MARTIN MARIETTA ENERGY SYSTEMS LIBRARIES
3 4456 0361472 9

CENTRAL RESEARCH LIBRARY
DOCUMENT COLLECTION

ORNL-2910
UC-34 – Physics and Mathematics
TID-4500 (15th ed.)

PHYSICS DIVISION

ANNUAL PROGRESS REPORT

FOR PERIOD ENDING FEBRUARY 10, 1960

CENTRAL RESEARCH LIBRARY
DOCUMENT COLLECTION
LIBRARY LOAN COPY
DO NOT TRANSFER TO ANOTHER PERSON
If you wish someone else to see this document, send in name with document and the library will arrange a loan.

OAK RIDGE NATIONAL LABORATORY
operated by
UNION CARBIDE CORPORATION
for the
U.S. ATOMIC ENERGY COMMISSION

Printed in USA. Price $2.50. Available from the
Office of Technical Services
Department of Commerce
Washington 25, D.C.

LEGAL NOTICE

This report was prepared as an account of Government sponsored work. Neither the United States, nor the Commission, nor any person acting on behalf of the Commission:

A. Makes any warranty or representation, expressed or implied, with respect to the accuracy, completeness, or usefulness of the information contained in this report, or that the use of any information, apparatus, method, or process disclosed in this report may not infringe privately owned rights; or

B. Assumes any liabilities with respect to the use of, or for damages resulting from the use of any information, apparatus, method, or process disclosed in this report.

As used in the above, "person acting on behalf of the Commission" includes any employee or contractor of the Commission, or employee of such contractor, to the extent that such employee or contractor of the Commission, or employee of such contractor prepares, disseminates, or provides access to, any information pursuant to his employment or contract with the Commission, or his employment with such contractor.

ORNL-2910
UC-34 – Physics and Mathematics
TID-4500 (15th ed.)

Contract No. W-7405-eng-26

PHYSICS DIVISION

ANNUAL PROGRESS REPORT

for Period Ending February 10, 1960

J. L. Fowler, Director
E. O. Wollan, Associate Director

DATE ISSUED

MAR 25 1960

OAK RIDGE NATIONAL LABORATORY
Oak Ridge, Tennessee
operated by
UNION CARBIDE CORPORATION
for the
U. S. ATOMIC ENERGY COMMISSION

MARTIN MARIETTA ENERGY SYSTEMS LIBRARIES
3 4456 0361472 9

FOREWORD

This is the second Physics Division progress report made on essentially an annual basis. The reporting period covers only 11 months as a result of the Physics Information Meeting having been scheduled for April.

The nature of the reporting is the same as previously. In those cases in which a paper has been written for publication, has been submitted to a journal, or has appeared in a journal, only the abstract will appear in the progress report. In such cases preprints of the original articles will be available. The reports of research in progress are given as previously when preliminary results are available

TABLE OF CONTENTS AND SUMMARY

PSEUDOSCALAR INTERACTION IN NUCLEAR BETA DECAY

C. P. Bhalla and M. E. Rose 1

The existence of pseudoscalar interaction is investigated by camparing the theoretical calculation with the experimental data on the Pr^{144} $0 \rightarrow 0$ (yes) beta transition. An upper limit on $|C_P/MC_A|$ has been set as 0.05.

NUCLEON FORM FACTORS AND THE MICROSCOPIC STRUCTURE OF SPACE

T. A. Welton 1

Arguments are given from the experimental information on the nucleon form factors to make plausible the assumption that a major breakdown of conventional space-time concepts occurs at distances comparable with the experimental nucleon radii.

THE SCATTERING AND POLARIZATION OF SPIN 1 PARTICLES

G. R. Satchler 4

Abstract of ORNL-2861.

SPIN-ORBIT COUPLING FOR SPIN 1 PARTICLES

G. R. Satchler 4

Abstract of paper to be submitted to *Nuclear Physics.*

$(d,p\gamma)$ ANGULAR CORRELATIONS PREDICTED BY THE DISTORTED WAVE BORN APPROXIMATION

G. R. Satchler and W. Tobocman 4

Abstract of paper submitted to the *Physical Review.*

CIRCULARLY POLARIZED GAMMA RAYS FROM DIRECT NUCLEAR REACTIONS

G. R. Satchler 5

Abstract of paper submitted to *Nuclear Physics.*

PHENOMENOLOGICAL WOODS-SAXON NUCLEAR POTENTIAL FOR SINGLE-PARTICLE STATES OF O^{17}

E. G. Corman and J. L. Fowler 5

A Woods-Saxon potential with a state dependent depth has been found which reproduces the single-particle states of O^{17}. The effective mass formalism for the velocity dependence was investigated.

LONGITUDINAL POLARIZATION OF P^{32} BETA RAYS

H. B. Willard, A. Galonsky, A. R. Brosi, and B. H. Ketelle 7

The longitudinal polarization of 618-kev betas from the decay of P^{32} has been measured by Mott scattering to be $(-0.981 \pm 0.012)v/c$. Corrections were made for background; wall scattering; foil location; multiple and plural foil scattering; instrumental asymmetry; finite solid angles; depolarization in the source and the window and by the plates of the electrostatic rotator.

GAMMA-GAMMA ANGULAR CORRELATION IN Ge^{74}

R. L. Robinson and E. Eichler 11

The angular correlation for the 0.60-0.60-Mev gamma-ray cascade in Ge^{74} has been measured. The cascade was found to have the spin sequence $2(D + Q)2(Q)0$ with $Q/D = 12^{+17}_{-7}$.

DECAYS OF Rh^{106} AND Ag^{106}

R. L. Robinson, F. K. McGowan, and W. G. Smith 12

Abstract of paper to be submitted to the *Physical Review.*

COULOMB EXCITATION OF EVEN-EVEN NUCLEI OF Ni, Zn, Ge, AND Se

P. H. Stelson and F. K. McGowan 12

Coulomb excitation results on 14 even-even nuclei of Ni, Zn, Ge, and Se are reported.

DECAY OF I^{132}

R. L. Robinson, E. Eichler, and N. R. Johnson 16

The gamma-ray spectrum of I^{132} has been studied with scintillation spectrometers. A tentative decay scheme has been proposed.

DECAY OF $Rh^{102} \longrightarrow Ru^{102}$

F. K. McGowan, P. H. Stelson, and W. G. Smith 19

The singles and coincident gamma-ray spectra from the decay of Rh^{102} have been measured with scintillation spectrometers. The branching ratio of cascade to crossover from the second 2^+ state is 1.5 ± 0.3, and $E2/M1$ for the $2^+ \rightarrow 2^+$ transition is greater than or equal to 225.

EVIDENCE FOR NEW ISOMERIC STATES

E. C. Campbell and P. F. Fettweis 24

Abstract of paper published in *Nuclear Physics.*

THE REACTION $C^{14}(p,n)N^{14}$

J. K. Bair, R. D. Edge, and H. B. Willard 24

Abstract of paper to be published in the *Physical Review.*

CROSS SECTIONS FOR (p,n) REACTIONS IN INTERMEDIATE-WEIGHT NUCLEI

C. H. Johnson, A. Galonsky, and C. N. Inskeep 25

Cross sections averaged over resonances for (p,n) reactions in 31 intermediate-weight ($37 \leqq A \leqq 133$) nuclei have been measured for proton energies from 1.5 to 5.5 Mev.

CROSS SECTION FOR THE $Li^6(n,\alpha)H^3$ REACTION FOR $1.2 \leqq E_n \leqq 8.0$ Mev

R. B. Murray and H. W. Schmitt 29

Abstract of paper published in the *Physical Review.*

NEUTRON-INDUCED FISSION CROSS SECTION OF Np^{237}

H. W. Schmitt and R. B. Murray 29

Abstract of paper to be published in the *Physical Review.*

DIFFERENTIAL NEUTRON SCATTERING FROM LEAD

J. L. Fowler 29

The total neutron cross section of normal lead and of an effectively 72% Pb^{208} sample of lead has been measured from 1 to 4.1 Mev, and the differential neutron scattering cross sections for these samples have been determined at 1.2, 2.2, and 3.2 Mev.

NEUTRON TOTAL CROSS SECTIONS IN THE kev ENERGY RANGE

J. H. Gibbons, W. M. Good, P. D. Miller, and J. H. Neiler 33

Automation and punched-tape output have made it possible to carry on the routine total cross section measurements while permitting time for other types of measurements. The isotopes Ge^{70}, Ge^{72}, Ge^{74}, and Ge^{76} have been studied with 2% or better energy resolution from 3 to 30 kev. Cobalt-59 and Cu^{63} have been examined at 3 to 10 kev and new structure found.

MILLIMICROSECOND PULSING – ITS APPLICATION AND TECHNIQUE
W. M. Good 33

Abstract of paper submitted to *Nuclear Instruments.*

ABSOLUTE NEUTRON ABSORPTION CROSS SECTIONS FOR ANTIMONY-BERYLLIUM PHOTONEUTRONS
H. W. Schmitt and C. W. Cook 34

Abstract of paper to be published in *Nuclear Physics.*

DETERMINATION OF THE ENERGY OF ANTIMONY-BERYLLIUM PHOTONEUTRONS
H. W. Schmitt 34

Abstract of paper to be published in *Nuclear Physics.*

MILLIMICROSECOND TIME-OF-FLIGHT: CAPTURE
J. H. Gibbons, R. L. Macklin, P. D. Miller, and J. H. Neiler 34

Measurements of capture cross sections have been carried out on a number of additional elements, and a considerable amount of time has been spent on improving the accuracy of the results.

NEUTRON RADIATIVE CAPTURE MEASUREMENTS WITH THE ORNL FAST-CHOPPER TIME-OF-FLIGHT NEUTRON SPECTROMETER
R. C. Block and G. G. Slaughter 35

Neutron radiative capture cross section measurements have been made with a new large-volume liquid scintillator recently installed at the ORNL fast-chopper time-of-flight neutron spectrometer. Data have been obtained in the low kev region, where the resolution averages over many resonances; and also in the 10 to 200 ev range, where individual resonances have been resolved.

THERMAL NEUTRON CROSS-SECTION MEASUREMENTS OF U^{233}, U^{235}, Pu^{240}, U^{234}, AND I^{129} WITH THE ORNL FAST-CHOPPER TIME-OF-FLIGHT NEUTRON SPECTROMETER
R. C. Block, G. G. Slaughter, and J. A. Harvey 41

Abstract of paper to be submitted to *Nuclear Science and Engineering.*

THE RESONANCE ENERGY NEUTRON CROSS SECTION OF U^{233}
N. J. Pattenden and J. A. Harvey 42

The variation with neutron energy of the total cross section of U^{233} has been measured up to 100 ev. The data up to 5 ev have been analyzed using a multilevel-multichannel formula.

ABSOLUTE MEASUREMENT OF ETA OF U^{233} AND U^{235}
R. L. Macklin, G. deSaussure, J. D. Kington, Jr., and W. S. Lyon 46

Abstract of paper submitted to *Nuclear Science and Engineering.*

RARE-EARTH SPECTROSCOPY
K. L. Vander Sluis 46

Having exhausted most of the Zeeman data available for Er II, an extension of the present energy level system has been attempted using existing wavelength data and the aid of the IBM-704 computer. This attempt verifies the statistical behavior of this method of using wavelength data, and also demonstrates the need for more wavelength data.

HYPERFINE STRUCTURE AND ISOTOPE SHIFT OF Po^{209}
G. W. Charles 47

Preliminary data and analysis of the hyperfine structure and isotope shift of Po^{209} are presented. Patterns are reported for 21 lines, and structures are presented for seven energy levels of Po^{209}. These preliminary results suggest the correctness of Mrozowski's identification of the lines λ5939.6 and λ4611.5.

INFRARED SPECTRA OF SOLID AMMONIA
H. W. Morgan and P. A. Staats 50

Infrared spectra of solid NH_3, NH_2D, NHD_2, and ND_3 in the stable cubic phase and in two metastable phases are discussed.

NEUTRON DIFFRACTION INVESTIGATION OF MAGNETIC ORDERING IN THE TRIFLUORIDES OF 4d TRANSITION ELEMENTS
M. K. Wilkinson, E. O. Wollan, H. R. Child, and J. W. Cable 50

Molybdenum trifluoride, MoF_3, becomes antiferromagnetic below 185°K with a spin-only magnetic moment corresponding to $S = 3/2$ and a magnetic structure which can be correlated with coupling rules applicable to the iron-group trifluorides. These results, together with the absence of observable magnetic neutron scattering from PdF_3 and RuF_3, suggest that Hund's rule does not apply to ions in the 4d transition series.

NEUTRON DIFFRACTION STUDY OF THE MAGNETIC PROPERTIES OF RARE-EARTH–IRON PEROVSKITES
W. C. Koehler, E. O. Wollan, and M. K. Wilkinson 54

Abstract of paper submitted to the *Physical Review.*

NEUTRON DIFFRACTION INVESTIGATIONS OF THE MAGNETIC ORDERING IN RARE-EARTH NITRIDES
M. K. Wilkinson, H. R. Child, J. W. Cable, E. O. Wollan, and W. C. Koehler 55

Abstract of paper scheduled for publication in the April 1960 issue of the *Journal of Applied Physics.*

NEUTRON DIFFRACTION STUDIES OF ANTIFERROMAGNETISM IN CrF_2 AND $CrCl_2$
J. W. Cable, M. K. Wilkinson, and E. O. Wollan 55

Abstract of paper submitted to the *Physical Review.*

NEUTRON DIFFRACTION INVESTIGATION OF ANTIFERROMAGNETISM IN $CrCl_3$
J. W. Cable, M. K. Wilkinson, and E. O. Wollan 56

Abstract of paper to be submitted to the *Physical Review.*

MAGNETIC COUPLING IN CRYSTALLINE COMPOUNDS – A PHENOMENOLOGICAL THEORY OF MAGNETISM IN 3d METALS
E. O. Wollan 56

Abstract of paper to be published in the *Physical Review.*

ANGULAR DISTRIBUTION OF ALPHA PARTICLES EMITTED BY ORIENTED Np^{237} NUCLEI
S. H. Hanauer, J. W. T. Dabbs, L. D. Roberts, and G. W. Parker 56

An experimental determination of the signs of the quadrupole and hyperfine coupling constants leading to nuclear alignment in NpO_2^{++} has shown that the original assignments of Eisenstein and Pryce ($A > 0$, $P < 0$) were incorrect.

FISSION FRAGMENTS FROM ALIGNED U^{233} AND U^{235} NUCLEI
J. W. T. Dabbs, F. J. Walter, L. D. Roberts, G. W. Parker, and J. O. Thomson 60

The fission of oriented U^{233} has been found to be isotropic, while U^{235} shows an anisotropy opposite to that of its alpha particles. A comparison with the predictions of the Bohr picture is made.

SIGN OF THE NUCLEAR QUADRUPOLE COUPLING IN UO_2^{++} AND NpO_2^{++} IONS
L. D. Roberts and J. W. T. Dabbs 62

Relativistic Hartree wave functions for atomic uranium and U^{5+} have been calculated. By use of these a discussion of the nuclear quadrupole coupling in UO_2^{++} and NpO_2^{++} is given.

SAMPLE SCATTERING CORRECTIONS IN NEUTRON BEAM EXPERIMENTS
H. W. Schmitt 69

Abstract of ORNL-2883.

MILLIMICROSECOND TIME-OF-FLIGHT: INSTRUMENTATION
J. H. Gibbons, W. M. Good, R. F. King, and J. Judish 70

Instrumental developments include (1) a better understanding of the limitations that accompany the use of pulsed beams, (2) designs for the production of 1-mμsec bursts of protons at 1 ma peak current, and (3) preparations for installing the Von Ardenne ion source including a 400-cps 3-kw generator, Freon cooling, and an enlarged high-voltage spinning.

SEMICONDUCTOR SURFACE BARRIER COUNTERS
F. J. Walter, J. W. T. Dabbs, L. D. Roberts, and S. H. Hanauer 70

A better understanding of the very low temperature behavior of semiconductor surface barrier counters has been obtained.

POLARIZED ION SOURCE
J. E. Sherwood, S. J. Ovenshine, and R. F. King 72

Construction of a source of polarized ions is under way. A status report and description of the apparatus are given.

SPHERICAL ABERRATION OF GRID-TYPE ELECTROSTATIC LENSES
N. B. Alexander, R. M. Chester, and D. G. Maeder 74

A study of the aberrations in electrostatic lenses is presented. A zero-spherical-aberration arrangement is shown feasible if a shaped wire grid is used in the cross section of the beam. This is not possible with conventional two-element lenses.

PUBLICATIONS 88

PAPERS PRESENTED AT SCIENTIFIC AND TECHNICAL MEETINGS 90

ANNOUNCEMENTS 94

PHYSICS DIVISION ANNUAL PROGRESS REPORT

PSEUDOSCALAR INTERACTION IN NUCLEAR BETA DECAY

C. P. Bhalla[1] M. E. Rose

The experiments on allowed transitions in nuclear beta decay indicate that the most probable interactions are vector and axial vector.

Due to the parity selection rule, these experiments do not have any bearing on the existence and, hence, the contribution of pseudoscalar interaction. To investigate this question, we have considered $0 \rightarrow 0$ (yes) beta transitions. In such a case, the vector interaction rigorously does not contribute. The relevant experimental data are the beta spectrum and the longitudinal polarization of beta particles.

For A and P interactions, we have calculated the expression for longitudinal polarization by using the scalar operator $\vec{\sigma}\cdot\hat{\mathbf{p}}$, where $\hat{\mathbf{p}}$ is a unit vector in the direction of the momentum of the beta particle. We use the operator for pseudoscalar interaction,[2] which one gets by applying the Foldy-Wouthysen transformation. It is in this respect that our treatment differs from the work of others. In the expressions for beta longitudinal polarization and spectrum, only two parameters occur, namely, C_P/MC_A, the ratio of the two coupling constants divided by nucleon mass, and $i\int\gamma_5/\int\vec{\sigma}\cdot\mathbf{r}$, the real ratio of the relevant nuclear matrix elements. The assumptions made are: (1) the two-component theory of the neutrino is valid, (2) time-reversal invariance in strong interactions is valid, and (3) time-reversal invariance in weak interactions is valid.

We have completed a detailed numerical analysis in the case of the ground-state transition of Pr^{144} ($0^- \rightarrow 0^+$), taking into account the finite size of the nucleus. In our analysis, we compare the calculated results with the most recent value of longitudinal polarization,[3] which is $-(0.986 \pm 0.030)v/c$ for the beta energy range of 1 to 3 Mev, and with the beta spectrum of Porter and Day.[4]

Our conclusions are the following: (1) Pure axial vector interaction can give a fit to the experimental results on beta longitudinal polarization and spectrum, and, as such, the experimental results are consistent with the absence of pseudoscalar interaction. (2) The upper limit for $|C_P/MC_A|$ which can also give a fit for the experimental spectrum and polarization is 0.05, with the real ratio of the matrix elements $i\int\gamma_5/\int\vec{\sigma}\cdot\mathbf{r}$ as large as ± 200. Our upper limit on C_P/MC_A is about half as much as previous estimates.[3,5]

[1] Physics Department, University of Tennessee.

[2] M. E. Rose and R. K. Osborn, *Phys. Rev.* 93, 1315 (1954).

[3] W. A. W. Mehlhap, Ph.D. dissertation, Washington University, Saint Louis, September 1959.

[4] F. T. Porter and P. Day, *Phys. Rev.* 114, 1286 (1959).

[5] R. Graham, J. Geiger, and T. Eastwood, *Can. J. Phys.* 36, 1084 (1958).

NUCLEON FORM FACTORS AND THE MICROSCOPIC STRUCTURE OF SPACE

T. A. Welton[1]

Evidence on the charge and current distributions of the nucleons comes from two sources. The results of Hughes *et al.*[2] and Melkonian *et al.*[3] on the low-energy neutron-electron interaction give an approximate upper limit for the magnitude of the mean square radius of the charge distribution of the neutron. Reasonably precise information on the charge and current distributions of the proton and somewhat less precise information on the current distribution of the neutron are available

[1] On year's assignment at Lawrence Radiation Laboratory, University of California, Berkeley.

[2] D. J. Hughes *et al.*, *Phys. Rev.* 90, 497 (1953).

[3] E. Melkonian, B. M. Rustad, and W. W. Havens, *Phys. Rev.* 114, 1571 (1959).

from the work of Hofstadter and collaborators.[4-7] These results can be summarized as follows. The experimental form factors will be represented by $F(k^2)$ with subscripts 1 or 2 for the electric or magnetic distributions and p or n for proton or neutron. The quantity k is the momentum transfer in the collision, in units of reciprocal fermis (10^{13} cm^{-1}). For small momentum transfer, F is conveniently represented by a series in k^2. Thus:

$$\begin{aligned} F_{1p}(k^2) &= 1 - \frac{1}{6} a_{1p}^2 k^2 + \dots , \\ F_{2p}(k^2) &= 1 - \frac{1}{6} a_{2p}^2 k^2 + \dots , \\ F_{1n}(k^2) &= - \frac{1}{6} a_{1n}^2 k^2 + \dots , \\ F_{2n}(k^2) &= 1 - \frac{1}{6} a_{2n}^2 k^2 + \dots . \end{aligned} \tag{1}$$

The Stanford work strongly indicates values for a_{1p}, a_{2p}, and a_{2n} all in the range 0.70 to 0.80 fermi. The neutron-electron scattering, on the other hand, will not allow a value for a_{1n} much greater than one-tenth this figure. It has become conventional to assume the three radii from the Stanford data to be identical. This exact equality is of course not compelled by the data, but deviations of the order of 10% would be noticed, and we accordingly write:

$$F_{1p} = F_{2p} = F_{2n} = F_H(k^2) = 1 - \frac{1}{6} a_H^2 k^2 . \tag{2}$$

Considerably more detail is in fact available, since F_H is quite well fitted over the known range of k^2 by a simple function:

$$F_H(k^2) = \left(1 + \frac{1}{12} a_H^2 k^2\right)^{-2} , \tag{3}$$

the so-called "exponential model" of Hofstadter.[7]

The information here summarized has been known for some time to be in serious conflict with any known theory of nucleon structure.[8-12] To summarize, four points must be emphasized:

1. The empirical assumption that $a_{1n} = a_H$, which is incomprehensible theoretically but is at least consistent with the Stanford observations (which are themselves incomprehensible theoretically), is in violent disagreement with the neutron-electron scattering measurement.

2. The charge and current distributions of the nucleons arise by mechanisms which are clearly quite different in detail. The equality of F_{1p} and F_{2p} therefore seems to be a strange coincidence.

3. Similarly, the details of the neutron and proton distributions are clearly quite different, so that the equality of F_{2p} and F_{2n} is again a strange coincidence.

4. The simplicity of the analytic form (3) is quite surprising, in view of the fact that the observations are well represented for $4 > k > 1$ fermi^{-1}. The analytic form contains only the single parameter a_H, while several different length parameters presumably should enter in a description of the nucleon charge and current distribution according to a correct meson theory. These length parameters include the reciprocal nucleon mass and the reciprocal of twice the pion mass. For comparison:

$$\left.\begin{aligned} a_H &= 0.80 \text{ fermi} , \\ \frac{1}{M} &= 0.21 \text{ fermi} , \\ \frac{1}{2\mu} &= 0.24 \text{ fermi} . \end{aligned}\right\} \tag{4}$$

Note that a_H is considerably larger than the other two parameters.

It has recently been suggested[13] that the element of coincidence could be explained and the fourth point circumvented by assuming a strong enough pion-pion interaction in a p state to permit

[4] R. Hofstadter and R. W. McAllister, *Phys. Rev.* 98, 217 (1955).

[5] M. R. Yearian and R. Hofstadter, *Phys. Rev.* 110, 552 (1958).

[6] R. Hofstadter, *Ann. Rev. Nuclear Sci.* 7, 231 (1957).

[7] E. E. Chambers and R. Hofstadter, *Phys. Rev.* 103, 1454 (1956).

[8] L. L. Foldy, *Revs. Modern Phys.* 30, 471 (1958).

[9] J. Bernstein and M. L. Goldberger, *Revs. Modern Phys.* 30, 465 (1958).

[10] P. Federbush, M. L. Goldberger, and S. B. Treiman, *Phys. Rev.* 112, 642 (1958).

[11] G. F. Chew *et al.*, *Phys. Rev.* 110, 265 (1958).

[12] S. D. Drell, *Proc. Ann. Intern. Conf. High Energy Phys., CERN, Geneva, 1958*, p 20, 27.

[13] W. R. Frazer and J. R. Fulco, *Phys. Rev. Letters* 2, 365 (1959).

a nearly bound two-pion state. The reciprocal of the energy of this state then would provide a third length parameter, which would be the same for F_{1p}, F_{2p}, and F_{2n} and might conceivably be large enough to explain the large value of a_H. It will be made clear that the study of high-energy electron-electron scattering can decide between this hypothesis and the one to be here presented. Lacking this result, it seems in any event unlikely that the pion-pion interaction can simultaneously explain the very small value for a_{1n} obtained from the neutron-electron interaction.

There exists one clear-cut hypothesis which seems able to account for all the outstanding difficulties. Suppose that all the nucleon charge and current distributions have rms radii comparable with the small value obtained from the neutron-electron interaction. Suppose that, in addition, the conventional description of the interaction of two point particles breaks down for some reason at distances of separation comparable with a_H. Under these conditions, the experimental form factors would be:

$$
\begin{aligned}
F_{1p}^{ex} &= F_{1p} \cdot F = \left(1 - \frac{1}{6} a_{1p}^2 k^2 + \dots\right)\left(1 - \frac{1}{6} a^2 k^2 + \dots\right), \\
F_{2p}^{ex} &= F_{2p} \cdot F = \left(1 - \frac{1}{6} a_{2p}^2 k^2 + \dots\right)\left(1 - \frac{1}{6} a^2 k^2 + \dots\right), \\
F_{1n}^{ex} &= F_{1n} \cdot F = \left(-\frac{1}{6} a_{1n}^2 k^2 + \dots\right)\left(1 - \frac{1}{6} a^2 k^2 + \dots\right), \\
F_{2n}^{ex} &= F_{2n} \cdot F = \left(1 - \frac{1}{6} a_{2n}^2 k^2 + \dots\right)\left(1 - \frac{1}{6} a^2 k^2 + \dots\right).
\end{aligned}
\tag{5}
$$

The quantities a_{1p}, a_{2p}, a_{1n}, and a_{2n} are the unknown rms radii of the actual distributions, all quite small compared with a_H. The universal constant a will be comparable with a_H in size and can therefore be determined roughly from the Stanford data. On this assumption, the absence of the leading term (unity) in F_{1n}, because of the electrical neutrality of the neutron, allows the experimental rms radius of the neutron to be much smaller than a_H, whereas the other experimental rms radii are composites of the form

$$a_{N\ \mathrm{exp}} = \left(a_N^2 + a^2\right)^{1/2} \tag{6}$$

and are much larger than the charge radius of the neutron. In this way, the contradictions between the various experiments are removed.

Once the force of the foregoing arguments is admitted, some theoretical framework must be sought for describing the postulated breakdown of the theory at small distances. A number of so-called "nonlocal" field theories have been proposed for this purpose. None have met with any important success, in large part because of grave questions of consistency. The previously reported work on the idea of a spherical momentum space,[14] originally proposed by Snyder,[15,16] has been much extended. Several apparent ambiguities and inconsistencies have been removed, the principal result being that the form factor to be used in calculating the Stanford results is given by

$$F(k^2) = \left(1 + \frac{1}{24} a^2 k^2\right)^{-4}, \tag{7}$$

with a given approximately by

$$a = 0.75 \times 10^{-13}\ \mathrm{cm} = \frac{3.56}{M}. \tag{8}$$

An essential point is that the form factor (7) is to be applied equally in the scattering of electrons

[14] T. A. Welton, *Phys. Semiann. Prog. Rep. Mar. 10, 1958*, ORNL-2501, p 1; *Phys. Semiann. Prog. Rep. Sept. 20, 1958*, ORNL-2610, p 7.

[15] H. S. Snyder, *Phys. Rev.* 71, 38 (1947).

[16] H. S. Snyder, *Phys. Rev.* 72, 68 (1947).

by electrons. This contrasts with the pion-pion proposal,[13] which would not affect the electron-electron case in any way. From (7), the effect should be easily observable under the conditions of the experiment to be performed by O'Neill and collaborators at Stanford. Unfortunately, the detailed form of (7) probably can neither be confirmed nor denied by the proposed experiment. Details of the work here reported are being prepared for publication.

THE SCATTERING AND POLARIZATION OF SPIN 1 PARTICLES[1]

G. R. Satchler

The theory of the scattering and polarization of spin 1 particles is reviewed and extended. After a discussion of optical models for spin 1 particles, the scattering amplitudes are given and used to construct formulas for the differential cross section and spin polarization moments. The transformation of the polarization from center-of-mass to laboratory systems, the interpretation of double-scattering experiments, and the effect on the polarization of magnetic deflection are also discussed.

[1] Abstract of ORNL-2861.

SPIN-ORBIT COUPLING FOR SPIN 1 PARTICLES[1]

G. R. Satchler

A one-body spin-orbit potential for spin 1 particles may contain, in addition to the familiar vector term $\mathbf{l} \cdot \mathbf{s}$ used with spin $\frac{1}{2}$ particles, certain tensor terms T. Here T is a scalar product of second-rank spherical tensors, $T = \mathbf{R}_2 \cdot \mathbf{S}_2$, where $\mathbf{S}_2$ operates in the spin space of the particle and $\mathbf{R}_2$ in coordinate space; $\mathbf{S}_2$ is uniquely determined, but several forms of $\mathbf{R}_2$ may be constructed from the position vector $\mathbf{r}$, momentum vector $\mathbf{p}$, and orbital angular momentum vector $\mathbf{l}$. The requirements of Hermiticity and parity conservation limit these to three. If a complex potential is allowed, as in the optical model for scattering from nuclei, time-reversal invariance is relaxed, but if we still demand symmetry for the scattering matrix, no other form of $\mathbf{R}_2$ becomes allowed. Only one of these forms of T remains diagonal in the orbital angular momentum $\mathbf{l}$. The implications for the scattering and polarization of spin 1 particles is discussed, with particular reference to deuterons.

[1] Abstract of paper to be submitted to *Nuclear Physics*.

(d,py) ANGULAR CORRELATIONS PREDICTED BY THE DISTORTED WAVE BORN APPROXIMATION[1]

G. R. Satchler W. Tobocman[2]

Angular correlations in (d,py) reactions have been calculated for several cases, using four different forms of stripping theory: (1) plane wave Born approximation with cutoff (Butler theory), (2) Coulomb wave Born approximation with cutoff, (3) optical potential wave Born approximation with cutoff, (4) optical potential wave Born approximation without cutoff. The distortion effects are found to be strongly dependent on the direction of the emerging proton and on the type of distortion assumed. The fact that in a given case the (d,p) angular distribution is only slightly changed by distortion effects seems to be no guarantee that distortion effects on the (d,py) angular correlation will be small. On the other hand, we have one case where distortion has an important effect on the angular distribution and a negligible effect on the angular correlation.

[1] Abstract of paper submitted to the *Physical Review*.

[2] The Rice Institute, Houston, Texas.

CIRCULARLY POLARIZED GAMMA RAYS FROM DIRECT NUCLEAR REACTIONS[1]

G. R. Satchler

The residual nuclei following a reaction are left in a polarized state in general. One way of measuring this polarization is to observe any gamma rays the residual nucleus emits. Their angular distribution reveals the even moments of the polarization, while their circular polarization depends upon the odd moments. Following a general discussion of circular polarization and the predictions of the direct-interaction picture of nuclear reactions, simple cases of stripping reactions and inelastic scattering are considered. Valuable information can be obtained concerning both the reaction mechanism and the reduced widths and nuclear spins involved.

[1]Abstract of paper submitted to *Nuclear Physics*.

PHENOMENOLOGICAL WOODS-SAXON NUCLEAR POTENTIAL FOR SINGLE-PARTICLE STATES OF O^{17}

E. G. Corman[1] J. L. Fowler

The bound-state information on O^{17} and neutron scattering from O^{16} allow one to construct a phenomenological nuclear potential which describes the essentially single-particle states of O^{17} (refs 2, 3). These include the $1d_{5/2}$ ground state, the $1d_{3/2}$ resonance in neutron scattering from O^{16}, the $2s$ bound state, and the s-wave scattering phase shifts. Figure 1 shows the experimentally determined phase shifts from neutron scattering from O^{16} (ref 2). The odd-parity $p_{3/2}$ levels at 0.44 and 1.32 Mev are compound-nucleus levels in O^{17}. The interference of an s compound-nucleus resonance with potential scattering indicates that the s-wave potential phase shift at 2.37 Mev is −90°. This s-wave potential scattering is interpreted as arising from the $2s$ bound state at −3.27 Mev. (See energy level diagram of O^{17} in Fig. 1.)

Now if we seek a single-particle phenomenological potential well which will reproduce the experimental data, we find that for any shape well the position of the $2s$ bound state and the s-wave phase shifts determine the depth and the effective radius of the potential. Equation (1) gives the radial wave function divided by r for a neutron in the presence of the potential $V(r)$ due to the O^{16} core:

$$\frac{d^2 u}{dr^2} = f(r) \times u \ , \qquad (1)$$

$$f(r) = -\frac{2m}{\hbar^2}\left[E - V(r)\right] + \frac{l(l+1)}{r^2} - \gamma \begin{Bmatrix} l \\ -(l+1) \end{Bmatrix} \frac{1}{2mc^2}\frac{1}{r}\frac{\partial V}{\partial r} \ . \qquad (2)$$

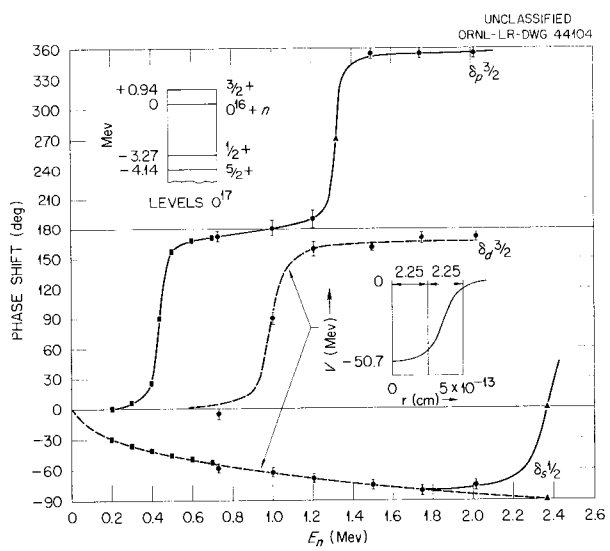

Fig. 1. Phase Shifts for Scattering of Neutrons from O^{16}. Dotted lines calculated with phenomenological potential shown as insert.

[1]Summer visitor from the University of Kansas.

[2]J. L. Fowler and H. O. Cohn, *Phys. Rev.* 109, 89 (1958).

[3]E. G. Corman and J. L. Fowler, *Bull. Am. Phys. Soc.* 5, 34 (1960).

As Eq. (2) indicates, the spin-orbit coupling is taken in the Thomas form multiplied by the constant γ. For s states, $l = 0$ and the last two terms in Eq. (2) drop out. Then $V(r)$ is the unknown. For the s resonance and s-wave potential scattering, the experimental information can be fitted with the following three potentials:

$$V = -35 \text{ Mev}, \quad r < 4.2 \text{ fermis}, \qquad V = 0, \quad r > 4.2 \text{ fermis}; \tag{3}$$

$$V = -44.2 \text{ Mev}, \quad r < 2.76 \text{ fermis}, \qquad V = -44.2 \exp\left(-\frac{r - 2.76 \text{ fermis}}{1.0 \text{ fermi}}\right) \text{Mev}, \quad r > 2.76 \text{ fermis}; \tag{4}$$

$$V = -\frac{50.7 \text{ Mev}}{1 + \exp[(r - 3.32 \text{ fermis})/0.5 \text{ fermi}]}. \tag{5}$$

In Eq. (5) the potential is taken in the Woods-Saxon form.

The next step in the calculation is the inclusion of the $1d$ states in the analysis. In Fig. 1 the energy positions of the d levels of O^{17} are listed in the upper left-hand corner. Shown on the right-hand side is the Woods-Saxon potential which gives the correct energy position of the $\frac{1}{2}^+$ state and the s-wave phase shifts as shown by the dotted line. Now the experimental width of the $d_{3/2}$ state at 0.94 Mev determines essentially the diffuseness of the well. From previous work[2] it has been found that a change in the diffuseness of an exponential well by 25% changed the theoretical width of the $d_{3/2}$ resonance by $\sim$100 kev. From this previous work one concluded that for the Woods-Saxon potential the constant which determines the diffuseness should be 0.5 fermi. Now for these calculations we assume that the depth of the well is state dependent. The dotted curve for the $d_{3/2}$ phase shifts was calculated with the Woods-Saxon potential -47.5 Mev deep and with γ, the constant multiplying the Thomas spin-orbit term, equal to 19.0. As can be seen, there is an excellent fit to the experimental data. These parameters also give the $d_{5/2}$ ground state of O^{17} at the correct energy, -4.14 Mev.

Next consider the case in which the velocity dependence is included with the effective mass formalism.[4] The Hamiltonian of the neutron and the O^{16} core used is of the form shown in Eq. (6). The effective mass of the neutron is a function of r:

$$\left[\mathbf{p} \frac{1}{2m} \mathbf{p} + V(r) \right] \psi = E\psi, \tag{6}$$

$$m = \frac{m_0}{1 + K\,V(r)}; \tag{7}$$

$$-\frac{\hbar^2}{2m_0} \frac{1}{r^2} \frac{d}{dr} \left\{ r^2 [1 + K\,V(r)] \frac{dR}{dr} \right\} + \left\{ V(r) + \frac{\hbar^2}{2m_0} \frac{l(l+1)}{r^2} [1 + K\,V(r)] - \gamma \begin{pmatrix} l \\ -(l+1) \end{pmatrix} \frac{\hbar^2}{4m_0^2 c^2} \frac{1}{r} \frac{dV}{dr} \right\} R = ER. \tag{8}$$

With

$$M(r) = r\sqrt{1 + K\,V(r)}\; R, \tag{9}$$

$$\frac{d^2 M(r)}{dr^2} = f(r)\, M(r), \tag{10}$$

as indicated by Eq. (7), since $V(r)$ is a function of r. The factor K is a constant. The radial wave function, R, is given by Eq. (8). With the substitution shown in Eq. (9) the radial wave equation can be put in the form of Eq. (10), where $f(r)$ is a function of $V(r)$ and the derivatives of $V(r)$. Now one proceeds as in the previous case of the state-dependent potential. One uses the same diffuseness constant for the Woods-Saxon potential as used previously, namely, 0.5 fermi. The depth and radius of the potential are determined by the $2s$ bound state and the s phase shifts. With the depth and radius so determined, γ is adjusted to give the energy position of the $d_{3/2}$ state. We have carried through the calculation for several values of K, or for several values of central reduced mass, with the results summarized in Table 1. The position of the $d_{5/2}$ state, which experimentally is at -4.14 Mev, in these calculations goes lower in energy as the

[4] A. A. Ross, R. D. Lawson, and H. Mark, *Phys. Rev.* 104, 401 (1956).

Table 1. Woods-Saxon Parameters for Different Values of Central Effective Mass

A = diffuseness constant = 0.5 fermi

m/m_0	R (fermis)	V_0 (Mev)	γ	$E_{d_{5/2}}$
1	3.32	50.7	27.0	7.1
$2/3$	2.84	85.1	15.2	8.0
$1/2$	2.55	121.7	10.8	8.6
$2/5$	2.35	158.7	8.4	8.6

effective mass decreases. With the diffuseness constant equal to 0.5 fermi, it appears that the effective-mass formalism does not give all of the single-particle properties of O^{17}. With the case $m_0/2$, the calculated width of the $d_{3/2}$ unbound level is ~5% low; it is possible that a correction of the diffuseness constant to increase the width of this level may allow a fit to the splitting of the d states.

We wish to acknowledge the assistance of M. Callihan, who aided in coding the latter stages of this problem for the 704 computer.

LONGITUDINAL POLARIZATION OF P^{32} BETA RAYS

H. B. Willard
A. Galonsky[1]
A. R. Brosi
B. H. Ketelle

The measurements previously reported[2] of the longitudinal polarization of P^{32} beta rays have been studied in considerably more detail. A spherical electrostatic analyzer converted the longitudinal polarization to transverse, and then the asymmetry in Mott scattering was observed. Multiple and plural scattering effects were investigated for 615.6-kev electrons scattered by gold foils from 0.1 to 12.6 mg/cm^2 thick. It was found that the asymmetry $e \equiv \vec{P}_e \cdot \vec{n}S$ is linear out to only 1.5 mg/cm^2 but that the function $e^{-1/2}$ is linear out to 12.6 mg/cm^2. These data are plotted as a function of foil thickness in Figs. 1 and 2 [$r \equiv (1 - e)/(1 + e)$, the up/down ratio]. The extrapolated (by $e^{-1/2}$) value of e is $e_0 = 0.3418$ ($\pm$0.64%).

In order to obtain an experimental determination of the source depolarization, up/down ratios were measured for two sources, which weighed 13.9 and 4.8 mg/cm^2. The thicker source was purposely thickened by adding $AlPO_4$ to the active material. Both 440-μg/cm^2 gold and 1-mil aluminum scattering foils were used. After correction for plural and multiple scattering and instrumental asymmetry, it was found that the depolarization is (0.01 $\pm$ 0.10)% per mg/cm^2. Thus the depolarization in the 1.2-curie source used to obtain gold scattering data out to 1.46 mg/cm^2 previously reported[2] was (0.03 $\pm$ 0.30)%, in good agreement with the theoretical estimate of 0.26% calculated from Mühlschlegel's[3] equations.

The problem of determining what happens to electrons scattered by the aluminum plates of the electrostatic rotator can be divided into three parts corresponding to energies (a) below 600 kev, (b) between 600 and 630 kev, and (c) above 630 kev. Since we accept in our pulse spectrum only electrons with energies between ~520 and ~710 kev, we can ignore all electrons which start out with energies below 520 kev. If the plate voltage is lowered to 22 kv so that only 360-kev electrons are transmitted without scattering, then the upper portion of this pulse spectrum will cut off well below the low energy limit we usually accept. However, the paths of high-energy electrons will not be greatly changed, and the intensity of electrons detected at a pulse height between 520 and 710 kev will be an approximate measure of the plate scattering from (a) and (c). The result of this experiment was a ratio of 1 to 2500 for the scattered beam at 22 kv to the direct beam at 34.9 kv (in the 12 channels customarily accepted). Even if the beam is completely depolarized, this will not change our final value of P by more than 0.06%.

The difficult problem is to determine part (b). Most of the scattering will occur near the source,

[1] Now at Midwestern Universities Research Association, Madison, Wis.

[2] A. R. Brosi *et al.*, *Phys. Ann. Prog. Rep. Mar. 10, 1959*, ORNL-2718, p 4.

[3] B. Mühlschlegel, *Z. Physik* 155, 69 (1959).

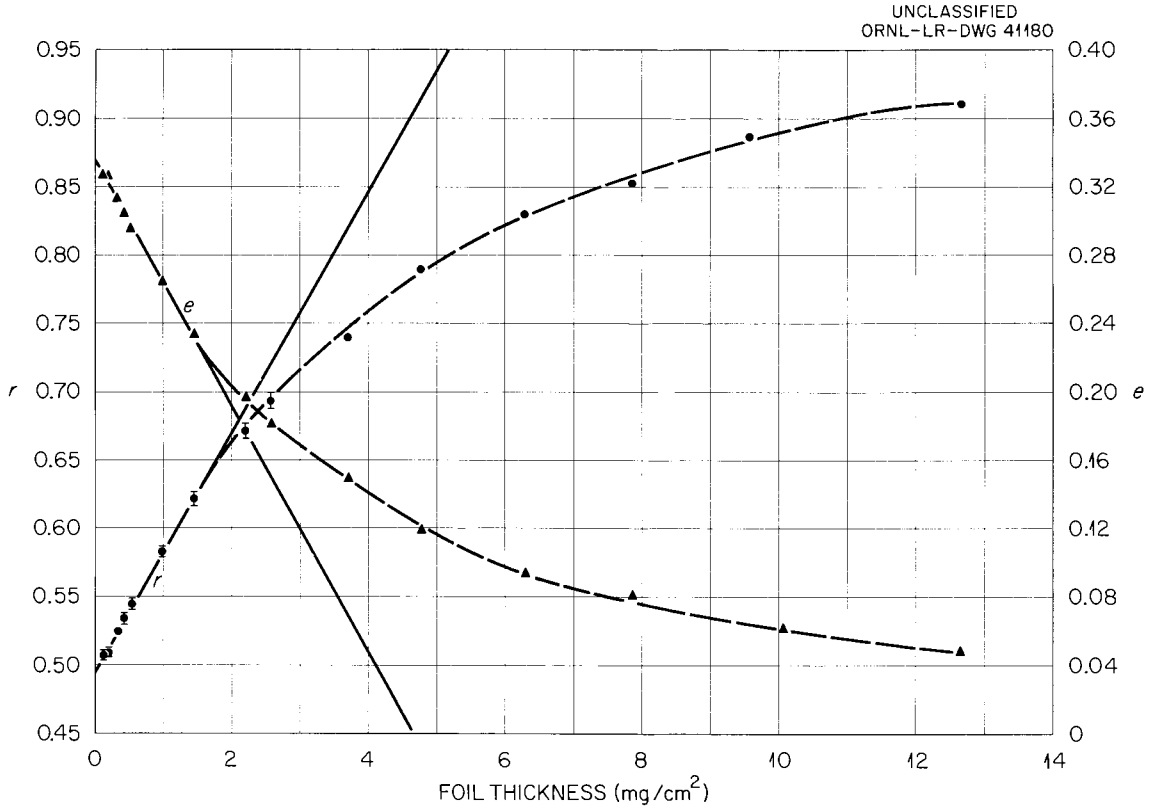

Fig. 1. Gold Asymmetry e and Up/Down Ratio r as a Function of Scattering Foil Thickness.

but will be limited to $\leq \pm 11°$. If the electrons make a single scattering from the plates, there will be no depolarization due to Mott scattering, since $S(\text{Al}, \leq 15°) \leq -0.0003$. If the electrons make two scatterings, both angles will be almost the same. Assuming a 100-kev energy loss, the two 90° scatterings will contribute 1 in 10^5 parts of the main beam, two 45° scatterings will contribute 1 in 450, etc. However, the two 45° scatterings will contribute less than 0.002% to the depolarization. Therefore we conclude that the plate depolarization is ($\leq 0.0 \pm 0.1$)%.

The finite extent of the beam on the target, its spatial distribution of intensity on the target, and especially the angle between the beam and the axis of rotation of the counters all contribute to an instrumental asymmetry not averaged out by counter rotation.

An ideal way to measure this asymmetry is to scatter from a low-Z material. In the (unattainable) limit of $Z = 0$, $S = 0$ and any deviation of r from unity must be ascribed to an instrumental asymmetry. The foil thickness necessary to obtain a given counting rate is proportional to $1/Z^2$. Because energy loss in the foil tends to smear out the pulse-height spectra in the detectors, thus reducing counting accuracy, we cannot go too low in Z; and the use of a high Z will give a large polarization asymmetry and defeat the very purpose of this subsidiary experiment. As a compromise we chose an aluminum foil 3.26 mg/cm^2 (nominally ½ mil) thick and found that $\bar{r} = 0.9509$ (± 0.42%). The foil location correction changes e by (0.19 ± 0.06)% and hence r by ($+0.012 \pm 0.003$)%. The differential wall-scattering background reduces this by (-0.016 ± 0.009)% to give finally 0.9508 (± 0.43%) for r. This value is for the same P^{32} source used to gather the gold data up to 1.46 mg/cm^2 thickness.

The plural and multiple scattering effect in aluminum was determined experimentally with a separate P^{32} source. Foil thickness values of 3.26, 7.19, and 13.51 mg/cm^2 were used. Although

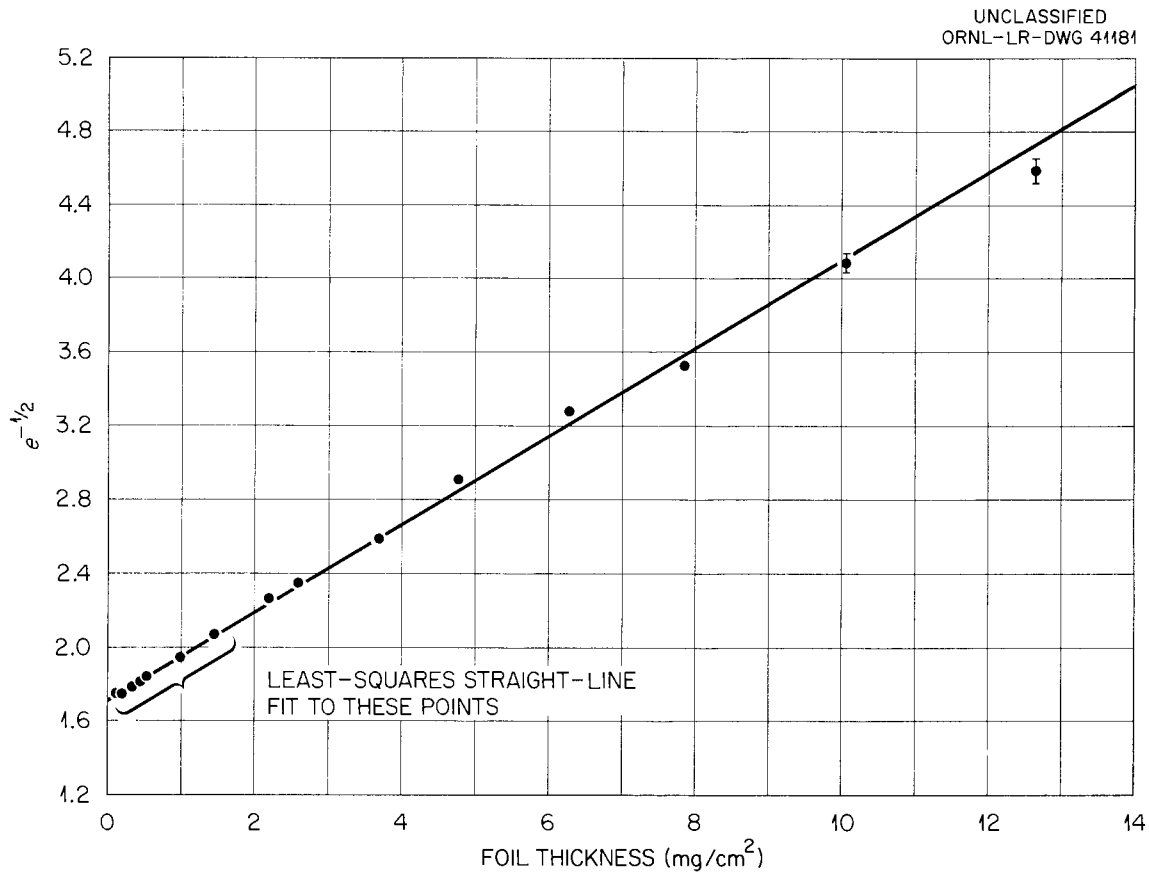

Fig. 2. Curve for $e^{-1/2}$ as a Function of Gold Scattering Foil Thickness.

each r value needs to be corrected for instrumental asymmetry, the experimental slope

$$\frac{1}{r}\frac{\Delta r}{\Delta d} = (0.00471 \pm 0.00048) \text{ per mg/cm}^2$$

is roughly independent of source asymmetry. Thus a $(-1.54 \pm 0.16)\%$ correction was applied to the value of r obtained with a 3.26-mg/cm^2 aluminum foil and the 1.2-curie P^{32} source used in evaluating e_0 for gold. Then $\bar{r}_0(\text{Al}) = 0.9354 \pm 0.0044$.

In order to determine the instrumental asymmetry we have only to compare this extrapolated value of $\bar{r}_0(\text{Al})$ with the theoretical $r_0(\text{th})$. Before proceeding with this task, it should be pointed out that since $e_0(\text{Al}) \sim 0.036$, a 1% error in its evaluation produces an error of only 0.07% in $r(\text{th})$. This is the extent to which aluminum approaches the ideal material where $S = e = 0$, and hence $r(\text{th})$ would be truly independent of e.

Anticipating our final value of the electron polarization, we use $P_e = -v/c = -0.8912$, the value at the scattering foil; $\overline{\cos\alpha}$ has been evaluated to give 0.8773, and Sherman's function for aluminum, averaged over the finite solid angles, is $\langle S(135°, 13, 0.8912)\rangle = -0.04578$. From this number we obtain $e_0 = -0.03579$ and $r(\text{th}) = 0.9309$.

The instrumental asymmetry is thus $\Delta r/r = (0.49 \pm 0.46)\%$ for aluminum. We may not apply this correction to the gold data until we investigate the nature of the asymmetry. The following example will clarify this problem:

Let us assume that the entire asymmetry is an angle $d\theta$ between the beam and the rotation axis in the vertical plane. Then

$$r(\theta \mp d\theta) = \frac{U(\theta - d\theta)}{D(\theta + d\theta)} = \frac{\sigma(\theta - d\theta)\,[1 - e(\theta - d\theta)]}{\sigma(\theta + d\theta)\,[1 + e(\theta + d\theta)]}\,,$$

and

$$\frac{dr}{r} = \frac{r(\theta \mp d\theta) - r(\theta)}{r(\theta)}$$

$$= 2d\theta \left(\frac{e^2}{1 - e^2} \frac{1}{S} \frac{dS}{d\theta} - \frac{1}{\sigma} \frac{d\sigma}{d\theta} \right) .$$

The above-mentioned problem is now clear: S and σ are not the same functions of θ for aluminum and gold; hence the instrumental asymmetries dr/r are not the same for aluminum and gold. Fortunately $(1/\sigma)(d\sigma/d\theta)$ is the same at 135°, –3.31% per degree, for both materials, and

$$\frac{e^2}{1 - e^2} \frac{1}{S} \frac{dS}{d\theta}$$

is, in both cases, much less than $(1/\sigma)(d\sigma/d\theta)$, namely, 0.14% per degree for gold and 0.00046% per degree for aluminum. Therefore we find $(dr/r)_{Au} = 1.044(dr/r)_{Al}$. This is a very likely source of asymmetry, because the large sensitivity, $(dr/r)_{Al} = 6.62\%$ per degree, means that the observed 0.49% asymmetry implies a $d\theta$ of only 0.08°.

The other source of asymmetry is the finite extent and the deviation from up-down asymmetry of the beam on the target. If we assume a parallel beam on the target, a displacement in the vertical scan by dx changes the scattering angle by $d\theta$ and the target-to-detector distance by dR. The average of r over the vertical scan, $N(x)$, gives for the deviation from that obtained with an infinitesimal beam

$$\frac{dr}{r} \cong \frac{2\sum_x [N(x) - N(-x)] \left[d\theta \left(\frac{1}{\sigma} \frac{d\sigma}{d\theta} - \frac{e^2}{1 - e^2} \frac{1}{S} \frac{dS}{d\theta} \right) + 2\frac{dR}{R} \right] - 2\sum_x N(x) \frac{d\theta}{1 - e^2} \left[\frac{e}{2} \frac{d\theta}{1} \frac{d^2S}{d\theta^2} + \frac{e}{S} \frac{dS}{d\theta} \left(\frac{d\theta}{\sigma} \frac{d\sigma}{d\theta} + 2\frac{dR}{R} \right) \right]}{\sum_x N(x)}$$

(The signs are arranged to make both $d\theta$ and dR positive.)

This is an interesting result in that there is no first-order term. That is, the terms linear in $d\theta$ and dR are multiplied by $N(x) - N(-x) \equiv dN(|x|)$, which is zero for a symmetrical scan. Hence the linear terms are really second order. We also note that the angle-dependent terms in the first summation are the same as those in the preceding example. Since dR/R (related to the change in solid angle at dx) is independent of the target material, the first summation must be the same for aluminum and gold to within less than 4.4%. In spite of the large asymmetry of the scan, this term contributes <0.1% to dr/r because the dominant parts, $(d\theta/\sigma)(d\sigma/d\theta) = -3.31\%$ per degree and $2(dR/R) = +3.49\%$ per degree, are of opposite sign and almost identical in magnitude.

Approximate cancellation of these terms also occurs in the second summation, so that it contributes to dr/r only ~0.01% for gold and about five times less for aluminum. Thus the instrumental asymmetry for gold will be

$$\frac{\Delta r}{r} = 1.044(0.49 \pm 0.46)\%$$

$$= (0.51 \pm 0.48)\% ,$$

or

$$\frac{\Delta e}{e} = (0.66 \pm 0.62)\% .$$

The various measured quantities with their errors and corrections are summarized in Table 1.

Thus the final ratio of nuclear polarization to nuclear v/c is –0.981 ± 0.012 for P^{32} beta rays emitted at the nucleus with an energy of 618 kev.

Table 1. Corrections and Errors

	Value	Correction (%)	Percentage Error
Asymmetry, e_0			
Extrapolated value (statistics)	0.3418		±0.64
Error due to foil location			±0.06
Differential wall scattering		+0.32	±0.18
Instrumental asymmetry		+0.66	±0.62
e_0	0.3452		±0.89
Spin Projection on Scattering Plane Normal			
cos α (median rays)	0.8807		±0.23
Finite solid angles		−0.38	±0.08
$\overline{\cos \alpha}$	0.8773		±0.24
Sherman's Function, S			
$-S$ (135°, 79, 0.8912) interpolated from Sherman's tables	−0.4573		±0.5
±0.2° error in scattering angle			±0.2
Finite solid angle		−1.54	±0.15
$\langle S \rangle$	−0.4503		±0.56
Polarization, P_e			
Value at foil	−0.8738		±1.08
Source and window depolarization		≤ -0.03	±0.30
Plate scattering depolarization			±0.1
Value at nucleus, P_N	−0.8741		±1.12
Beta-Ray Velocity, β_N, at Emission from Nucleus	0.8915		±0.04

GAMMA-GAMMA ANGULAR CORRELATION IN Ge^{74}

R. L. Robinson E. Eichler[1]

The angular correlation of the 0.60-0.60-Mev gamma-ray cascade which originates at the 1.20-Mev level in Ge^{74} has been measured. For this study an 18-day As^{74} source was used. The relative intensities of the two 0.60-Mev gamma rays in this decay are 3 and 100.

The gamma rays were detected by two 3 × 3 in. NaI crystals. The distance between the source and each detector was 15 cm. The source consisted of ~20 μl of a dilute Na_3AsO_4 solution which was placed in a fluorothene container. One-quarter inch of Lucite was placed around the source to absorb electrons and positrons. Data were taken every 10° between 90 and 180°. At each angle the region of the spectrum which included the 0.60-Mev peak was observed in coincidence with gamma rays of energies around 0.60 Mev. The random coincidences, which accounted for 20 to 60% of the gross coincidences, were also measured. To correct for coincidences with events not due to the 0.60-Mev gamma ray, the same region of the spectrum was observed in coincidence with gamma rays of energies around 0.70 Mev. The data were least-squares fitted to the function $W(\theta) = 1 + A_2P_2 (\cos \theta) + A_4P_4 (\cos \theta)$

[1]Chemistry Division.

on an IBM-704 and then corrected for the finite angular resolution of the detectors.[2]

The experimental correlation coefficients are $A_2 = -0.248 \pm 0.044$ and $A_4 = +0.251 \pm 0.070$. They are compatible only with the spin sequence $2(D + Q)2(Q)0$. The experimental value of A_2 is obtained for $\delta = (E2/M1)^{1/2} = -0.85$ and -3.4, in the notation of Biedenharn and Rose[3] (see Fig. 1).

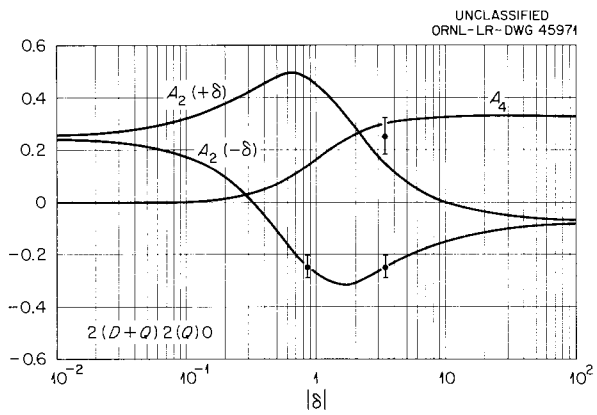

Fig. 1. Angular Correlation Coefficients as a Function of Dipole-Quadrupole Mixing for 2-2-0 Sequence.

The A_4 coefficient is in best agreement with the latter value of δ. For this value the $E2/M1$ ratio is 12^{+17}_{-7}. This predominance of $E2$ radiation for transitions between the second and first 2^+ levels is typical of even-even medium-weight nuclei and is consistent with several proposed nuclear models.[4-6] From the axially asymmetric model of Davydov and Filippov, the predicted value for the $E2/M1$ ratio is 7.6. From the present results and the Coulomb excitation data of McGowan and Stelson,[7] a value of 18×10^{-4} $(e\hbar/2mc)^2$ has been obtained for the $B(M1)$ of the upper 0.60-Mev transition.

[2] M. E. Rose, *Phys. Rev.* 91, 610 (1953).

[3] L. C. Biedenharn and M. E. Rose, *Revs. Modern Phys.* 25, 729 (1953).

[4] G. Scharff-Goldhaber and J. Weneser, *Phys. Rev.* 98, 212 (1955).

[5] B. J. Raz, *Phys. Rev.* 114, 1116 (1959).

[6] A. S. Davydov and G. F. Filippov, *Nuclear Phys.* 8, 237 (1958).

[7] F. K. McGowan and P. H. Stelson, *Bull. Am. Phys. Soc.* 4, 232 (1959).

DECAYS OF Rh^{106} AND Ag^{106}[1]

R. L. Robinson F. K. McGowan W. G. Smith[2]

The gamma-ray spectra of 30-sec Rh^{106} and 8.3-day Ag^{106}, which both decay to Pd^{106}, have been studied with scintillation spectrometers. Three gamma-gamma angular correlations have also been measured. The results are consistent with the following level scheme for Pd^{106}: $0.513(2^+)$, $1.131(2^+)$, $1.137(0^+)$, 1.360 or 1.213, $1.563(2^+)$, 1.73(2 or 3), 1.84, 1.88, $1.94(3^-$ or $4^+)$, 2.01, $2.052(4^+)$, 2.09(3), 2.28, 2.305(3 or 4), $2.352(4^+)$, 2.46, 2.62, $2.764(5^-)$, 2.87, and 3.08 Mev. The transition between the first and second 2^+ levels was found to consist primarily of $E2$ radiation. The branching ratio obtained for the cascade to crossover gamma rays from the second 2^+ level is 2.1 ± 0.3. This ratio, combined with Coulomb excitation data of Stelson and McGowan, gives a value of 1.0 ± 0.3 for the ratio $B(E2, 2' \to 2)/B(E2, 2 \to 0)$.

[1] Abstract of paper to be submitted to the *Physical Review.*

[2] Purdue University, Lafayette, Ind.

COULOMB EXCITATION OF EVEN-EVEN NUCLEI OF Ni, Zn, Ge, AND Se

P. H. Stelson F. K. McGowan

The determination by Coulomb excitation of the energy and $B(E2)_{ex}$ for the first 2^+ state of even-even nuclei has previously been reported for 29 nuclei with $40 \leq Z \leq 52$ (ref 1). An extension of the work to lighter nuclei with $28 \leq Z \leq 34$ is reported here.

Thick metallic targets of isotopically enriched material were bombarded by alpha particles with energies variable from 3 to 10 Mev. The gamma-ray yields were measured for an extended range

[1] P. H. Stelson and F. K. McGowan, *Phys. Rev.* 110, 489 (1958).

of alpha-particle energies to determine whether or not the observed variation in yield followed that expected for Coulomb excitation. In some cases the change in yield was followed for four decades. In general, the relative yield of gamma rays at different alpha-particle energies was determined to an accuracy of 2 to 3%. The results of these yield measurements are given in Table 1. The gamma-ray yields in column 3 are for the corresponding alpha-particle energies listed in column 2. The errors given are relative errors, since we are here interested in the variation of the gamma-ray yield with energy. The absolute error in the gamma-ray yields may be obtained approximately by combining the error given with an additional 4% error. The isotopic abundance of the nucleus of interest is given in column 3 of Table 2. The yields given in column 3 (Table 1) have not been converted to a 100% isotopic enrichment basis.

To obtain the reduced electric quadrupole transition probabilities, $B(E2)_{ex}$, one must convert from gamma-ray yields to the number of nuclear excitations. This is done by taking into account (1) the isotopic abundance, that is, converting to a 100% basis, (2) the total internal-conversion coefficient, and (3) the angular distribution of the gamma rays. For these light nuclei the correction for internal conversion is negligible. A discussion of the angular distribution correction has been given previously.[1] The excitations per microcoulomb (He^{++} ions) are given in column 4 of Table 1 (corrected to a 100% isotopic enrichment basis). The theoretical thick-target integral Y given has also been discussed previously.[1]

Our best values for the $B(E2)_{ex}$ are given in column 4 of Table 2. The relative error includes all the errors in N (excitations/μcoulomb) and in Y which enter into the comparison of the relative transition rates for the different nuclei. The absolute percentage error contains additional sources of error (mainly the error in the absolute stopping power) which are common to all the transitions measured. In the ratio of the observed $B(E2)_d$ to that expected for a transition between states of the single-particle model, we have taken $B(E2)_{sp}$ to be equal to $(\frac{1}{4}\pi)|\frac{3}{5}R_0^2|^2$, where $R_0 = 1.20 \times 10^{-13} A^{1/3}$ cm.

Two types of collective motion have been proposed to account for "near harmonic" spectra: the free oscillation of a nucleus about the spherical shape,[2,3] and the "γ unstable" motion.[4] From the $B(E2)_{ex}$ and the E_{2+} are obtained the parameters B_2 and C_2, which are appropriate to the description of quadrupole vibrations about the spherical shape.[3,5] The effective surface tension is represented by C_2 and the mass transported by the collective motion by B_2. Formulas (1) and (2) show the relation between these quantities:

$$C_2\,(\text{Mev}) = \frac{0.995 Z^2 E_{2+}(\text{Mev})}{[B(E2)_d/B(E2)_{sp}]}\,, \qquad (1)$$

$$\frac{B_2}{(B_2)_{irrot}} = \frac{241(Z^2/A^{5/3})}{E_{2+}(\text{Mev})\,[B(E2)_d/B(E2)_{sp}]}\,. \qquad (2)$$

The value $(B_2)_{irrot}$ is that expected for the case of irrotational flow. The values for C_2 and $B_2/(B_2)_{irrot}$ are listed in Table 2. Of the two experimental quantities, E_{2+} and $B(E2)_d$, which enter into the calculation of the parameters C_2 and $B_2/(B_2)_{irrot}$, the $B(E2)_d$ has the dominant error. Since both parameters vary inversely with $B(E2)_d$, the relative and absolute percentage errors given in Table 2 will also be approximately correct for C_2 and $B_2/(B_2)_{irrot}$.

The parameters appropriate to the "shape unstable" model are β and $B_2/(B_2)_{irrot}$, where

$$\beta = 2.91 \times 10^{26}\,\frac{[B(E2)_{ex}]^{1/2}}{ZA^{2/3}}\,. \qquad (3)$$

The values of β are listed in Table 2. Since β depends on the square root of $B(E2)_{ex}$, the percentage error in β is approximately one-half the relative and absolute percentage errors.

---

[2] G. Scharff-Goldhaber and J. Weneser, *Phys. Rev.* **98**, 212 (1955).

[3] See review article by K. Alder *et al.*, *Revs. Modern Phys.* **28**, 432 (1956).

[4] L. Wilets and M. Jeans, *Phys. Rev.* **102**, 788 (1956).

[5] G. T. Temmer and N. P. Heydenburg, *Phys. Rev.* **104**, 967 (1956).

Table 1. Information on Variation of Gamma-Ray Yields from Coulomb Excitation

Nucleus (E_γ in kev)	E_α (Mev)	Yield at $\theta = 55^\circ$ (gammas/μcoulomb)	Excitations/μcoulomb	Y (kev × mg/cm^2)	$B(E2)_{ex}$ (cm^4)
					$\times 10^{-49}$
Ni^{58} (1460)	8.013	$(9.38 \pm 0.66) \times 10^4$	$(9.18 \pm 0.64) \times 10^4$	1.93×10^3	0.77 ± 0.05
	7.012	$(2.05 \pm 0.09) \times 10^4$	$(2.01 \pm 0.09) \times 10^4$	4.64×10^2	0.70 ± 0.05
	6.020	$(2.49 \pm 0.14) \times 10^3$	$(2.43 \pm 0.14) \times 10^3$	5.96×10	0.66 ± 0.04
	5.535	$(7.00 \pm 0.52) \times 10^2$	$(6.79 \pm 0.50) \times 10^2$	1.52×10	0.72 ± 0.05
	5.036	$(1.50 \pm 0.17) \times 10^2$	$(1.45 \pm 0.16) \times 10^2$	2.51	0.93 ± 0.11
	4.532	$(3.2 \pm 1.0) \times 10$	$(3.08 \pm 1.0) \times 10$	2.08×10^{-1}	2.4 ± 0.8
Ni^{60} (1332)	8.013	$(2.18 \pm 0.09) \times 10^5$	$(2.15 \pm 0.09) \times 10^5$	3.03×10^3	1.15 ± 0.05
	7.012	$(5.03 \pm 0.22) \times 10^4$	$(4.97 \pm 0.22) \times 10^4$	8.34×10^2	0.96 ± 0.04
	6.020	$(7.92 \pm 0.33) \times 10^3$	$(7.78 \pm 0.33) \times 10^3$	1.36×10^2	0.93 ± 0.04
	5.535	$(2.20 \pm 0.09) \times 10^3$	$(2.15 \pm 0.09) \times 10^3$	3.97×10	0.88 ± 0.04
	5.036	$(4.57 \pm 0.24) \times 10^2$	$(4.46 \pm 0.24) \times 10^2$	8.20	0.88 ± 0.05
	4.532	$(4.4 \pm 0.9) \times 10$	$(4.2 \pm 0.9) \times 10$	0.98	0.70 ± 0.15
Ni^{62} (1171)	8.013	$(2.56 \pm 0.14) \times 10^5$	$(2.57 \pm 0.14) \times 10^5$	5.19×10^3	0.80 ± 0.04
	7.012	$(8.60 \pm 0.42) \times 10^4$	$(8.65 \pm 0.41) \times 10^4$	1.67×10^3	0.84 ± 0.04
	6.020	$(1.77 \pm 0.07) \times 10^4$	$(1.77 \pm 0.07) \times 10^4$	3.44×10^2	0.83 ± 0.03
	5.535	$(6.14 \pm 0.27) \times 10^3$	$(6.10 \pm 0.27) \times 10^3$	1.23×10^2	0.80 ± 0.04
	5.036	$(1.70 \pm 0.06) \times 10^3$	$(1.69 \pm 0.06) \times 10^3$	3.15×10	0.87 ± 0.04
	4.532	$(2.83 \pm 0.14) \times 10^2$	$(2.79 \pm 0.14) \times 10^2$	5.31	0.85 ± 0.04
	4.030	$(3.9 \pm 1.4) \times 10$	$(3.9 \pm 1.4) \times 10$	0.46	1.3 ± 0.5
Zn^{64} (995)	8.013	$(5.94 \pm 0.21) \times 10^5$	$(6.53 \pm 0.23) \times 10^5$	7.83×10^3	1.73 ± 0.06
	7.012	$(2.15 \pm 0.08) \times 10^5$	$(2.35 \pm 0.09) \times 10^5$	2.83×10^3	1.72 ± 0.07
	6.020	$(5.00 \pm 0.18) \times 10^4$	$(5.48 \pm 0.20) \times 10^4$	6.91×10^2	1.65 ± 0.06
	4.532	$(1.32 \pm 0.14) \times 10^3$	$(1.43 \pm 0.14) \times 10^3$	1.83×10	1.61 ± 0.16
Zn^{66} (1040)	8.013	$(5.77 \pm 0.18) \times 10^5$	$(5.81 \pm 0.18) \times 10^5$	6.89×10^3	1.74 ± 0.05
	7.012	$(1.80 \pm 0.05) \times 10^5$	$(1.80 \pm 0.05) \times 10^5$	2.37×10^3	1.57 ± 0.04
	6.020	$(3.88 \pm 0.12) \times 10^4$	$(3.90 \pm 0.12) \times 10^4$	5.43×10^2	1.49 ± 0.05
	5.535	$(1.39 \pm 0.05) \times 10^4$	$(1.39 \pm 0.05) \times 10^4$	2.08×10^2	1.39 ± 0.05
	5.036	$(4.28 \pm 0.14) \times 10^3$	$(4.26 \pm 0.14) \times 10^3$	6.02×10	1.47 ± 0.05
	4.532	$(7.86 \pm 0.44) \times 10^2$	$(7.79 \pm 0.44) \times 10^2$	1.20×10	1.34 ± 0.08
	4.030	$(7.06 \pm 0.84) \times 10$	$(6.96 \pm 0.84) \times 10$	1.33	1.08 ± 0.13
Zn^{68} (1078)	8.013	$(3.68 \pm 0.12) \times 10^5$	$(3.74 \pm 0.12) \times 10^5$	6.08×10^3	1.27 ± 0.04
	7.012	$(1.23 \pm 0.04) \times 10^5$	$(1.24 \pm 0.04) \times 10^5$	2.02×10^3	1.27 ± 0.04
	6.020	$(2.76 \pm 0.09) \times 10^4$	$(2.79 \pm 0.09) \times 10^4$	4.42×10^2	1.31 ± 0.04
	5.535	$(9.30 \pm 0.30) \times 10^3$	$(9.37 \pm 0.30) \times 10^3$	1.64×10^2	1.19 ± 0.04
	5.036	$(2.79 \pm 0.09) \times 10^3$	$(2.80 \pm 0.09) \times 10^3$	4.53×10	1.28 ± 0.04
	4.532	$(4.88 \pm 0.25) \times 10^2$	$(4.88 \pm 0.25) \times 10^2$	8.40	1.20 ± 0.06
	4.030	$(5.49 \pm 0.66) \times 10$	$(5.45 \pm 0.66) \times 10$	0.84	1.34 ± 0.16
Zn^{70} (887)	8.013	$(5.09 \pm 0.25) \times 10^5$	$(8.48 \pm 0.42) \times 10^5$	1.11×10^4	1.58 ± 0.05
	7.012	$(2.13 \pm 0.07) \times 10^5$	$(3.52 \pm 0.12) \times 10^5$	4.45×10^3	1.63 ± 0.06
	6.020	$(6.04 \pm 0.23) \times 10^4$	$(1.00 \pm 0.04) \times 10^5$	1.33×10^3	1.55 ± 0.06
	5.535	$(2.58 \pm 0.09) \times 10^4$	$(4.27 \pm 0.15) \times 10^4$	5.62×10^2	1.57 ± 0.05
	5.036	$(9.58 \pm 0.41) \times 10^3$	$(1.58 \pm 0.07) \times 10^4$	2.01×10^2	1.63 ± 0.07
	4.532	$(2.53 \pm 0.13) \times 10^3$	$(4.15 \pm 0.21) \times 10^3$	5.23×10	1.64 ± 0.08
	4.030	$(5.01 \pm 0.50) \times 10^2$	$(8.21 \pm 0.82) \times 10^2$	8.91	1.91 ± 0.19

Table 1 (continued)

Nucleus (E_γ in kev)	E_α (Mev)	Yield at $\theta = 55°$ (gammas/μcoulomb)	Excitations/μcoulomb	Y (kev × mg/cm^2)	$B(E2)_{ex}$ (cm^4)
					$\times 10^{-49}$
Ge^{72} (834)	8.013	$(8.90 \pm 0.30) \times 10^5$	$(9.75 \pm 0.34) \times 10^5$	1.19×10^4	2.14 ± 0.08
	7.012	$(3.47 \pm 0.11) \times 10^5$	$(3.78 \pm 0.12) \times 10^5$	4.18×10^3	2.36 ± 0.08
	6.020	$(1.11 \pm 0.03) \times 10^5$	$(1.21 \pm 0.03) \times 10^5$	1.38×10^3	2.29 ± 0.06
	5.535	$(4.91 \pm 0.17) \times 10^4$	$(5.35 \pm 0.19) \times 10^4$	6.20×10^2	2.25 ± 0.08
	5.036	$(1.82 \pm 0.06) \times 10^4$	$(1.98 \pm 0.07) \times 10^4$	2.24×10^2	2.31 ± 0.08
	4.532	$(5.47 \pm 0.39) \times 10^3$	$(5.91 \pm 0.44) \times 10^3$	6.00×10	2.57 ± 0.19
Ge^{74} (600)	9.965	$(7.09 \pm 0.21) \times 10^6$	$(7.26 \pm 0.21) \times 10^6$	6.43×10^4	2.95 ± 0.09
	8.996	$(4.73 \pm 0.11) \times 10^6$	$(4.84 \pm 0.11) \times 10^6$	4.12×10^4	3.07 ± 0.07
	8.013	$(2.87 \pm 0.07) \times 10^6$	$(2.92 \pm 0.07) \times 10^6$	2.39×10^4	3.19 ± 0.08
	7.012	$(1.39 \pm 0.03) \times 10^6$	$(1.41 \pm 0.03) \times 10^6$	1.18×10^4	3.12 ± 0.07
	6.020	$(5.52 \pm 0.14) \times 10^5$	$(5.56 \pm 0.14) \times 10^5$	4.61×10^3	3.15 ± 0.08
	5.535	$(3.01 \pm 0.07) \times 10^5$	$(3.04 \pm 0.07) \times 10^5$	2.57×10^3	3.09 ± 0.07
	5.036	$(1.48 \pm 0.03) \times 10^5$	$(1.49 \pm 0.03) \times 10^5$	1.22×10^3	3.19 ± 0.07
	4.532	$(5.95 \pm 0.15) \times 10^4$	$(5.99 \pm 0.15) \times 10^4$	4.79×10^2	3.26 ± 0.08
	4.030	$(1.68 \pm 0.04) \times 10^4$	$(1.68 \pm 0.04) \times 10^4$	1.43×10^2	3.07 ± 0.07
	3.522	$(3.62 \pm 0.17) \times 10^3$	$(3.60 \pm 0.17) \times 10^3$	2.64×10	3.56 ± 0.17
	3.022	$(3.84 \pm 0.74) \times 10^2$	$(3.80 \pm 0.73) \times 10^2$	2.63	3.77 ± 0.70
Ge^{76} (567)	9.965	$(5.63 \pm 0.18) \times 10^6$	$(5.71 \pm 0.18) \times 10^6$	6.86×10^4	2.17 ± 0.07
	8.996	$(3.93 \pm 0.09) \times 10^6$	$(3.99 \pm 0.09) \times 10^6$	4.45×10^4	2.34 ± 0.05
	8.013	$(2.53 \pm 0.06) \times 10^6$	$(2.56 \pm 0.06) \times 10^6$	2.63×10^4	2.54 ± 0.06
	7.012	$(1.32 \pm 0.03) \times 10^6$	$(1.33 \pm 0.03) \times 10^6$	1.33×10^4	2.61 ± 0.06
	6.020	$(5.54 \pm 0.13) \times 10^5$	$(5.57 \pm 0.13) \times 10^5$	5.32×10^3	2.73 ± 0.06
	5.535	$(3.06 \pm 0.07) \times 10^5$	$(3.07 \pm 0.07) \times 10^5$	3.10×10^3	2.58 ± 0.06
	5.036	$(1.58 \pm 0.04) \times 10^5$	$(1.58 \pm 0.04) \times 10^5$	1.53×10^3	2.69 ± 0.07
	4.532	$(6.53 \pm 0.15) \times 10^4$	$(6.52 \pm 0.15) \times 10^4$	6.31×10^2	2.70 ± 0.06
	4.030	$(2.02 \pm 0.06) \times 10^4$	$(2.01 \pm 0.06) \times 10^4$	2.00×10^2	2.62 ± 0.08
	3.522	$(4.16 \pm 0.12) \times 10^3$	$(4.12 \pm 0.12) \times 10^3$	4.10×10	2.62 ± 0.08
	3.022	$(5.07 \pm 0.84) \times 10^2$	$(4.98 \pm 0.84) \times 10^2$	4.46	2.91 ± 0.49
Se^{76} (560)	8.008	$(3.35 \pm 0.06) \times 10^6$	$(3.79 \pm 0.07) \times 10^6$	2.53×10^4	4.80 ± 0.09
	7.040	$(1.72 \pm 0.04) \times 10^6$	$(1.93 \pm 0.04) \times 10^6$	1.30×10^4	4.75 ± 0.09
	6.041	$(7.02 \pm 0.14) \times 10^5$	$(7.88 \pm 0.16) \times 10^5$	5.23×10^3	4.81 ± 0.09
	5.035	$(1.90 \pm 0.04) \times 10^5$	$(2.12 \pm 0.04) \times 10^5$	1.41×10^3	4.82 ± 0.09
Se^{78} (612)	8.008	$(2.39 \pm 0.05) \times 10^6$	$(2.65 \pm 0.06) \times 10^6$	2.18×10^4	3.88 ± 0.08
	7.040	$(1.12 \pm 0.02) \times 10^6$	$(1.23 \pm 0.02) \times 10^6$	1.075×10^4	3.66 ± 0.08
	6.041	$(4.50 \pm 0.09) \times 10^5$	$(4.93 \pm 0.10) \times 10^5$	4.07×10^3	3.87 ± 0.08
	5.035	$(1.12 \pm 0.02) \times 10^5$	$(1.23 \pm 0.02) \times 10^5$	9.94×10^2	3.96 ± 0.08
Se^{80} (665)	8.008	$(1.63 \pm 0.03) \times 10^6$	$(1.65 \pm 0.03) \times 10^6$	1.86×10^4	2.84 ± 0.06
	7.040	$(7.53 \pm 0.15) \times 10^5$	$(7.60 \pm 0.15) \times 10^5$	8.80×10^3	2.76 ± 0.06
	6.041	$(2.73 \pm 0.06) \times 10^5$	$(2.74 \pm 0.06) \times 10^5$	3.11×10^3	2.82 ± 0.06
	5.035	$(6.30 \pm 0.20) \times 10^4$	$(6.30 \pm 0.20) \times 10^4$	6.69×10^2	3.01 ± 0.09
Se^{82} (654)	8.008	$(6.20 \pm 0.25) \times 10^5$	$(1.19 \pm 0.05) \times 10^6$	1.91×10^4	2.00 ± 0.08
	7.040	$(3.21 \pm 0.13) \times 10^5$	$(6.18 \pm 0.25) \times 10^5$	9.20×10^3	2.14 ± 0.08
	6.041	$(1.18 \pm 0.06) \times 10^5$	$(2.26 \pm 0.11) \times 10^5$	3.28×10^3	2.20 ± 0.10
	5.035	$(2.67 \pm 0.13) \times 10^4$	$(5.12 \pm 0.26) \times 10^4$	7.26×10^2	2.26 ± 0.11

Table 2. Summary of Information Obtained from Coulomb Excitation

Nucleus	E_γ (kev)	Isotopic Abundance (%)	$B(E2)_{ex}$ (cm^4)	Relative Error (%)	Absolute Error (%)	$\frac{B(E2)_d}{B(E2)_{sp}}$	$T_{1/2}$ (sec)	β	C_2 (Mev)	$\frac{B_2}{(B_2)_{irrot}}$
			$\times 10^{-49}$							
Ni^{58}	1460 ± 20	99.6 ± 1.0	0.72	±6	±10	11	5.9×10^{-13}	0.187	105	13.6
Ni^{60}	1332 ± 15	99.1 ± 0.1	0.91	±5	±9	13	7.4×10^{-13}	0.204	80	11.8
Ni^{62}	1171 ± 12	97.8 ± 0.1	0.83	±5	±9	11	1.7×10^{-12}	0.190	80	14.4
Zn^{64}	995 ± 10	89.6 ± 0.1	1.70	±5	±9	22	1.7×10^{-12}	0.252	40	9.6
Zn^{66}	1040 ± 10	97.8 ± 0.05	1.45	±5	±9	18	1.6×10^{-12}	0.227	51	10.5
Zn^{68}	1078 ± 10	96.8 ± 0.1	1.25	±5	±9	15	1.55×10^{-12}	0.206	69	11.8
Zn^{70}	887 ± 9	59.3 ± 0.5	1.60	±5	±9	19	3.2×10^{-12}	0.228	42	11.0
Ge^{72}	834 ± 8	89.2 ± 1.0	2.30	±4	±8	26	3.05×10^{-12}	0.252	33	9.2
Ge^{74}	600 ± 6	97.7 ± 0.1	3.17	±4	±8	34	1.15×10^{-12}	0.292	18	9.2
Ge^{76}	576 ± 6	98.6 ± 0.1	2.63	±4	±8	27	1.83×10^{-12}	0.260	21	11.7
Se^{76}	560 ± 5	88.51 ± 0.04	4.80	±5	±9	51	1.07×10^{-11}	0.328	13	7.3
Se^{78}	612 ± 6	90.24 ± 0.03	3.85	±5	±9	39	8.6×10^{-12}	0.291	18	8.2
Se^{80}	665 ± 7	98.39 ± 0.04	2.83	±5	±9	27	7.7×10^{-12}	0.245	28	10.2
Se^{82}	654 ± 8	51.6 ± 0.5	2.13	±5	±9	20	1.12×10^{-11}	0.210	41	13.6

DECAY OF I^{132}

R. L. Robinson E. Eichler[1] N. R. Johnson[1]

The ground-state spin of I^{132} has recently been measured as 4 by Sherwood, Ovenshine, and Parker.[2] With this new information it seemed probable that the spins of some of the Xe^{132} higher-energy levels could be determined through additional studies of the decay of I^{132}. This has led us to examine the gamma-ray spectrum of I^{132} by means of scintillation spectrometers and to measure several gamma-gamma angular correlations.

The 2.3-hr I^{132} was obtained in an equilibrium condition with 77-hr Te^{132} from the Brookhaven National Laboratory. The I^{132} was separated from the equilibrium sample and then chemically purified. The singles spectrum, which was observed for a source-to-detector distance of 9.3 cm, is given in Fig. 1. The spectra in coincidence with the 0.515-, 0.667-, 0.775-, 0.953-, 1.142-, and 1.392-Mev gamma rays were also studied. The

[1] Chemistry Division.

[2] J. E. Sherwood, S. J. Ovenshine, and G. W. Parker, *Bull. Am. Phys. Soc.* 4, 386 (1959). More recently this spin value was also obtained by E. Lipworth, H. L. Garvin, and W. A. Nierenberg, *Bull. Am. Phys. Soc.* 4, 353 (1959).

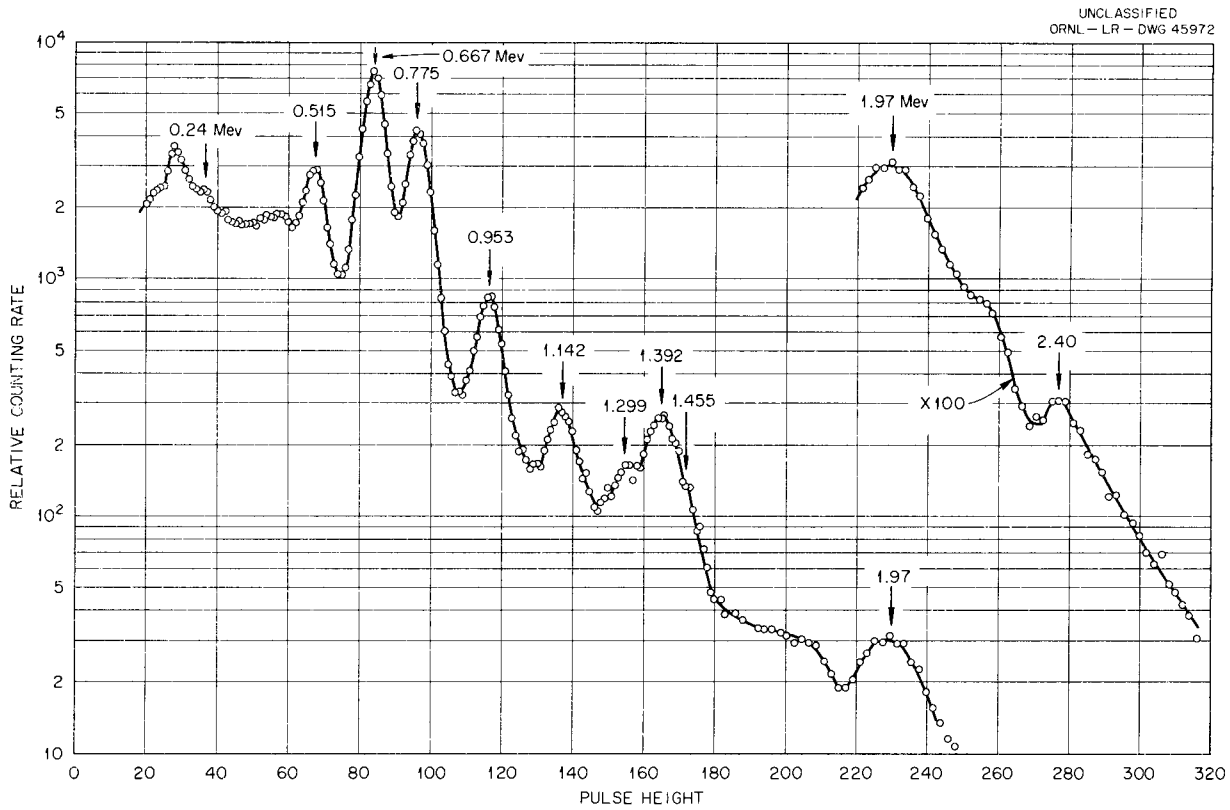

Fig. 1. Gamma-Ray Spectrum of I^{132}.

coincident spectra, besides revealing new gamma rays with energies of 0.75 and 1.75 Mev, indicate that the 0.667-Mev peak in the singles spectrum is composed of two gamma rays with energies of 0.673 and ~0.64 Mev. The intensities of the gamma rays in all spectra were determined in the same manner as described in a previous report.[3] A tentative decay scheme which is consistent with most of our results is given in Fig. 2. This decay scheme is similar to that proposed by Finston and Bernstein.[4]

From the comparative half life given by Finston and Bernstein[4] for the beta-ray group to the 1.448-Mev level (log $ft = 7.5$) and the spin of I^{132} (ref 2), the spin of the 1.448-Mev level is expected to be 3, 4, or 5. From the observed systematic properties of even-even nuclei in this region, spin 4 is the most probable of these three spins. If spin 4 is taken for the 1.448-Mev level, the angular correlation function obtained for the 0.64-0.673-Mev, 1-3 gamma-ray cascade is in best agreement with an assignment of spin 4 for the 2.10-Mev level. The angular correlation functions of the 0.953-0.775-Mev cascade and the 0.953-0.673-Mev, 1-3 cascade are consistent with a spin assignment of 3, 4, or 5 for the 2.40-Mev level. The presence of a ground-state transition from this level makes spin 4 or 5 unlikely. The angular correlation functions for the 1.392-0.775-Mev cascade and the 1.392-0.673-Mev, 1-3 cascade suggest that the 2.84-Mev level has spin 3 or 5.

[3] R. L. Robinson, F. K. McGowan, and W. G. Smith, *Phys. Ann. Prog. Rep. Mar. 10, 1959*, ORNL-2718, p 8.

[4] H. L. Finston and W. Bernstein, *Phys. Rev.* **96**, 71 (1954).

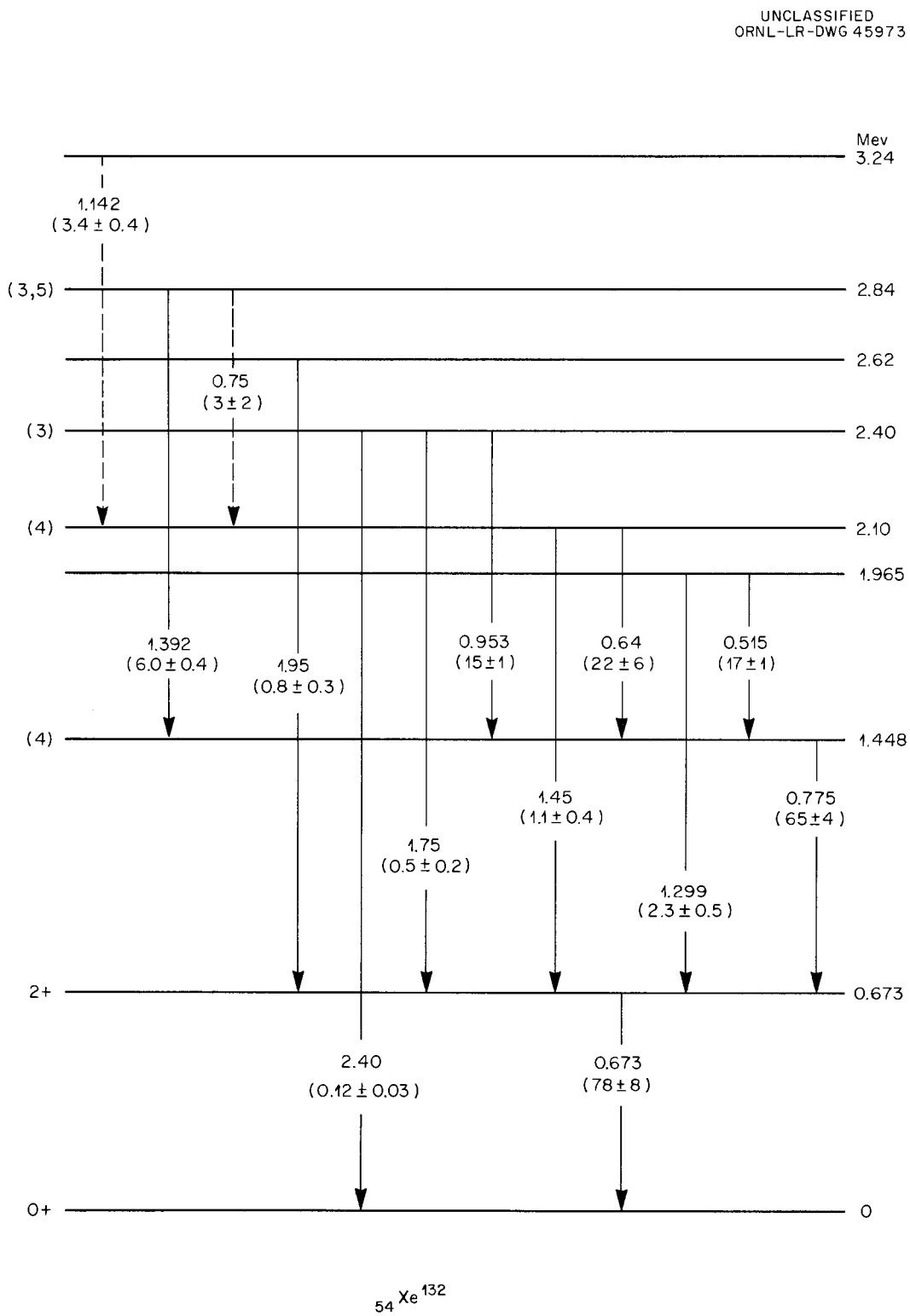

Fig. 2. Proposed Transitions and Energy Levels in Xe^{132} Which Occur in the Decay of I^{132}. The pair of numbers associated with each transition gives its energy in Mev and relative intensity.

DECAY OF $Rh^{102} \longrightarrow Ru^{102}$

F. K. McGowan P. H. Stelson W. G. Smith[1]

The previously reported[2] measurements of the weak Coulomb excitation of the second 2^+ state in medium-weight even-even nuclei have provided information on the $B(E2)$ for decay of the second 2^+ state. For many of these nuclei the ratio of cascade to crossover transitions from the second 2^+ state is not known. This ratio is needed to determine the $B(E2)_d$ for the cascade and the crossover transitions. Values for $B(E2,\ 2 \rightarrow 2)/B(E2,\ 2 \rightarrow 0)$ provide a valuable test of the various models.[3-5] Therefore it is important to have more information on nuclei in the medium-weight region in order to determine the extent and degree of the applicability of the models. A knowledge of the branching ratio of cascade to crossover from the second 2^+ state and of the $E2/M1$ ratio for the upper cascade transition would be very desirable for the medium-weight nuclei in which the second 2^+ state has been observed in Coulomb excitation. We wish to report some information obtained from the decay of $Rh^{102} \rightarrow Ru^{102}$.

The ground state of Rh^{102} is known to decay by β^- to the ground state of Pd^{102} and by β^+ and electron capture to the ground state and excited states of Ru^{102}. From measurements by other workers, the branching ratio of cascade to crossover from the second 2^+ state at 1105 kev ranges from 10 to 100 (ref 6). This value appears to be unreasonably large compared with branching ratios for similar transitions of other medium-weight nuclei.

Rhodium-102 was produced with the ORNL cyclotron by the (p,n) reaction on a 50-mg sample of ruthenium containing 97.2% Ru^{102}. The beam energy was degraded to enhance the yield of Rh^{102} relative to Rh^{101} from the $Ru^{102}(p,2n)Rh^{101}$ reaction. Sources of Rh^{102} were prepared from a chemical separation of the rhodium from the ruthenium. The gamma rays from the decay of Rh^{102} were detected with a 3 × 3 in. NaI scintillation spectrometer. Pulse-height spectra were measured with a 120-channel analyzer of Bell-Kelley design[7] and an RCL 256-channel analyzer. For the coincident spectra and the angular correlation measurements, two 3 × 3 in. NaI scintillation spectrometers were used. The singles gamma-ray spectrum of Rh^{102} is shown in Figs. 1 and 2. The results from an analysis of this spectrum are given in Table 1. The intensity of the annihilation radiation was obtained from measurements of the coincident spectrum of the annihilation gamma rays from the Rh^{102} source and an Na^{22} source.

The directional angular correlations of several gamma-ray cascades were measured. Representative coincident spectra taken at $\theta = 90°$ are shown in Figs. 3–8. A least-squares analysis

[1]Summer research participant from Purdue University, Lafayette, Ind.

[2]P. H. Stelson and F. K. McGowan, *Bull. Am. Phys. Soc.* **2**, 267 (1957); **4**, 232 (1959).

[3]G. Scharff-Goldhaber and J. Weneser, *Phys. Rev.* **98**, 212 (1955).

[4]A. S. Davydov and G. F. Fillippov, *Nuclear Phys.* **8**, 237 (1958).

[5]B. J. Raz, *Phys. Rev.* **114**, 1116 (1959).

[6]See for instance, K. Way *et al.* (eds.), *Nuclear Data Sheets*, p NRC 58-10-50 Rh^{102}-1, 2, National Academy of Sciences – National Research Council, Washington, D.C., 1958.

[7]G. G. Kelly, P. R. Bell, and C. C. Harris, *Phys. Semiann. Prog. Rep. Sept. 10, 1953*, ORNL-1620, p 50; *Sept. 10, 1955*, ORNL-1975, p 99.

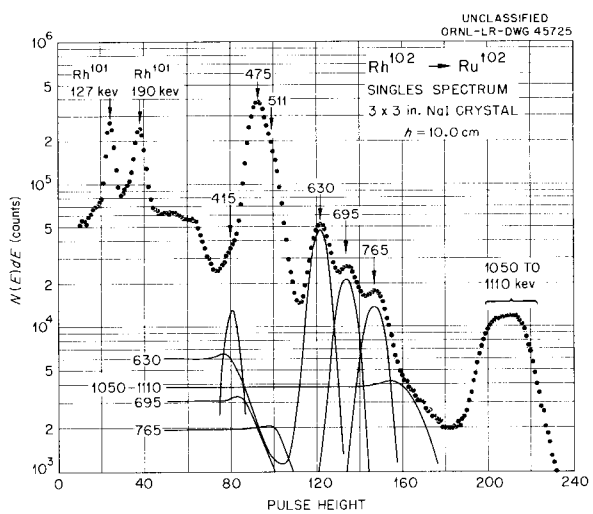

Fig. 1. Pulse-Height Spectrum of the Gamma Rays (Low Energy) from Rh^{102}.

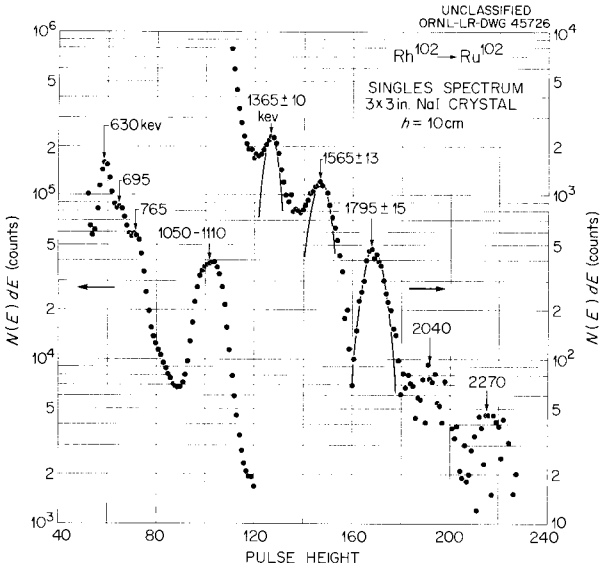

Fig. 2. Pulse-Height Spectrum of the Gamma Rays (High Energy) from Rh^{102}.

Table 1. Relative Intensities of Gamma Rays from Rh^{102}

E_γ (kev)	Relative Intensity
415 ± 5	2.6 ± 0.3
475 ± 5	100
630 ± 6	17.4 ± 1
695 ± 7	9.4 ± 0.6
765 ± 8	6.9 ± 0.4
1050 to 1110	18.0 ± 1.1
1365 ± 10	0.67 ± 0.07
1565 ± 13	0.27 ± 0.04
1795 ± 15	0.07 ± 0.02
2040 ± 14	0.06 ± 0.01
511	31.6 ± 1.9

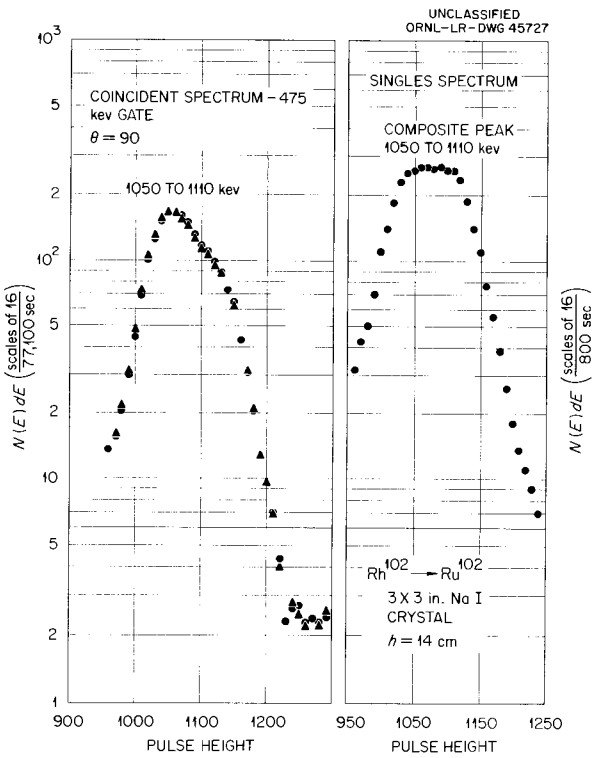

Fig. 3. Pulse-Height Spectrum of the Gamma Rays from Rh^{102} with a 50-kev Gate at 475 kev.

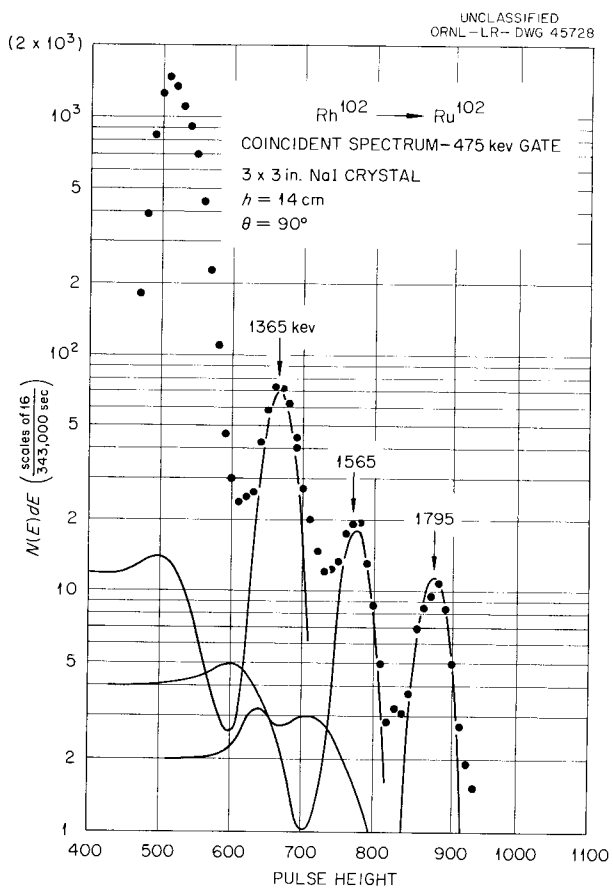

Fig. 4. Pulse-Height Spectrum of the Gamma Rays from Rh^{102} with a 50-kev Gate at 475 kev.

of the data from the angular correlation measurements in terms of a series of Legendre polynomials,

$$W(\theta) = A_0 + A_2 P_2(\cos\theta) + A_4 P_4(\cos\theta) \ ,$$

was carried out on an IBM-704. In Table 2 are listed the angular distribution coefficients which have been corrected for finite angular resolution. The spin assignments, which fit the angular correlation data, are listed in column 4; δ is defined

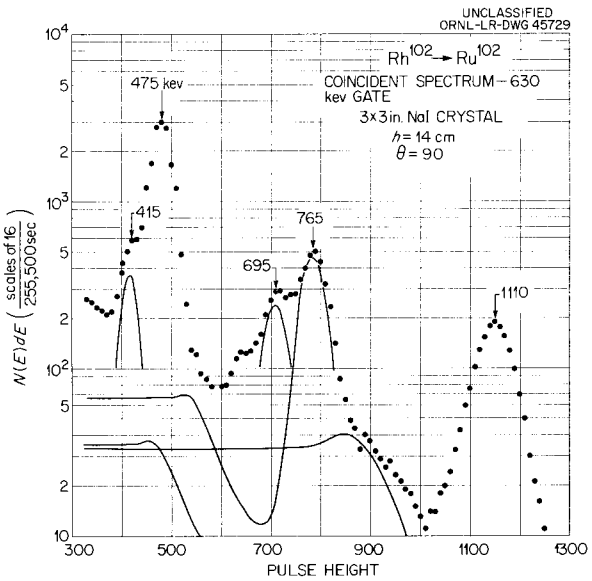

Fig. 5. Pulse-Height Spectrum of the Gamma Rays from Rh^{102} with a 50-kev Gate at 630 kev.

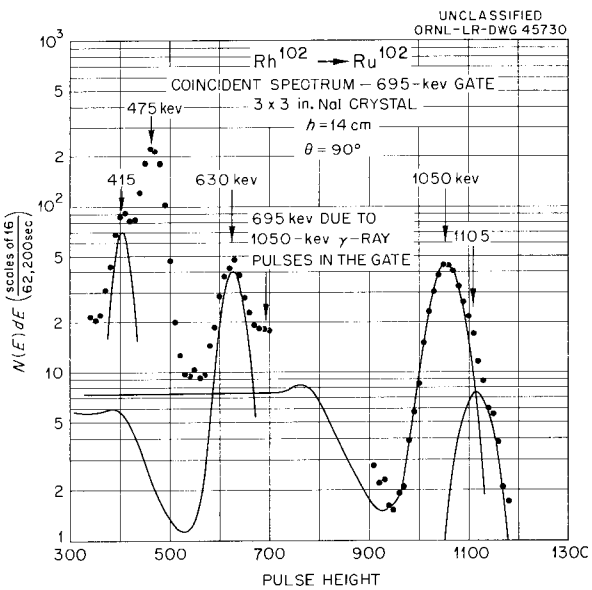

Fig. 6. Pulse-Height Spectrum of the Gamma Rays from Rh^{102} with a 30-kev Gate at 695 kev.

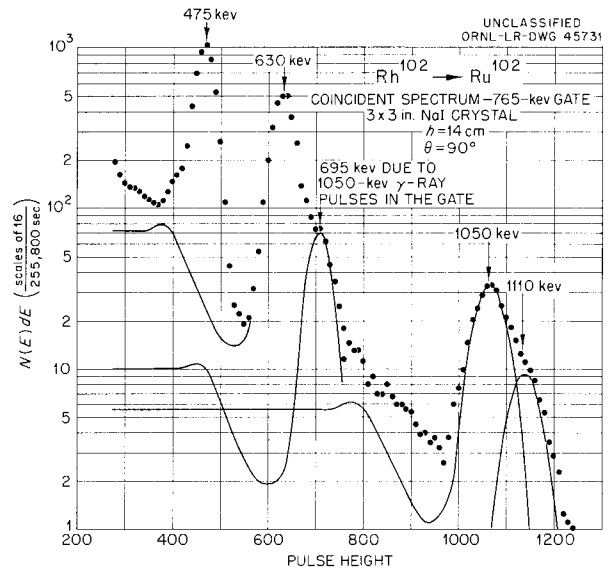

Fig. 7. Pulse-Height Spectrum of the Gamma Rays from Rh^{102} with a 50-kev Gate at 765 kev.

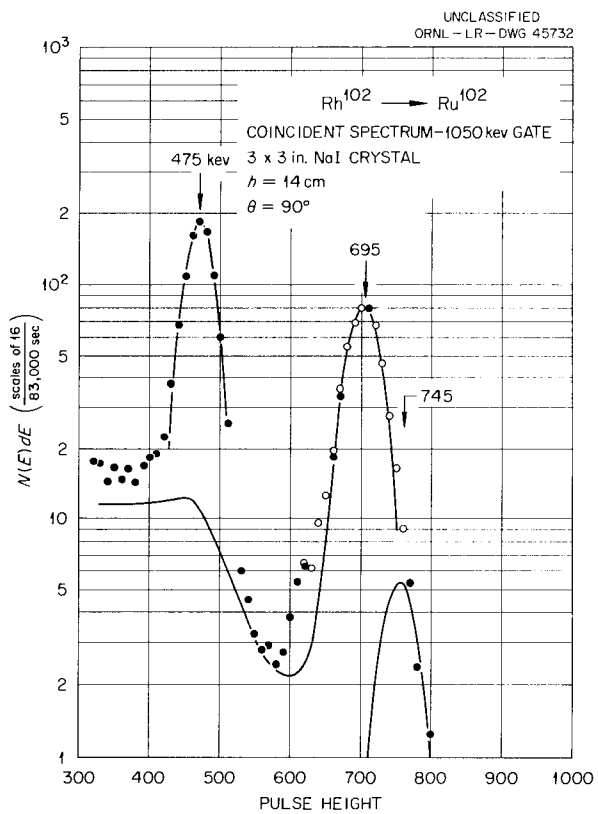

Fig. 8. Pulse-Height Spectrum of the Gamma Rays from Rh^{102} with a 50-kev Gate at 1050 kev.

as $(Q/D)^{1/2}$ in the notation of Biedenharn and Rose.[8]

The coincident spectra were, also, analyzed to obtain the absolute intensities of the gamma rays. These intensities are given in Table 3, together with the intensities obtained from the singles spectrum. A level scheme for Ru^{102} based on the study of the singles and coincident gamma-ray intensities and the angular correlation results is given in Fig. 9. The number in parentheses accompanying the energy of the transition is the relative intensity of the gamma ray. The 2^+ state at 1105 kev has been previously observed in Coulomb excitation.[2] It is not possible to fit the 630-475 and the 1110-630 angular correlation data and the gamma-ray yields from the coincident measurements with a single state at 1105 kev. As a result, to account for the data, we have placed a 4^+ state coincident to within ±8 kev with the second 2^+ state at 1105 kev. The value of $E2/M1$ for the 630-kev transition ($2^+ \rightarrow 2^+$), deduced from the composite correlation of the 630-475 cascades, is greater than or equal to 225. The branching ratio of cascade to crossover from the second 2^+ state is 1.5 ± 0.3, which was obtained from the gamma-ray intensities with the 695-kev gate.

With a knowledge of the gamma intensities into and out of each state in Ru^{102}, it is possible to obtain the relative intensities of the beta decay groups from Rh^{102}. The log (ft) values for the beta decay groups are listed in Table 4. The relative intensity of the β^- decay group was taken from measurements of other workers[6] because we

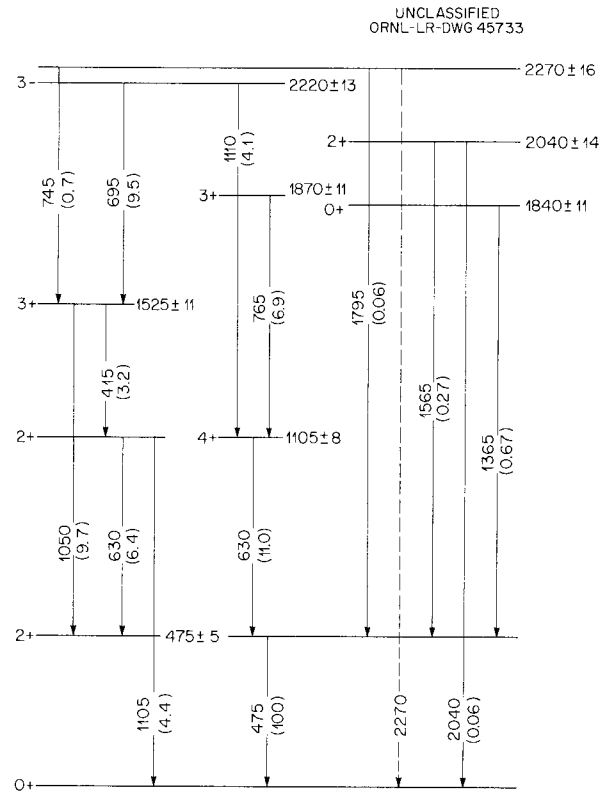

Fig. 9. Transitions and Energy Levels in Ru^{102} Which Occur in the Decay of Rh^{102}. Energies of the transitions are in kev.

did not measure this group. The log (ft) values for the ground-state groups to Pd^{102} and Ru^{102} are characteristic of first-forbidden unique transitions ($\Delta I = 2$, yes). The relative parities of the states in Ru^{102} are based on a 2^- assignment to Rh^{102}. The states at 1840 and 2040 kev could be populated by gamma transitions from the 2220-kev state rather than by direct beta decay from Rh^{102}. The energy of the state at 2270 kev is, within the experimental error, equal to the total decay energy of Rh^{102}.

[8] L. C. Biedenharn and M. E. Rose, *Revs. Modern Phys.* 25, 729 (1953).

Table 2. Angular Distribution Coefficients of the Terms in the Correlation Function Expressed in Legendre Polynomials

Cascade (E in kev)	A_2	A_4	Decay Sequence	δ_1	δ_2
1365-475	0.29 ± 0.04	1.00 ± 0.13	$0(E2)2(E2)0$		
1565-475	$-(0.20 \pm 0.02)$	0.30 ± 0.03	$2(Q+D)2(E2)0$	2.8 ± 0.2	
1050, 1110 -475	$-(0.26 \pm 0.02)$	$-(0.003 \pm 0.03)$	$3(Q+D)2(E2)0$ $3(Q+D)4(E2)2(E2)0$	2.6×10^{-1} $-(2.4 \times 10^{-1})$	
630-475	0.043 ± 0.005	0.146 ± 0.010	$4(Q)2(E2)0$ $2(Q+D)2(E2)0$	≥ 15	
765-630	0.107 ± 0.010	$-(0.010 \pm 0.018)$	$3(Q+D)4(E2)2$	3.1×10^{-1}	
765-630	0.113 ± 0.011	0.007 ± 0.017	$3(Q+D)4(E2)2$	3.1×10^{-1}	
765-475	0.08 ± 0.02 0.14 ± 0.03	0.02 ± 0.03 0.02 ± 0.04	$3(Q+D)4(E2)2(E2)0$	3.1×10^{-1}	
1050-475	$-(0.274 \pm 0.015)$	0.019 ± 0.024	$3(Q+D)2(E2)0$	$(2.6 \pm 0.15) \times 10^{-1}$	
695-1050	$-(0.048 \pm 0.010)$	$-(0.003 \pm 0.02)$	$3(Q+D)3(Q+D)2$	$-(3.8 \times 10^{-1})$	$-(2.6 \times 10^{-1})$
1110-630	$-(0.32 \pm 0.02)$	$-(0.03 \pm 0.03)$	$3(Q+D)4(E2)2$	$-(2.4 \times 10^{-1})$	

Table 3. Intensities of Gamma Rays (gammas/sec) from Rh^{102} in the Singles and Coincident Spectro

		Gating Gamma Ray					
E_γ (kev)	Singles	475	630	695	765	1050	1050–1110
	$\times 10^3$	$\times 10^3$	$\times 10^3$	$\times 10^3$	$\times 10^3$	$\times 10^3$	$\times 10^3$
415 ± 5	2.8		2.3	3.2			0.7
475 ± 5	107		21.1	10.5	8.7	10.4	14.7
630 ± 6	18.6			2.26	7.7		4.6
695 ± 7	10.2		2.5			9.1	10.2
745 ± 8						0.7	0.8
765 ± 8	7.4		7.5				
1050 ± 10				8.5	1.1		
1105 ± 8				1.57	0.35		0.27
1110 ± 11			4.4				
1050 to 1110	19.3	14.6					
1365 ± 10	0.72	0.62					
1565 ± 13	0.29	0.22					
1795 ± 15	0.07	0.06					
2040 ± 14	0.06						

Table 4. Log (ft) Values for the Beta Decay Groups from Rh^{102}

Nucleus	Level Position	Type of Decay	Relative Intensity (%)	Log (ft)	(W_0^2-1) log (ft)
Pd^{102}	Ground state	β^-	16.4	9.64	10.6
Ru^{102}	Ground state	β^+	6.6	9.11	10.2
	Ground state	Electron capture	11.7	9.02	
	475 (2^+)	β^+	3.3	8.54	
	475 (2^+)	Electron capture	41.8	8.27	
	1105 (2^+)	Electron capture	4.5	8.85	
	1525 (3^+)	Electron capture	1.6	8.90	
	1840 (0^+)	Electron capture	0.4	9.0	
	1870 (3^+)	Electron capture	4.3	7.92	
	2040 (2^+)	Electron capture	0.18	8.7	
	2220 (3^-)	Electron capture	8.6	5.42	
	2270	Electron capture	0.5		

EVIDENCE FOR NEW ISOMERIC STATES[1]

E. C. Campbell P. F. Fettweis[2]

By means of a fast pneumatic transfer tube installed in the Belgian reactor BR1, at Mol, samples irradiated in a flux of 10^{12} neutrons·cm^{-2}·sec^{-1} could be examined within 0.1 sec by a shielded 2 × 2 in. NaI pulse-height spectrometer. Decay measurements were made with a set of ten electronically switched fast scalers. Two previously unreported isomeric states were found and identified as Ga^{72m} (0.040 ± 0.002 sec, ~90 kev) and Ba^{135m} (0.33 ± 0.03 sec, ~700 and ~800 kev). Measurement of the decay of Na^{24m} produced in the reaction $Na^{23}(n,\gamma)Na^{24m}$ gave 0.020 ± 0.002 sec for the half life. Irradiation of separated isotopes permitted the identification of short-period isomeric states in In, Hf, Ir, and Yb.

[1]Abstract of published paper: *Nuclear Phys.* 13, 92 (1959).

[2]Centre d'Etude de l'Energie Nucléaire, Mol, Belgium.

THE REACTION $C^{14}(p,n)N^{14}$[1]

J. K. Bair R. D. Edge[2] H. B. Willard

The yield of neutrons from the proton bombardment of C^{14} has been extended to 5 Mev with good resolution using targets of high isotopic enrichment. Measurements were made at three angles with the long counter and at one angle with a proton recoil counter. The region of the thresholds for the second and third neutron groups was investigated with a lithium iodide detector. The very narrow level at 13.15-Mev excitation did not appear, but the 6-kev wide level just above threshold was observed, and a level (13.36 Mev) was resolved on the low-energy side of the previously observed level at E_p = 3.41 Mev. In the previously

[1]Abstract of paper to be published in the *Physical Review.*

[2]Summer research participant from the University of South Carolina, Columbia.

unobserved region above E_p = 3.41 Mev, anomalies were found in the excitation curves at E_p = 3.63 mev (Γ = 13 kev); 3.89 Mev (Γ = 35 kev); 4.19 Mev (Γ = 112 kev); 4.24 Mev (Γ = 27 kev); 4.60 Mev (Γ = 140 kev); and 4.93 Mev (Γ = 106 kev). There is some indication that the anomaly at 4.24 Mev may be double. The threshold for the third group of neutrons is observed at 4.910 ± 0.008 Mev, in good agreement with the known energy of the second excited state in N^{14}.

CROSS SECTIONS FOR (p,n) REACTIONS IN INTERMEDIATE-WEIGHT NUCLEI

C. H. Johnson A. Galonsky[1] C. N. Inskeep[2]

This report is a continuation of measurements of (p,n) cross sections which were initiated to study proton strength functions, isotope effects on cross sections, and (p,n) thresholds. The experimental method was described previously.[3] Briefly, protons which are accelerated in the energy range 1.5 to 5.5 Mev by a Van de Graaff accelerator impinge on the target, and neutrons produced in the (p,n) reaction are counted by a 4π flat-response graphite-sphere detector.[4] A total of 40 cross-section curves was obtained for nuclei with $37 \leqq A \leqq 133$. Nine of these (five isotopes of Cd and four isotopes of Te) were reported previously,[3] and it is the intent here to present the remaining 31 cross-section curves. A discussion in terms of proton strength functions is deferred to a later report.

Table 1 lists the 31 nuclei, their isotopic abundances in the targets, and the target thicknesses at 3 Mev. Targets (excepting Nb^{93}) were either electroplated[5] or evaporated onto 10-mil platinum blanks, and their weights were measured on a microbalance. Target thicknesses (excepting Nb^{93}) are much less than the range of proton energies used in the measurements but several times the level spacings in the compound nuclei; thus the observed neutron yields are averaged over resonances. The Nb^{93} excitation curve was found by differentiating the thick-target yield, and its cross sections were obtained with the use of the atomic stopping powers.[6]

In order to find the cross section for the primary target nucleus, it was necessary to correct for neutron yields from other isotopes of the target element, other elements in the target compound, target contaminants, and backgrounds from the target backing and from the accelerator. These corrections will be reviewed briefly.

In a few cases a correction for another isotope of the target element was straightforward, because that other isotope was included in the set of 31 targets. Examples are the two isotopes each of Cu, Ga, and Ag. In other cases only the most abundant other isotope was included in the set; for example, measurements were made on targets enriched in Zn^{67} and in Zn^{68} but not on targets enriched in Zn^{64}, Zn^{66}, or Zn^{70}. In this example, since the Zn^{64} and Zn^{66} thresholds are at least 6 Mev,[7] no correction is made for their presence in the Zn^{67} or Zn^{68} targets. Less than 1% of Zn^{70} is present in each target, so that its cross section can be approximated as being equal to the Zn^{67} cross section.

Five of the targets are compounds: NaCl for Cl^{37}, KI for K^{41}, TiO_2 for Ti^{49}, PbI_2 for I^{127}, and CsI for Cs^{133}. For two of these, NaCl and TiO_2, the primary isotope of the other element has a (p,n) threshold above the energy range of the measurements. The yield from lead in PbI_2 is assumed to be negligible because of the high Coulomb barrier. Corrections for iodine in the KI and CsI targets are provided by the PbI_2 target.

Background corrections were made for neutrons from target contaminants, the target backing, and the accelerator. The only serious target contaminant was Cl^{37}; its characteristic threshold and yield curve were generally observed in heavier targets: $A > 100$. Backgrounds from the target backing and from the accelerator were measured using a platinum blank target.

Figures 1 and 2 show the cross sections for all the nuclei except Ag^{107}, Pd^{105}, Pd^{106}, and

[1]Now at MURA.

[2]Now at the University of Tennessee.

[3]C. H. Johnson, A. Galonsky, and C. N. Inskeep, *Phys. Semiann. Prog. Rep. Mar. 10, 1958*, ORNL-2501, p 29.

[4]R. L. Macklin, *Nuclear Instr.* 1, 335 (1957).

[5]Most of the targets were electroplated by E. B. Olszewski of the Isotopes Division.

[6]W. Whaling, *Handbuch der Physik* (ed. by S. Flugge), vol. XXXIV, p 193, Springer, Berlin, 1958.

[7]R. W. King, *Revs. Modern Phys.* **26**, 327 (1954).

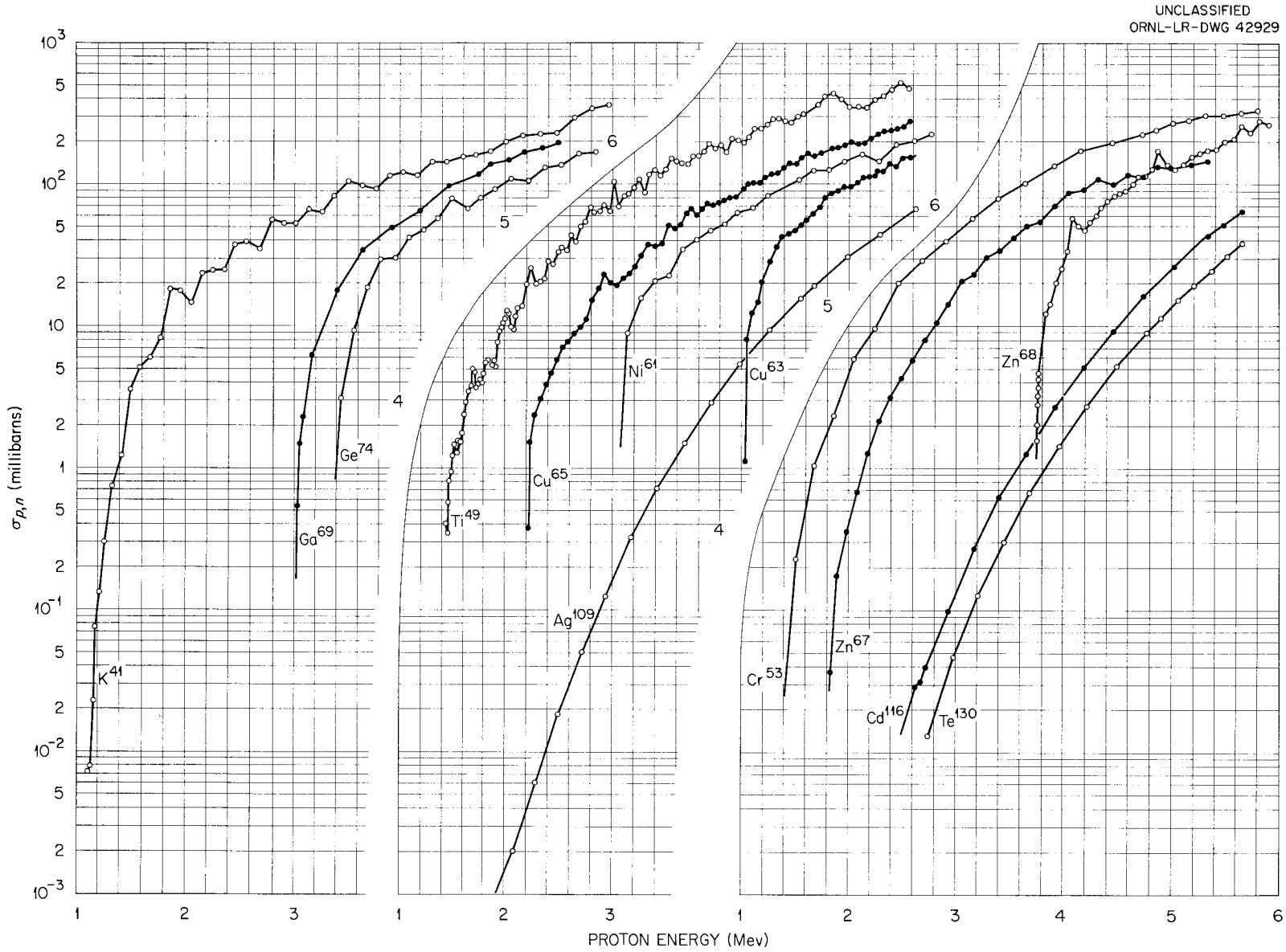

Fig. 1. Cross Sections for (p,n) Reactions in Intermediate-Weight Nuclei. Each curve is labeled with the target nucleus.

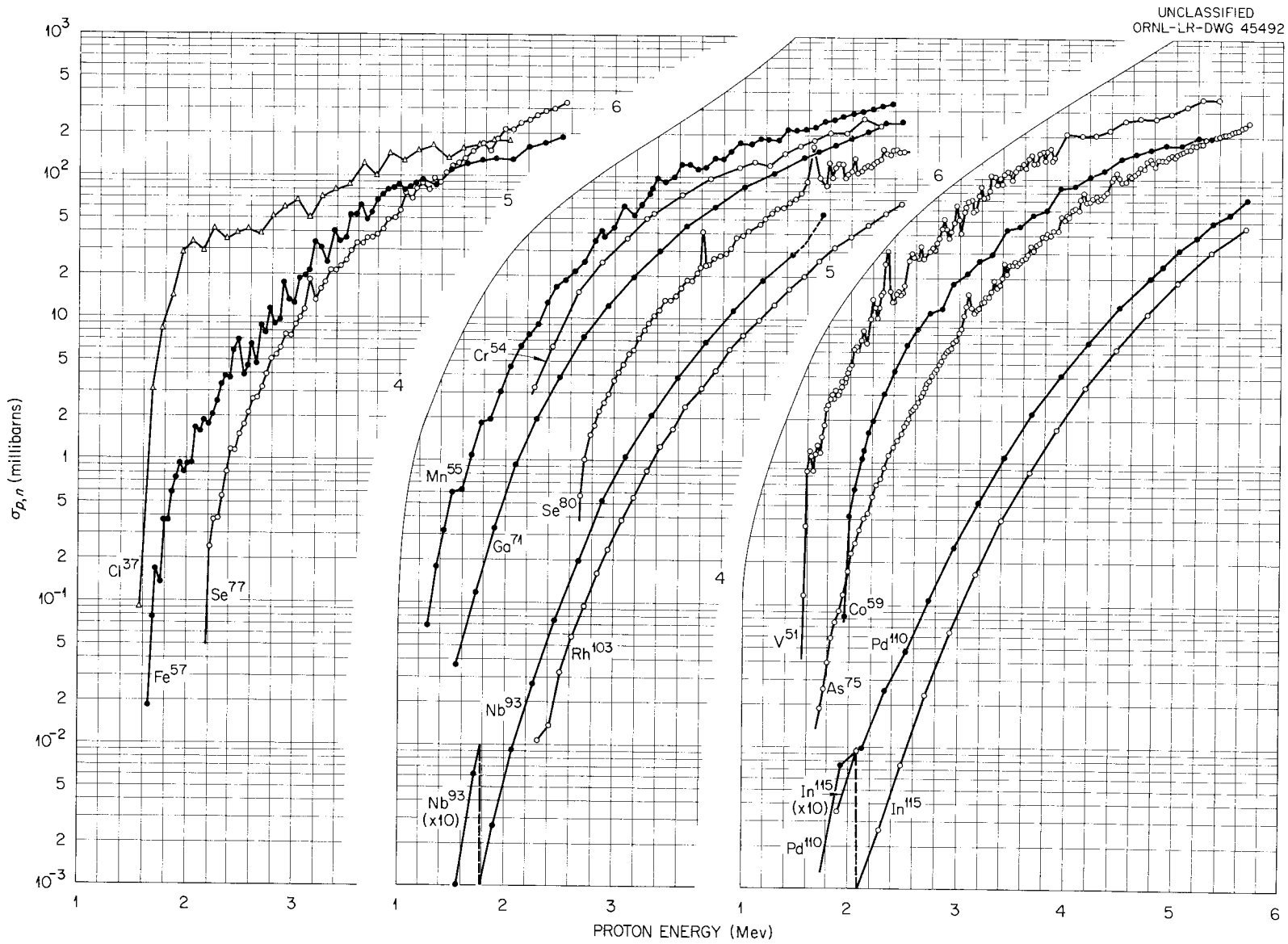

Fig. 2. Cross Sections for (p,n) Reactions in Intermediate-Weight Nuclei. Each curve is labeled with the target nucleus.

Table 1. Properties of Targets

Target Nucleus	Abundance (at. %)	Target Thickness at 3 Mev (kev)	Target Nucleus	Abundance (at. %)	Target Thickness at 3 Mev (kev)
Cl^{37}	24.6	115	Ge^{74}	97.7	15
K^{41}	6.91	130	As^{75}	100.0	20
Ti^{49}	77.6	30	Se^{77}	49.4	12
V^{51}	99.8	15	Se^{80}	98.4	20
Cr^{53}	96.5	130	Nb^{93}	100.0	Thick
Cr^{54}	94.3	180	Rh^{103}	100.0	60
Mn^{55}	100.0	75	Ag^{107}	98.8	110
Fe^{57}	84.1	30	Ag^{109}	99.5	90
Co^{59}	100.0	140	Pd^{105}	78.2	40
Ni^{61}	85.0	120	Pd^{106}	82.3	40
Cu^{63}	99.7	130	Pd^{108}	94.7	60
Cu^{65}	98.2	105	Pd^{110}	91.4	35
Zn^{67}	57.2	90	In^{115}	95.7	110
Zn^{68}	96.8	75	I^{127}	100.0	130
Ga^{69}	98.1	70	Cs^{133}	100.0	110
Ga^{71}	98.4	90			

Pd^{108}. The cross section of Ag^{107} averages about 10% less than that for Ag^{109}. Cross sections for the three lighter palladium isotopes are shown in Fig. 3 relative to Pd^{110}. Figure 1 also includes the previously reported[3] curves for Cd^{116} and Te^{130}.

There has been no attempt in the figures to arrange the cross sections in a logical order; the purpose is simply to present the data in readable form in a small space.

Thresholds were determined for Fe^{57}, Ni^{61}, Ga^{69}, Ge^{74}, Se^{80}, Pd^{106}, and Pd^{108}. These may be read approximately from the graphs; a later report will give the accurate values with their uncertainties.

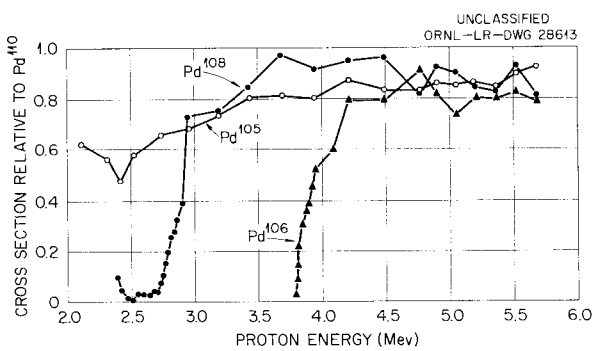

Fig. 3. Cross Sections for the (p,n) Reaction in Pd^{105}, Pd^{106}, and Pd^{108} Relative to the $Pd^{110}(p,n)Cd^{110}$ Cross Section. Thresholds are exhibited for the Pd^{106} and Pd^{108} targets.

CROSS SECTION FOR THE $Li^6(n,\alpha)H^3$ REACTION FOR $1.2 \leqq E_n \leqq 8.0$ Mev[1]

R. B. Murray H. W. Schmitt

The cross section for the reaction $Li^6(n,\alpha)H^3$ has been measured as a function of neutron energy in the range $1.2 \leqq E_n \leqq 8.0$ Mev. An essentially back-to-back method was used, with a thin cylindrical $Li^6I(Eu)$ scintillation crystal placed concentric with and adjacent to a thin-walled ionization chamber containing a deposit of fissile material (U^{238} or Np^{237}). The magnitude of $\sigma_{n,\alpha}$ as measured in this experiment depends on the absolute value of $\sigma_{fiss}(U^{238})$, while the shape of the curve of cross section *vs* energy depends on the known energy dependence of $\sigma_{fiss}(U^{238}$ or $Np^{237})$. Statistical and other point-to-point uncertainties in the data range from ±5 to ±9%, while the uncertainty in absolute value of the cross section is ±7%. The cross section obtained from these measurements decreases monotonically from a value of 0.28 barn at E_n = 1.2 Mev to 0.051 barn at E_n = 8.0 Mev.

[1]Abstract of published paper: *Phys. Rev.* **115**, 1707 (1959).

NEUTRON-INDUCED FISSION CROSS SECTION OF Np^{237}[1]

H. W. Schmitt R. B. Murray

The neutron-induced fission cross section of Np^{237} has been measured as a function of neutron energy in the range 0.9 to 8.0 Mev. Measurements above 1.7 Mev were made relative to the fission cross section of U^{238} by using 2π counting of fission fragments from thin fissile deposits placed back to back in a gridded ionization chamber. In the range 0.9 to 2.8 Mev the energy dependence of the Np^{237} fission cross section was determined relative to the $T(p,n)He^3$ yield, and the results were normalized to those of the comparison counting experiment in the overlapping energy range. Results show that the cross section increases above threshold to a maximum value of 1.75 barns at ~2 Mev, decreases to 1.40 barns at ~5 Mev, and increases again to 2.14 barns at 8 Mev. Estimated uncertainty in the absolute magnitude of $\sigma_f(Np)$ is ±7%.

[1]Abstract of paper to be published in the *Physical Review.*

DIFFERENTIAL NEUTRON SCATTERING FROM LEAD

J. L. Fowler

In the case of interaction of a neutron with the doubly closed shell light nuclei He^4 and O^{16}, the bound states and the neutron scattering phase shifts together permit one to find a phenomenological nuclear potential which describes these states.[1-3] It is of interest, therefore, to investigate the situation for the case of the heavy doubly closed shell nucleus, Pb^{208}. In normal lead the isotope Pb^{208} is only 51.4% abundant; Pb^{206} (26.7%), Pb^{207} (20.6%), and Pb^{204} (1.3%) are the other stable isotopes of the normal element. There is available, however, a radiogenic lead which is mostly Pb^{206} with the following approximate analysis: Pb^{206} (88.3%), Pb^{207} (8.6%), and Pb^{208} (3.1%). By choosing appropriate weight samples for measurements of the total and differential cross sections, the effect of the Pb^{206} can be subtracted so that data are obtained for the following mixture of isotopes: Pb^{208} (72.4%), Pb^{207} (25.8%), and Pb^{204} (1.8%).

[1]E. Vander Spuy, *Nuclear Phys.* 1, 381 (1956).

[2]J. L. Fowler and H. O. Cohn, *Phys. Rev.* 109, 89 (1958).

[3]E. G. Corman and J. L. Fowler, *Bull. Am. Phys. Soc.* 5, 34 (1960).

By this technique the total cross section of the effectively 72% Pb^{208} sample was measured between 1 and 4.1 Mev, and the differential cross section was determined at three selected energies in this range. In the course of this work the cross sections of normal lead were also obtained.

For the total cross-section measurement, $T(p,n)$ neutrons were produced in a 3-cm-long gas cell. The energy spread of the neutrons (25 kev full width at half maximum) was determined by the rise in the neutron yield at threshold. Measurements were made by the standard transmission technique, with the center of a biased propane neutron detector located 38 cm from the center of the gas cell. The 2.86-cm-dia samples were positioned approximately halfway between the neutron source and the detector. Counts were taken with no sample, with the normal lead sample, and with the radiogenic lead sample. The scattered neutron background was evaluated by placing a 30.5-cm-long polyethylene rod between the source and the neutron counter.

Figure 1 shows the results of the measurement of the total cross section of normal lead from 1.0 to 4.1 Mev. The typical errors shown every ½ Mev were calculated from the counting statistics. Inscattering corrections were made to the data by use of the differential cross sections plotted in Fig. 2. The resonance at 1.75 Mev also appears in the published results of Miller *et al.*[4] Since it shows up more prominently in the 72% Pb^{208} sample measurements (Fig. 3), it is undoubtedly a resonance in the Pb^{208} cross section. Fluctuations in the points at other energies are

[4] D. W. Miller *et al.*, *Phys. Rev.* 88, 83 (1952).

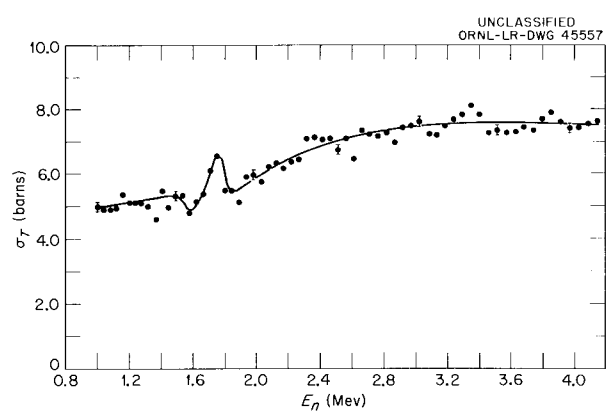

Fig. 1. Total Cross Section of Normal Lead.

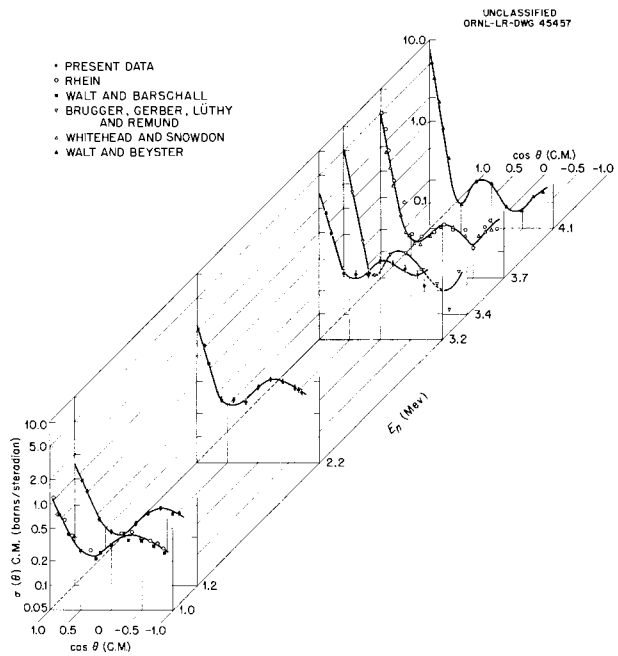

Fig. 2. Differential Cross Section for Neutron Scattering from Normal Lead as a Function of Neutron Energy. Data in center-of-mass system (see refs 8–12 in text).

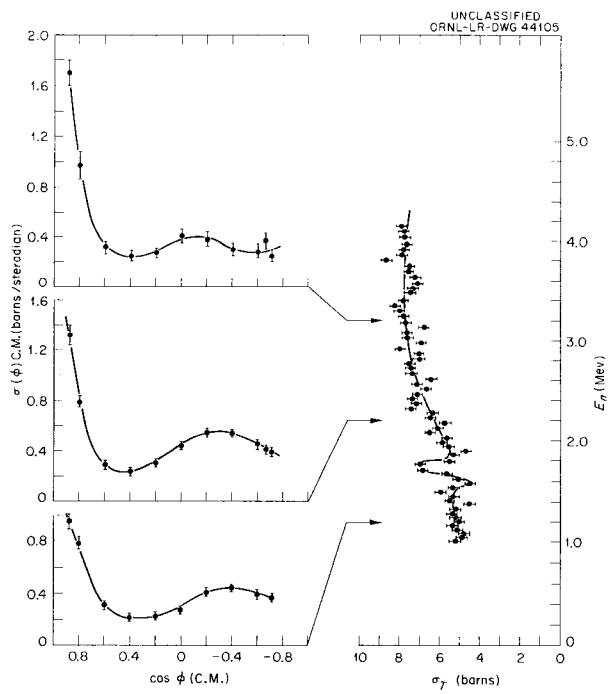

Fig. 3. Total and Differential Cross Sections of Lead Containing 72.4% Pb^{208}, 25.8% Pb^{207}, and 1.8% Pb^{204}.

possibly due to resonances from the 27% Pb^{206} isotope or the 21% Pb^{207} isotope.

The differential cross sections of normal lead and of the 72% Pb^{208} sample were measured by the technique of detecting neutrons scattered from cylinders with a biased propane counter[5] which was shielded from the direct neutrons by a lithiated paraffin collimator.[6] Neutrons from the $T(p,n)$ reactions were produced in a helium-cooled double-foiled gas cell.[7] The neutron energy spread was approximately 50 kev full width at half maximum. The sample diameter (2.22 cm) was chosen so that the error due to the multiple scattering correction was the same order of magnitude as that due to counting statistics.

In Fig. 2 the present differential measurements of the scattering of neutrons from normal lead are compared with other published curves.[8-12] On the horizontal scale is plotted the cosine of the center-of-mass scattering angle, and on the vertical scale is plotted the center-of-mass differential cross section in barns per steradian; the skew scale gives the laboratory energy of the incident neutrons. For the data of Walt and Barschall[8] and Rhein,[9] the estimated errors were ±15%. The errors of the other curves are probably of the same order of magnitude. Within this range of errors the differential cross sections from the various sets of data agree, as the plots in Fig. 2 indicate.

In Fig. 3 on the right-hand side, the measured total neutron cross section of the effectively 72% Pb^{208} sample is plotted as a function of neutron energy. Errors shown are calculated from statistics. Inscattering corrections calculated with the use of the set of curves plotted in Fig. 2 have been applied. The peak at 1.75 Mev corresponds to a resonance of ~3.2 ± 0.5 barns in Pb^{208}. Since a $J = 3/2$ resonance at this energy has a peak cross section of 3.0 barns, whereas for a $J = 5/2$ resonance this value is 4.5 barns, the 1.75-Mev peak is probably a $J = 3/2$ resonance in Pb^{208}. Comparison with other p-wave resonances[13] in Pb^{208}, which are characterized by a small dip before the resonance due to interference with p-wave potential scattering, suggests that the 1.75-Mev resonance is also due to a p level and therefore is a $J = 3/2^-$ resonance.

The left-hand side of Fig. 3 shows the differential cross section of 72% Pb^{208} at 1.2, 2.2, and 3.2 Mev. The data are in the center-of-mass system and have been corrected for multiple scattering, and the errors shown are the root mean square of statistical errors and errors in the multiple-scattering correction which were estimated to be 1/3 of this correction.

Although a phase-shift analysis of the scattering of neutrons from lead in this energy range is greatly complicated by the large number of partial waves involved (probably up to f waves), it is perhaps not hopeless. Low-energy cross sections give some idea of the s-wave phase shifts. The magnitude of the interference dips before the p resonances[13] allows an estimate of the p-wave potential scattering. The $d_{3/2}$ and $d_{5/2}$ phase shifts then have to be adjusted to give the differential data below ~2.0 Mev. Above this energy, f-wave phase shifts enter, but possibly they are small.

It is extremely helpful for such an analysis to know the bound-state assignments in Pb^{209}. The experimental situation, as reported in the literature,[14-16] is summarized in Fig. 4. The net conclusion to be drawn from this information is that the ground state in Pb^{209} is a $g_{9/2}$ single-particle state, the second excited state is probably a $d_{5/2}$ single-particle state, and possibly the 2.54-Mev level is an $s_{1/2}$ state. Even the $d_{5/2}$

[5] J. L. Fowler and C. H. Johnson, *Phys. Rev.* 98, 728 (1955).

[6] H. O. Cohn and J. L. Fowler, *Phys. Rev.* 114, 194 (1959).

[7] Designed by R. W. Lamphere. For references to such a cell see J. H. Coon, *Fast Neutron Physics, Part I: Techniques* (ed. by J. B. Marion and J. L. Fowler), p 707, Interscience, New York, 1960.

[8] M. Walt and H. H. Barschall, *Phys. Rev.* 93, 1062 (1954).

[9] W. J. Rhein, *Phys. Rev.* 98, 1300 (1955).

[10] H. R. Brugger *et al.*, *Helv. Phys. Acta* 28, 331 (1955).

[11] W. D. Whitehead and S. C. Snowdon, *Phys. Rev.* 92, 114 (1953).

[12] M. Walt and J. R. Beyster, *Phys. Rev.* 98, 677 (1955).

[13] H. H. Barschall *et al.*, *Phys. Rev.* 76, 1146 (1949); R. E. Peterson, R. K. Adair, and H. H. Barschall, *Phys. Rev.* 79, 935 (1950).

[14] J. A. Harvey, *Can. J. Phys.* 31, 278 (1953).

[15] D. Strominger, F. S. Stephens, Jr., and J. O. Rasmussen, *Phys. Rev.* 103, 748 (1956).

[16] M. T. McEllistrem *et al.*, *Phys. Rev.* 111, 1636 (1958).

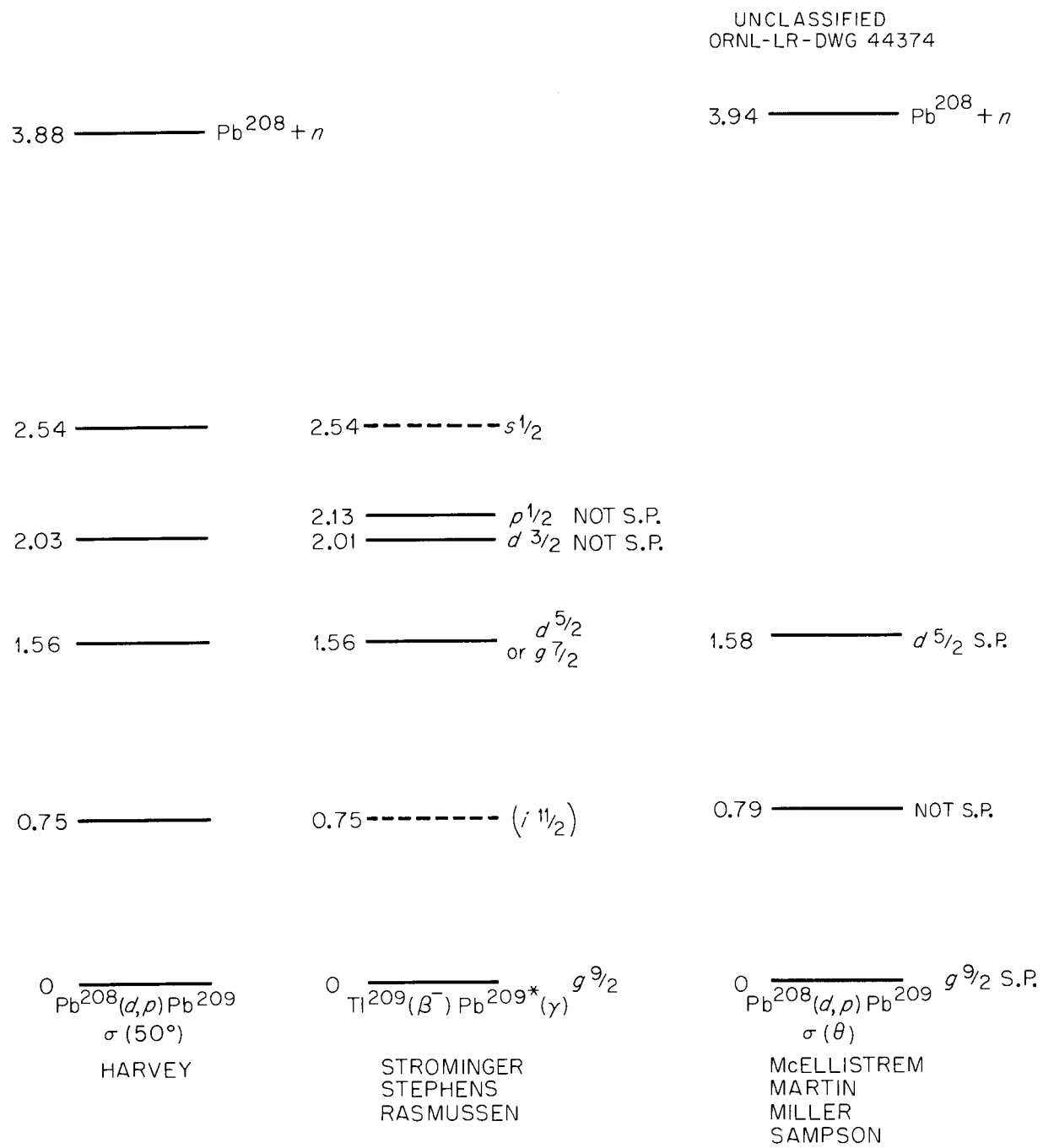

Fig. 4. Energy Level Schemes for Pb^{209} for Bound-State Levels. (See refs 14–16.)

assignment is not completely unambiguous. The angular distribution of protons from (d,p) stripping was not exactly that expected for a $d_{5/2}$ level.[16] Certainly more information is needed on the bound-state levels of Pb^{209}.

An initial phase-shift analysis of the neutron scattering data has been started under the assumption that the broad rise of the total cross section at 3 to 4 Mev (Fig. 3) is due to a $d_{3/2}$ essentially single-particle level in Pb^{209}, the other member of the $3d$ doublet corresponding to the $d_{5/2}$ bound state either at 1.58 Mev in Pb^{209} or at some higher energy. While a completely satisfactory phase-shift fit to the scattering data has not been

obtained, the possibility that the broad rise in the neutron cross section at 3 to 4 Mev is due to a $d_{3/2}$ single-particle resonance has not been ruled out.

In the meantime a naturally occurring lead, rich in Pb^{208}, has been discovered in Tennessee shale. The approximate analysis is as follows: Pb^{208} (72.8%), Pb^{206} (25.4%), and Pb^{207} (1.8%). By use of an 88% Pb^{206} sample for subtracting the effects of Pb^{206}, one can obtain results for a practically pure sample of Pb^{208}. Suitable samples have been requested so that the neutron scattering experiment can be continued with this enriched sample of Pb^{208}.

NEUTRON TOTAL CROSS SECTIONS IN THE kev ENERGY RANGE

J. H. Gibbons W. M. Good P. D. Miller J. H. Neiler

The measurement of neutron total cross sections of separated isotopes is a very time-consuming routine. It takes on the average about 8 hr to obtain numbers for cross sections over the energy range E_n to $E_n + 0.4E_n$. In order to carry on an extensive amount of this type of measurement and still permit other experiments with the millimicrosecond-pulsed beam and time analyzer, automation has been incorporated in addition to punch-tape analyzer output. The latter permits data processing on the Oracle. The automation presently consists of automatically taking the alternate sample-in and sample-out spectra. In this way 24-hr/day operation is possible. The result has been not only more running hours per week, but improved performance as well.

The germanium isotopes Ge^{70}, Ge^{72}, Ge^{74}, and Ge^{76} are being studied carefully for purposes of publication. In the energy interval 3 to 30 kev, the following resonances have been found: for Ge^{70}, 4.35, 4.95, 5.55, 6.65, 8.5, 9.8, 10.2, 11.7, 13.2, 18.5, 23.8, 25.7, and 28.1; for Ge^{72}, 4.52, 4.92, 8.9, 11.1, and 19.2; for Ge^{74}, 4.95 and 19.3; and for Ge^{76}, 4.95, 14.9, 22.3, and 29.3. While the peak positions are well established, some of the measurements have to be repeated before a really reliable figure can be given for the strength functions. Cobalt-59 has been thought to have a relatively sharp resonance at 4.2 kev and a broad resonance at about 5 kev. With the best resolution achievable at the time, Co^{59} was reexamined; there was definite evidence that the resonance at about 5 kev is in fact two resonances peaking respectively at 4.8 and 5.0 kev. Finally, the measurements on Cu^{63} have been repeated and extended up to 10 kev with the following resonances: 4.35, 4.77, 5.14, 5.71, 7.40, 7.80, 9.00, and 9.70.

MILLIMICROSECOND PULSING – ITS APPLICATION AND TECHNIQUE[1]

W. M. Good

A terminal-pulsed Van de Graaff generator is capable of delivering 500 μa and more peak currents in bursts of 2 to 10 mμsec duration at arbitrary repetition rates. It is shown how millimicrosecond intervals relative to these bursts can be measured and recorded. Applications of such measurements to nuclear physics are given. Some of the problems encountered in producing bursts of ions at the terminal of a Van de Graaff are outlined by considering the application of a simple sinusoidally varying voltage to obtain bursts. It is shown that existing techniques can be improved substantially in a number of ways.

[1]Abstract of paper submitted to *Nuclear Instruments*.

ABSOLUTE NEUTRON ABSORPTION CROSS SECTIONS FOR ANTIMONY-BERYLLIUM PHOTONEUTRONS[1]

H. W. Schmitt C. W. Cook[2]

Absolute absorption cross sections of Cu, Zn, Ag, Cd, In, Sb, I, Au, Hg, and Pb have been measured for antimony-beryllium photoneutrons, the average energy of which is given as 24.8 ± 1.1 kev. A specially designed antimony-beryllium neutron source was used in spherical-shell transmission measurements. A detailed account of the method, including discussion of the experimental measurements and analysis of data, is given. Absorption cross sections obtained are as follows: Cu, 42 ± 15 mb; Zn, 64 ± 20 mb; Ag, 1185 ± 80 mb; Cd, 515 ± 70 mb; In, 823 ± 60 mb; Sb, 565 ± 45 mb; I, 885 ± 90 mb; Au, 585 ± 60 mb; Hg, 380 ± 100 mb; and Pb, 3 ± 9 mb.

[1]Abstract of paper to be published in *Nuclear Physics*.
[2]Convair, San Diego, California.

DETERMINATION OF THE ENERGY OF ANTIMONY-BERYLLIUM PHOTONEUTRONS[1]

H. W. Schmitt

The transmission of a spherical shell of enriched B^{10} has been measured and used to determine the average energy of neutrons from a spherical antimony-beryllium source. Analysis of the transmission data in terms of the known absorption and total cross sections of B^{10}, including effects of single and multiple neutron scattering in the shell and source, permits determination of the effective energy neutrons in the shell, the average energy of neutrons emitted from the particular source, and an estimate of the initial antimony-beryllium photoneutron energy. The average energy of neutrons from the neutron source of this experiment is 24.8 ± 1.1 kev; the initial energy of the primary group of antimony-beryllium photoneutrons is 25.6 ± 1.3 kev. A discussion of the source-neutron energy as a function of source dimensions is included.

[1]Abstract of paper to be published in *Nuclear Physics*.

MILLIMICROSECOND TIME-OF-FLIGHT: CAPTURE

J. H. Gibbons R. L. Macklin P. D. Miller J. H. Neiler

Although much of the past year was spent in attempts to improve the accuracy of experimental results, cross section vs energy measurements were extended to include a total of 24 elements. Cross sections are now completed over the energy range from about 10 to 170 kev for F, Br, Nb, Pd, Ag, Cd, In, Sb, I, Pr, Sm, Gd, Tb, Dy, Ho, Er, Tm, Yb, La, Ta, W, Pt, Au, and U^{235}. Cross sections at 29 and 63 kev have been determined for these and 26 other elements.

The following is the abstract of an article (describing this work) being submitted for publication in the *Physical Review*.

Measurements of neutron radiative capture cross sections in the kev region have been made possible by a new method involving fast (millimicrosecond) time-of-flight techniques and a large liquid-scintillator tank. Two series of measurements have been completed on a number of elements: (1) accurate determinations of cross sections near 29 and 63 kev and (2) cross sections as a function of neutron energy from about 10 to 170 kev. Using known average nuclear parameters the value for the *p*-wave strength function has been obtained in all cases where *s*-wave parameters are known.

Significant improvement in data processing has been accomplished by coding the Oracle to process

the punched-tape output of the analyzer to a completed cross section (vs energy). A code for computation of (theoretical) capture cross section vs energy, given average *s*- and *p*-wave nuclear parameters, has also been completed. It is used to fit the experimental results. Finally, the very important correction for scattering effects[1] has been coded for Oracle calculation, resulting in more accurate and detailed correction factors.

The feasibility of studying neutron absorption by radioactive materials has been examined. Studies of neutron absorption by U^{235} have indicated good relative cross-section results but difficulties, as yet not fully understood, in obtaining absolute cross sections. The difficulties are related to the high detector counting rate caused by the sample's own activity.

[1]H. W. Schmitt, *Sample Scattering Corrections in Neutron Beam Experiments*, ORNL-2883 (Jan. 12, 1960).

NEUTRON RADIATIVE CAPTURE MEASUREMENTS WITH THE ORNL FAST-CHOPPER TIME-OF-FLIGHT NEUTRON SPECTROMETER

R. C. Block G. G. Slaughter

A 28-in.-dia liquid-scintillator detector (see Fig. 1) has been installed at an 11.5-m flight station of the ORNL fast-chopper time-of-flight neutron spectrometer. Neutrons that are "chopped" by the M1 rotor are collimated to pass through a hole through the scintillator tank. (This scintillator tank was originally used as an anticoincidence mantle for scintillation spectrometry.[1]) Samples are placed in the center of the tank, and capture gamma rays from the sample are detected by the scintillator. Four 5-in.-dia photomultipliers are used to collect the light. An A-8 double-delay-line amplifier is used with this detector. A 4-in.-thick shield of lead surrounding the tank reduces the gamma-ray background. A $\frac{3}{4}$-in.-thick layer of paraffin and $Li_2^6CO_3$ lines the inside of the hole through the tank to prevent neutrons scattered by the sample from entering the scintillator and producing unwanted capture gamma rays. The scintillator solution consists of xylene, a *p*-terphenyl phosphor, and an αNPO (α-naphthylphenyloxazole) wavelength shifter. To this solution 6% by volume methyl borate has been added. This "boron additive" has a twofold purpose: (1) it reduces the lifetime of the fast neutrons which are scattered into the tank when the chopper rotor is in the open position, and (2) neutrons which are captured in the tank are captured mainly by the boron, which can result only in a 480-kev gamma ray, instead of being captured by hydrogen, which produces a 2.2-Mev gamma ray.

This equipment is useful for investigating radiative capture from resolved resonances, and radiative capture in the low kev energy range, where the resolution of the equipment is such that only the average over many resonances is obtained. With the M1 rotor spinning at 6000 rpm the resolution was approximately 0.2 μsec/m, that is, about 6% at 100 ev and about 20% at 1 kev (this resolution can be improved by spinning the M1 rotor at its designed speed of 10,000 rpm). The results of a typical measurement with this equipment are shown in Fig. 2. The capture counting rates per time channel observed with three different thicknesses of tungsten foils are plotted vs channel number. Channel zero corresponds to about 50 kev. Individual resonances are resolved below $\sim$150 ev, whereas only results averaged over resonances are obtained at higher energies. It is interesting to note how the 18.9-ev tungsten resonance shows up in these measurements. Only in the thinnest sample measurement (upper curve in Fig. 2) was one peak observed; while in the other measurements, where quite thick samples were used, two peaks were observed.

In order to convert these counting data to absolute capture cross sections, the following must first be determined: (1) the neutron flux incident upon the sample, (2) the liquid-scintillator efficiency for detecting a capture reaction, and (3) the background counting rates. Part (1) is determined by measuring the neutron flux with a BF_3 counter of known geometry and pressure. Part (3) is determined by placing in the sample position a sample of lead which scatters as many neutrons into the tank as the capture sample. This is done because the background caused by neutrons scattered into the tank is appreciable

[1]R. C. Davis *et al.*, *IRE Trans. on Nuclear Sci.* NS-3, 82 (1956).

UNCLASSIFIED
ORNL-LR-DWG 41775R

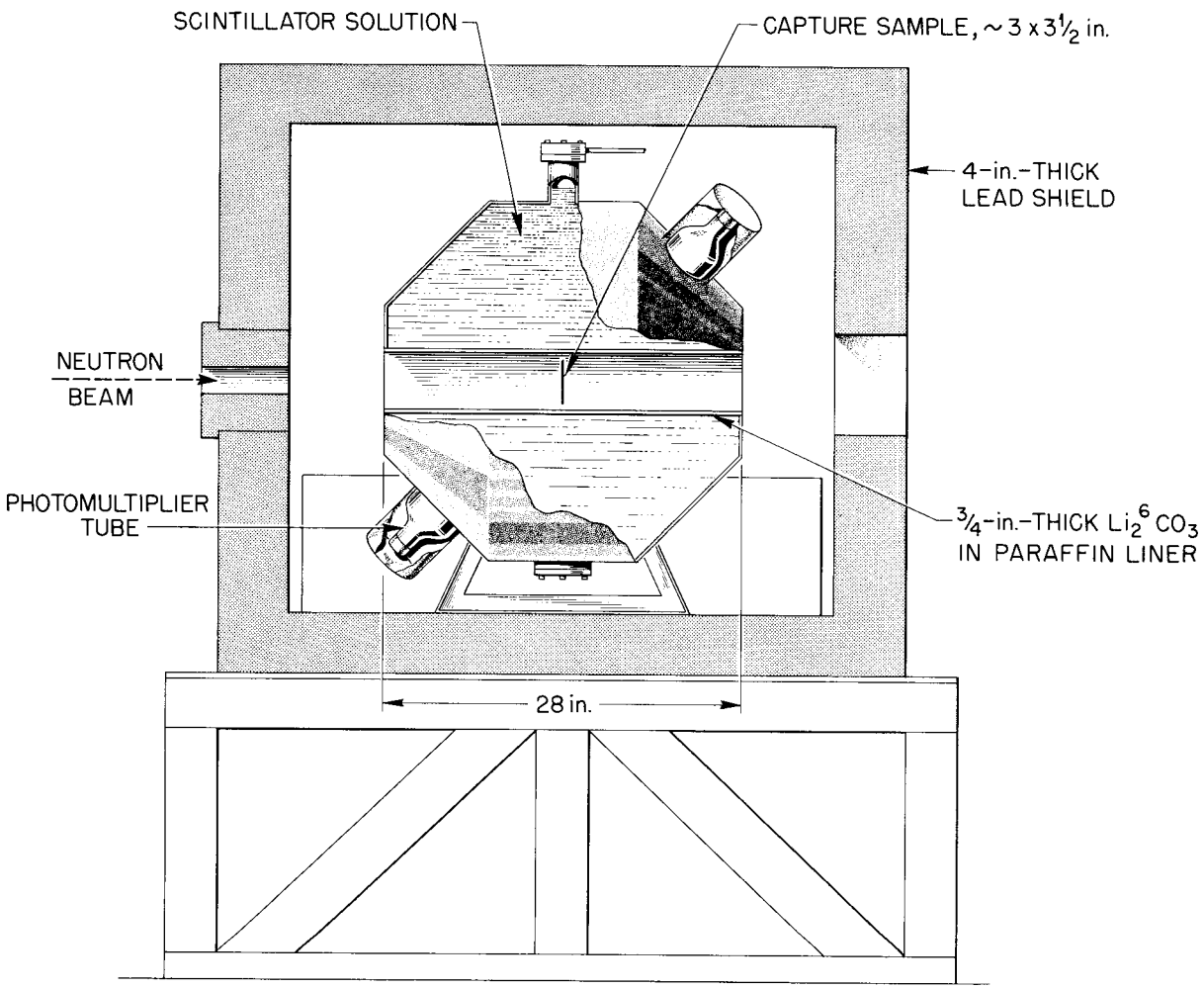

Fig. 1. The 28-in.-dia Liquid Scintillator Radiative Capture Detector.

in the kev region even though the $Li_2^6CO_3$-paraffin liner is used inside the tank. Part (2) is the most difficult to determine. The differential pulse-height spectrum in the scintillator is determined for each capture sample by means of a 256-channel magnetic-core pulse-height analyzer. This spectrum is plotted and the spectrum is extrapolated back to zero pulse height. The discriminator bias is also plotted as a vertical line at the correct pulse-height setting, and the efficiency for detecting interactions in the tank is the ratio

$$\frac{\text{area above bias setting}}{\text{total area}} ,$$

where the areas are taken beneath the differential pulse-height curve. It is also estimated that the efficiency for at least one interaction to take place inside the scintillator per capture is ~90%. (This is based on thermal energy measurements, where an average of about two to three gamma rays per neutron capture is observed.) Therefore, the efficiency of the scintillator tank for a given bias setting is:

$$\text{tank eff} \simeq 0.9 \times \frac{\text{area above bias setting}}{\text{total area}} .$$

It is estimated that the determination of parts (1),

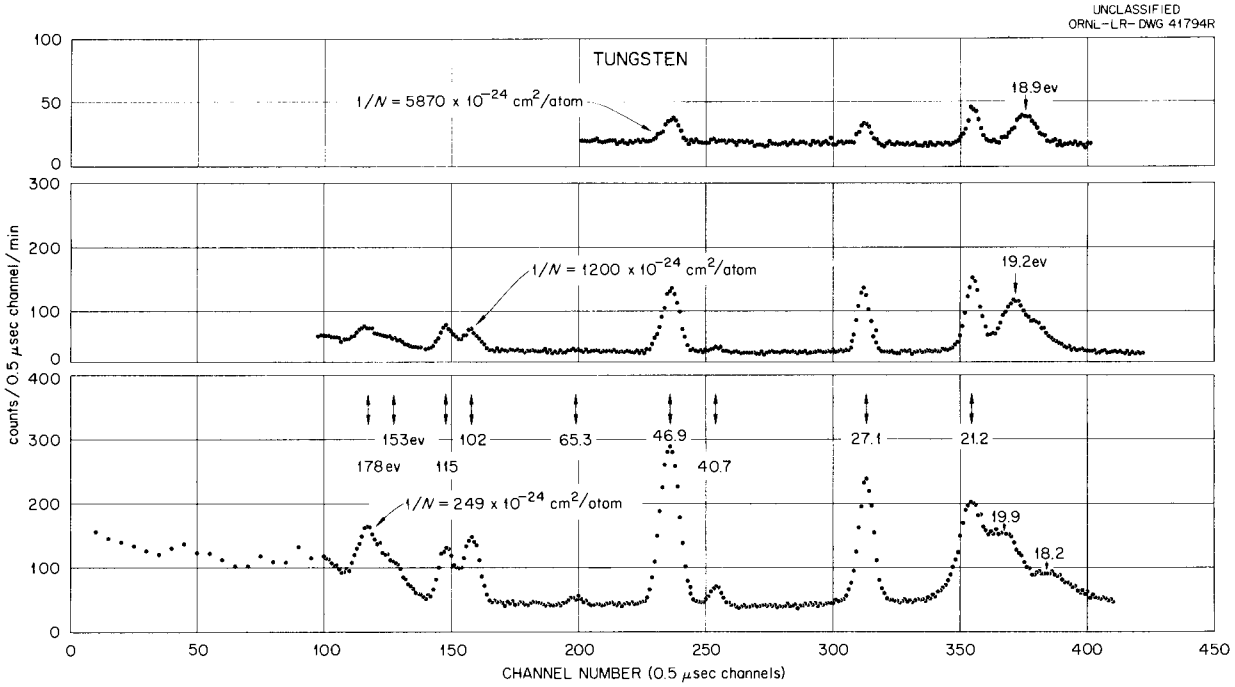

Fig. 2. Capture Measurements on Tungsten.

(2), and (3) results in an over-all uncertainty of about 15 to 25% in the absolute value of the capture cross sections.

Results of capture cross section measurements on naturally abundant samples of Nb, Mo, Rh, Pd, Ag, Cd, In, Sn, W, Pt, Au, and Th are plotted in Figs. 3–14. These results are to be considered as only preliminary because the data have not been corrected for multiple scattering and for resonance self-absorption. Both of those corrections are relatively small above a few kev for the sample thicknesses used for these measurements, but they will affect the data at lower energies. On the curves for Ag, In, W, Pt, and Au are also plotted the higher energy results obtained with the ORNL pulsed Van de Graaff accelerator. Although an accuracy of only 15 to 25% is claimed for these chopper measurements, the agreement with the higher energy results is quite good. In Fig. 15 are plotted results obtained with highly enriched silver isotopes.

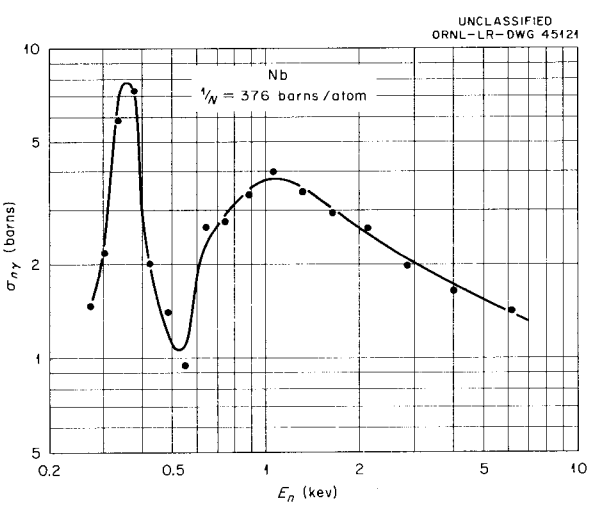

Fig. 3. Radiative Capture Cross Section of Niobium.

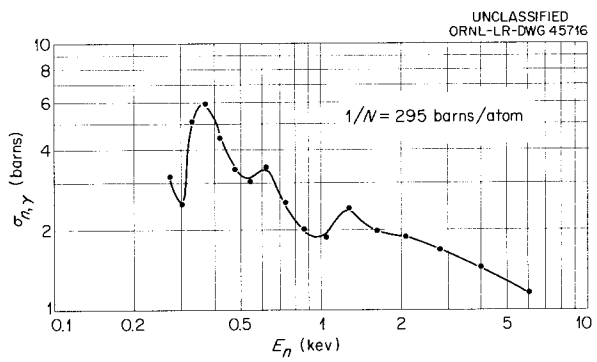

Fig. 4. Radiative Capture Cross Section of Molybdenum.

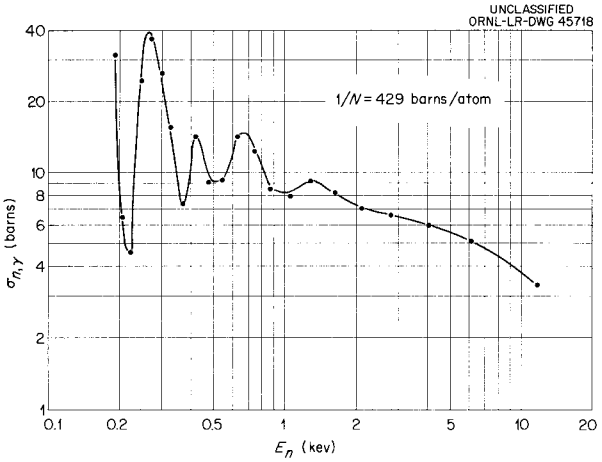

Fig. 5. Radiative Capture Cross Section of Rhodium.

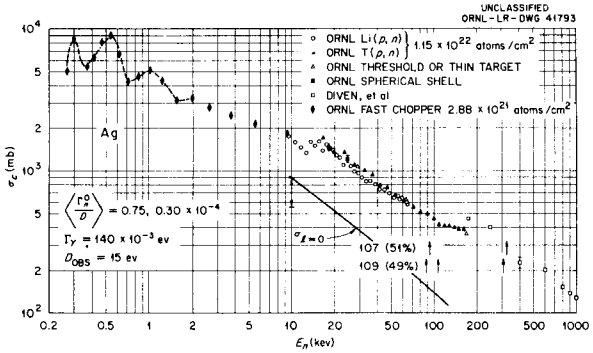

Fig. 7. Radiative Capture Cross Section of Silver.

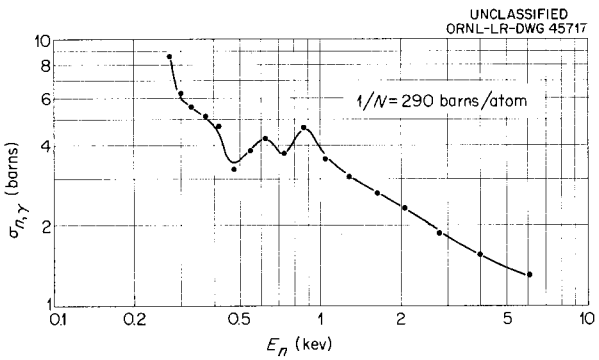

Fig. 6. Radiative Capture Cross Section of Palladium.

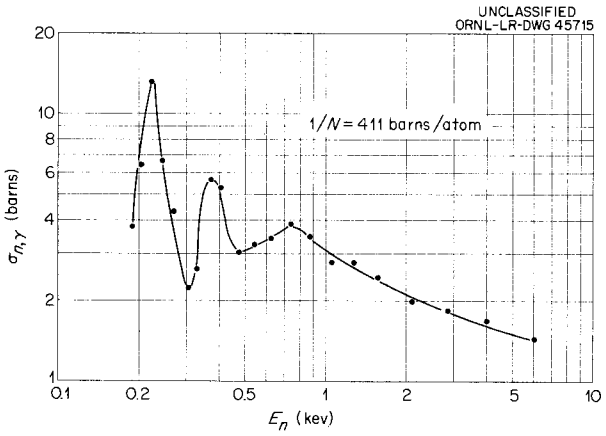

Fig. 8. Radiative Capture Cross Section of Cadmium.

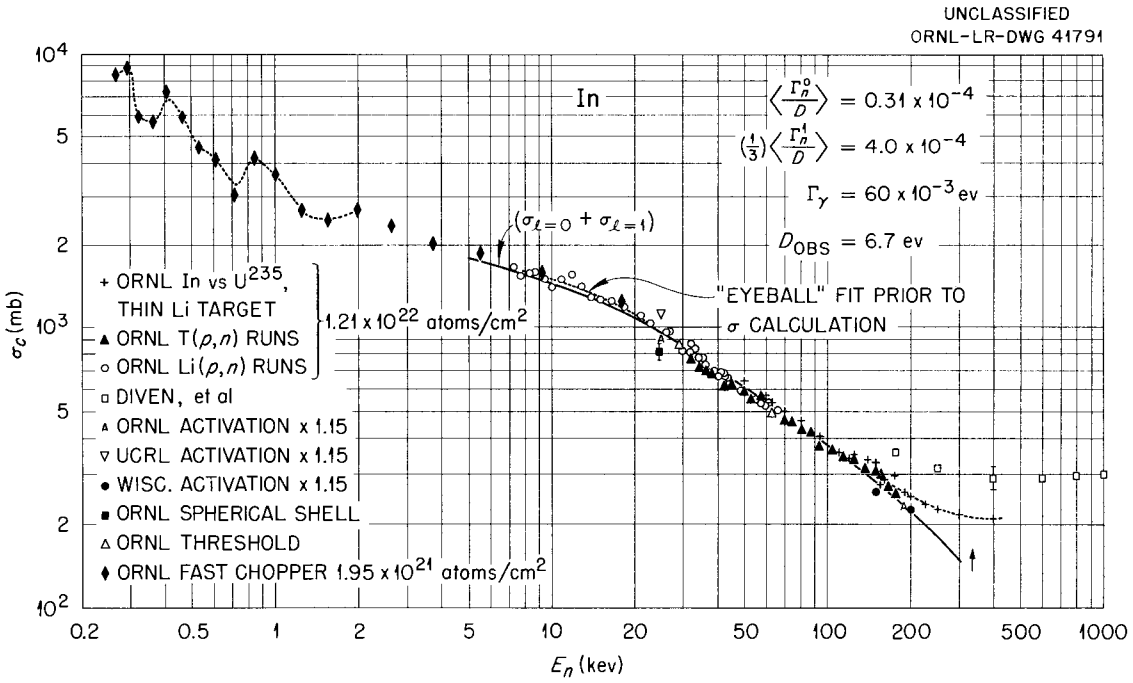

Fig. 9. Radiative Capture Cross Section of Indium.

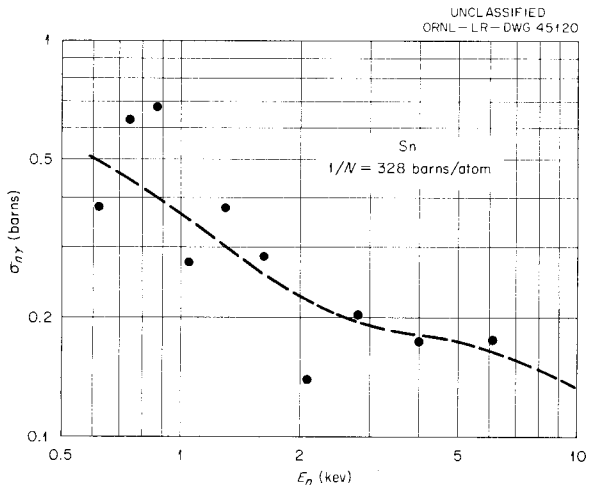

Fig. 10. Radiative Capture Cross Section of Tin.

The capture counting rate from the 132-ev cobalt resonance, as measured with a thin sample, is shown at the bottom of Fig. 16. In order to obtain the ratio of Γ_γ to Γ a transmission measurement was also performed on this sample, as indicated in the upper portion of Fig. 16. The ratio Γ_γ/Γ is then extracted from the ratio of the two shaded areas, the incident neutron flux, and the liquid-scintillator efficiency. From these data a radiative width of 0.9 ± 0.2 ev was deduced. An estimate of multiple scattering of about 10% reduces this to 0.8 ± 0.2. The effects of multiple scattering will have to be more accurately determined (with the aid of high-speed computers) before these results can be improved. Other preliminary results are: Γ_γ/Γ is 0.61 ± 0.10, 0.22 ± 0.04, 0.74 ± 0.12, and 0.29 ± 0.04 for the resonances, respectively, at 102 and 115 ev in tungsten and at 67 and 96

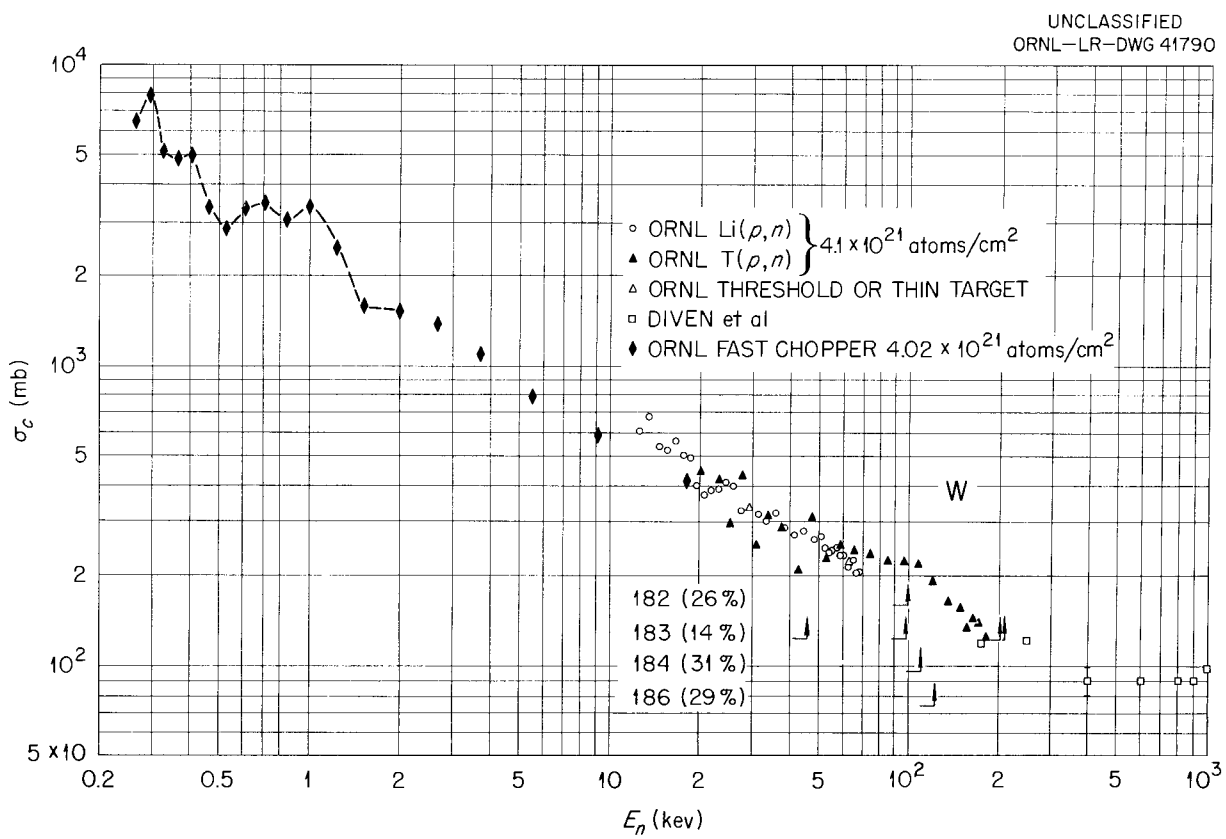

Fig. 11. Radiative Capture Cross Section of Tungsten.

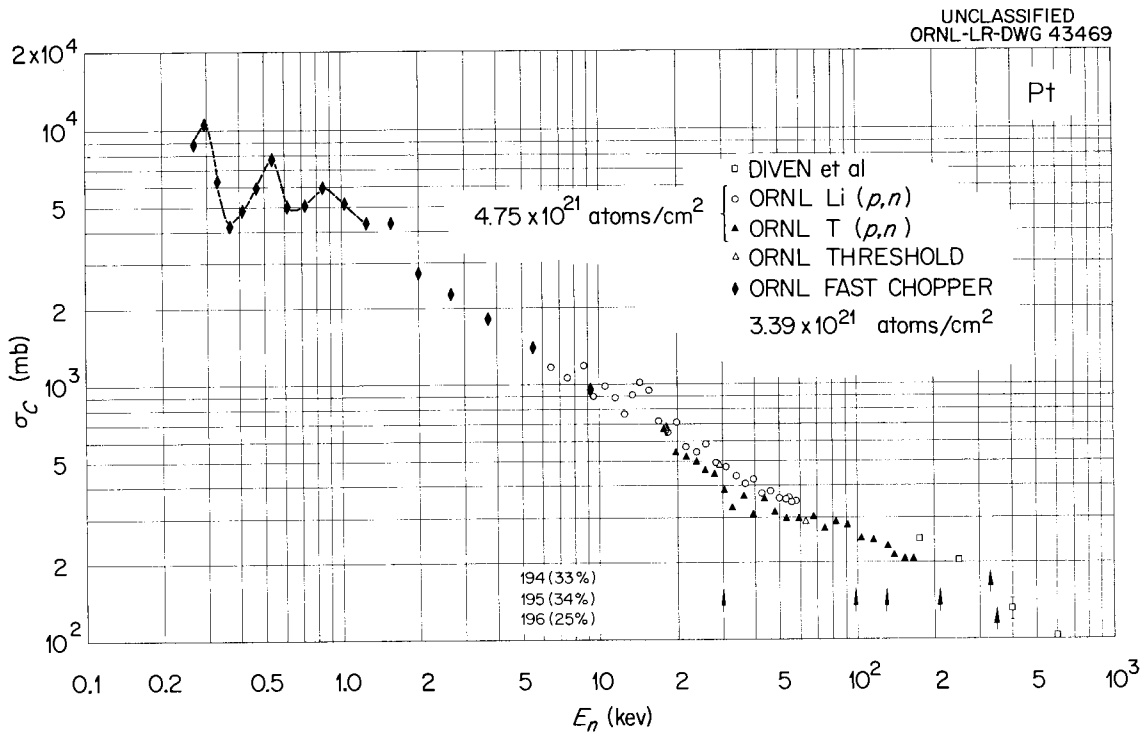

Fig. 12. Radiative Capture Cross Section of Platinum.

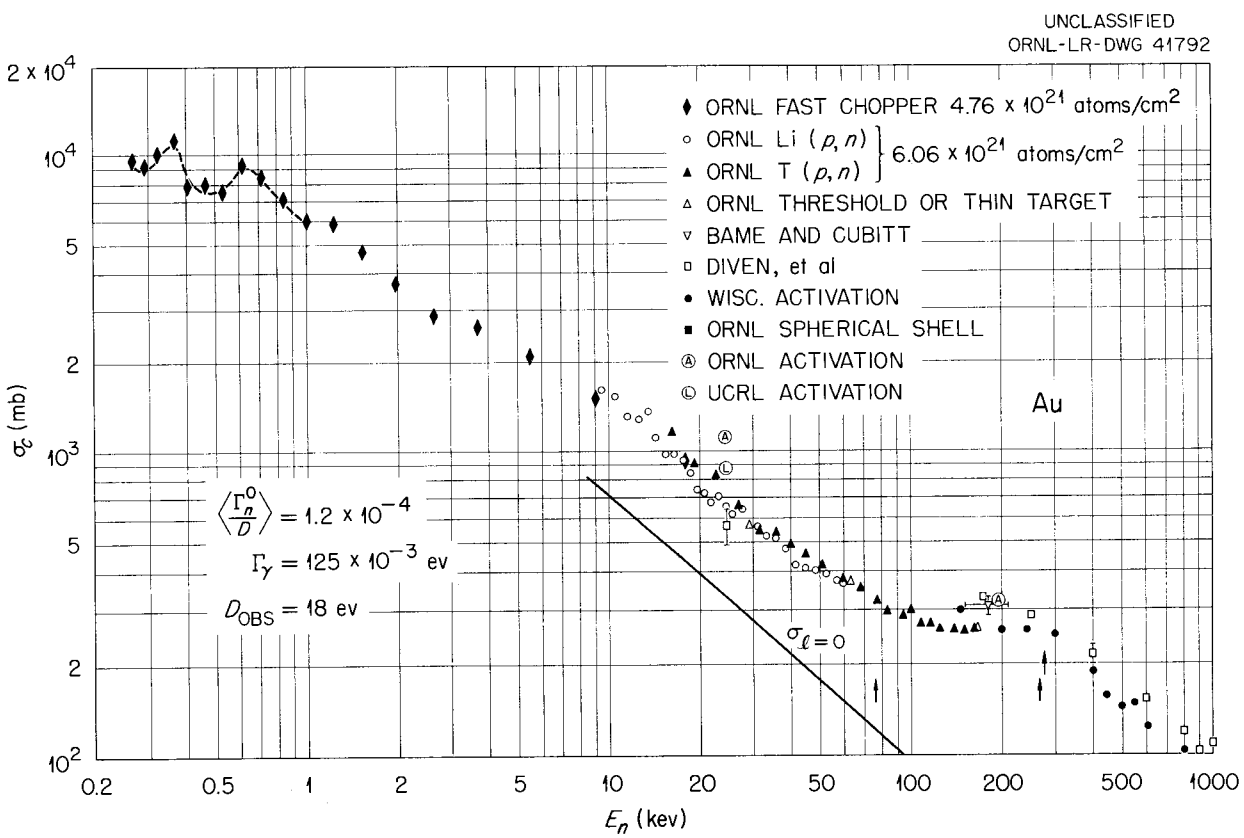

Fig. 13. Radiative Capture Cross Section of Gold.

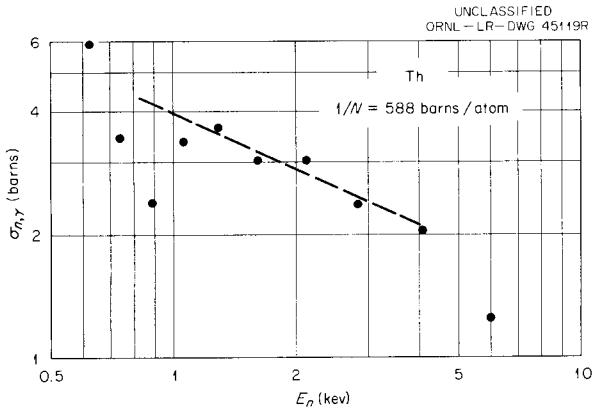

Fig. 14. Radiative Capture Cross Section of Thorium.

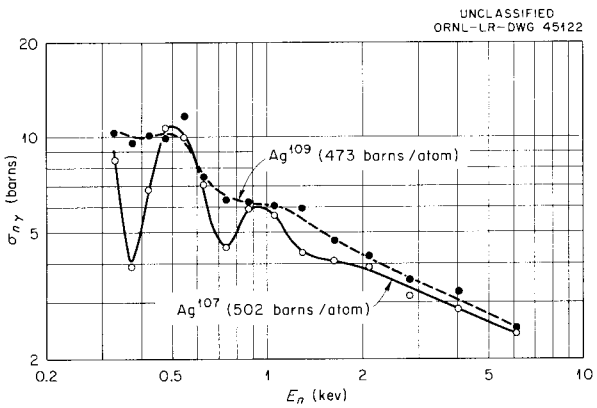

Fig. 15. Radiative Capture Cross Section of Ag^{107} and Ag^{109}.

ev in platinum. (The resonance observed at 67 ev in platinum is actually two unresolved resonances.) These results have not been corrected for multiple scattering.

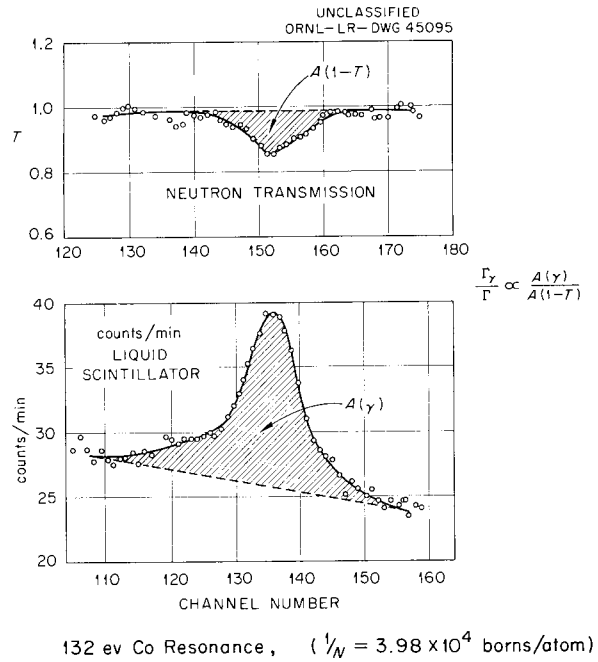

Fig. 16. Transmission and Capture Measurements of the 132-ev Cobalt Resonance.

THERMAL NEUTRON CROSS-SECTION MEASUREMENTS OF U^{233}, U^{235}, Pu^{240}, U^{234}, AND I^{129} WITH THE ORNL FAST-CHOPPER TIME-OF-FLIGHT NEUTRON SPECTROMETER[1]

R. C. Block G. G. Slaughter J. A. Harvey

The neutron total cross sections of U^{233}, U^{235}, Pu^{240}, U^{234}, and I^{129} were measured with the new ORNL fast-chopper time-of-flight neutron spectrometer over an energy range from approximately 0.02 to 0.20 ev. The cross-section data have been fitted in the energy range from approximately 0.02 to 0.04 ev by the least-mean-squares method to the following equation:

$$\sigma_T - \sigma_{sc} = \frac{a}{\sqrt{E}} + b \ ,$$

where σ_T and σ_{sc} are the total and scattering cross sections, E is the neutron energy, and a and b are the coefficients of fit. From this least-mean-squares fit the 2200-m/sec neutron total cross sections of U^{233}, U^{235}, Pu^{240}, U^{234}, and I^{129} are 587 ± 3, 693 ± 5, 290 ± 8, 110 ± 4, and 35 ± 4 barns, respectively. A brief description of the new ORNL fast-chopper time-of-flight neutron spectrometer is included in this paper.

[1]Abstract of paper to be submitted to *Nuclear Science and Engineering*.

THE RESONANCE ENERGY NEUTRON CROSS SECTION OF U^{233}

N. J. Pattenden[1] J. A. Harvey

The fission widths of the levels in the compound nucleus $U^{233} + n$ are relatively large and the level spacing is small. Consequently, conditions exist for the occurrence of strong interference between the levels, which can significantly distort the resonance shapes. Current fission theory[2] implies that only a few channels may be available for the low-energy-neutron-induced fission process, so the interference is assumed to occur between the fission components of the resonance. Thus a study of the extent of the interference can give information on the number of fission channels. We have measured the variation with neutron energy of the total cross section of U^{233} up to 100 ev, and we have fitted to our data at low energies the result of a multilevel method of analysis involving a small number of fission channels.

MEASUREMENTS

Transmission measurements as a function of neutron time of flight were made on uranium metal foils using the time-of-flight spectrometer on the ORR. The metal had the following isotopic analysis:

Isotope	Amount
232	<0.6 ppm
233	99.76 ± 0.01 at. %
234	0.022 ± 0.001 at. %
235	0.007 ± 0.0007 at. %
236	<1 ppm
238	0.21 ± 0.01 at. %

The thicknesses of the foils were as follows:

Sample	$1/n$ (barns/atom)
1	82.0 ± 0.2
2	324.5 ± 0.8
3	1743.0 ± 4.4

The thicknesses refer to the area of the foils in the neutron beam and include a correction for the fact that the foils were about 1% thicker at the center than at the edges, a consequence of their manufacture by rolling. The foils were sealed in an inert atmosphere inside aluminum holders.

The spectrometer was operated with the high-intensity M1 chopper, the 45-m flight path, and BF_3 proportional counters as neutron detectors. Runs were taken covering a neutron energy range from 0.072 ev upward for each sample thickness, and in general, runs were repeated several times. For energies of less than 100 ev, the spectrometer had an energy resolution of approximately 1½%. The statistical accuracy of each cross-section point was better than ½% at the lowest neutron energies, but deteriorated to about 2% at 22.5 ev.

MULTILEVEL ANALYSIS METHOD

We have adopted the multilevel analysis method of Vogt,[3] which stems from the general Wigner-Eisenbud[4] resonance theory. The method puts the theory in a more convenient form by converting relations involving the collision matrix, whose rows and columns refer to channels, into relations involving a defined level matrix A, whose rows and columns refer to levels. The level matrix is specified in terms of its inverse, which is a complex matrix. The diagonal elements of A^{-1} correspond to the single-level contributions to the cross section, and the off-diagonal elements correspond to interference between levels.

Interference between levels is assumed to exist only in the fission cross section. The fission width of each level is symbolized by a vector in fission channel space; the interference between any two levels is given by the scalar product of their vectors, and these scalar products give the off-diagonal elements of A^{-1}. In a two-dimensional channel space, the amount of interference between any two levels λ and λ' is most easily given in terms of the angle $\theta_{\lambda\lambda'}$ between their fission

[1] Participant in exchange program from AERE, Harwell, Berkshire, England.

[2] J. A. Wheeler, *Physica* 22, 1103 (1956).

[3] E. Vogt, *Phys. Rev.* 112, 203 (1958); *Bull. Am. Phys. Soc.* [2]4, 271 (1959).

[4] E. P. Wigner and L. Eisenbud, *Phys. Rev.* 72, 29 (1947).

vectors. The contribution of the capture channels to the off-diagonal elements is considered to be negligible because of sign fluctuations in the many channels involved. Since the neutron widths are small their contribution to the off-diagonal elements is also neglected.

Only a small number of levels are considered together, and, hence, the matrix A^{-1} may be inverted readily. In our case, this operation (and the other calculations discussed by Vogt[3]) has been performed on an IBM-704 computer, the program for which was written by A. Culkowski and N. Dismuke, of the Mathematics Panel. The effect of distant levels is included in a non-interfering term. The method enables one to compute cross sections, postulating a number of fission channels from one up to the number of levels being considered. The effects of Doppler and resolution broadening have also been included in the computer program.

DISCUSSION OF ANALYSIS

The levels involved in the interaction of low-energy neutrons with U^{233} nuclei may be in either of two spin states which cannot interfere with each other. Hence, to attempt a multilevel analysis it is first necessary to make spin assignments of the observed resonances. Regier *et al.*[5] find that the peak-to-valley ratio of the fission product mass distribution curve varies from one neutron resonance to another. The 1.775- and 2.31-ev resonances fall into one group, and the thermal value and the 4.82-ev resonance fall into another. This is considered as evidence for different spin assignments. Fluharty *et al.*[6] and Vogt,[3] in previous attempts to analyze the U^{233} cross section, have pointed out that the resonance widths (and, hence, the fission widths) tend to fall into two groups, which are not inconsistent with this grouping. Therefore, we have used these indications to make the spin assignments for the purposes of the analysis.

In the neutron-energy region below 1 ev, there are two significant features to the observed cross-section curve; the cross section is too large to be explained by contributions from the observed resonances, and there is a small step in the curve at about 0.2 ev. The step may be explained by a small, narrow resonance at 0.185 ev, whose shape is so strongly distorted by interference that a distinct peak is almost unobservable in the total cross section. This resonance has been assigned to the narrow-width group. To fit the extremely distorted shape it is necessary to postulate almost full interference between this and the 1.775-ev resonance, and also to postulate the existence of a bound level with which it interferes fully. The parameters of the bound level and its spacing from the 0.185-ev level were chosen as being typical of the levels in this spin state.

When the effects due to all the narrow-width levels are subtracted from the observed cross section, a large fraction remains, which, below about 0.25 ev, varies approximately inversely with the square root of neutron energy. We have fitted this by postulating another bound level, with a resonance energy at about −0.3 ev and a broad width, which interferes significantly with the broad-width levels at positive energy. The parameters of this level are quite consistent with those of the broad levels at positive energy.

In the energy region from 1.0 to 2.5 ev, where the first two prominent resonances are observed, and additional resonance at 1.62 ev is required to fit the data. The resonance has a large width and hence is included with the broad-width group. Another broad resonance is observed at 4.82 ev, which shows some asymmetry. It is not clear whether any more observed resonances should be grouped with the broad-width levels. The 8.75- and 16.28-ev resonances are intermediate cases, with widths of about 0.39 and 0.5 ev respectively. Also, the latter is difficult to determine with accuracy. The 23.86-ev resonance is sufficiently broad, but it may be an unresolved doublet due to the poor resolution in this region.

From consideration of their widths, the other resonances observed may be included in the narrow-width group. The six large resonances observed below 15 ev all show marked asymmetry, with the exception of the 6.835-ev resonance, in which the asymmetry is small.

Figure 1 shows the observed total cross section multiplied by the square root of the neutron energy for the region below 1 ev. The data in the 0 to 0.08-ev region are those of Block *et al.* ("Thermal

[5] R. B. Regier, W. H. Burgus, and R. L. Tromp, *Phys. Rev.* 112, 1589 (1959).

[6] R. S. Fluharty, M. S. Moore, and J. E. Evans, *Proc. U.N. Intern. Conf. Peaceful Uses Atomic Energy, 2nd, Geneva, 1958* 15, 111 (1858).

Neutron Cross-Section Measurements of U^{233}, U^{235}, Pu^{240}, U^{234}, and I^{129} with the ORNL Fast-Chopper Time-of-Flight Neutron Spectrometer," this report). Figures 2 and 3 show the observed total cross section in the regions 0.5 to 5.0 ev and 0 to 30 ev respectively. In the figures the solid line is the cross-section curve computed from the multilevel analysis, using two fission channels

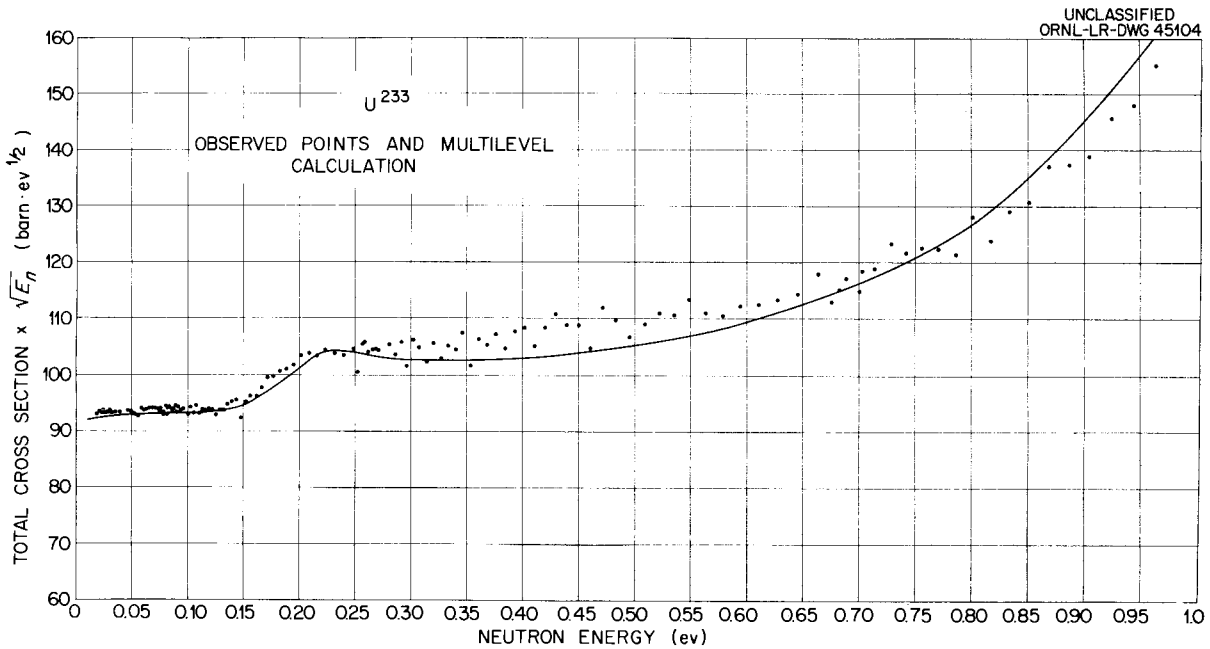

Fig. 1. Total Cross Section of $U^{233} \times \sqrt{E_n}$.

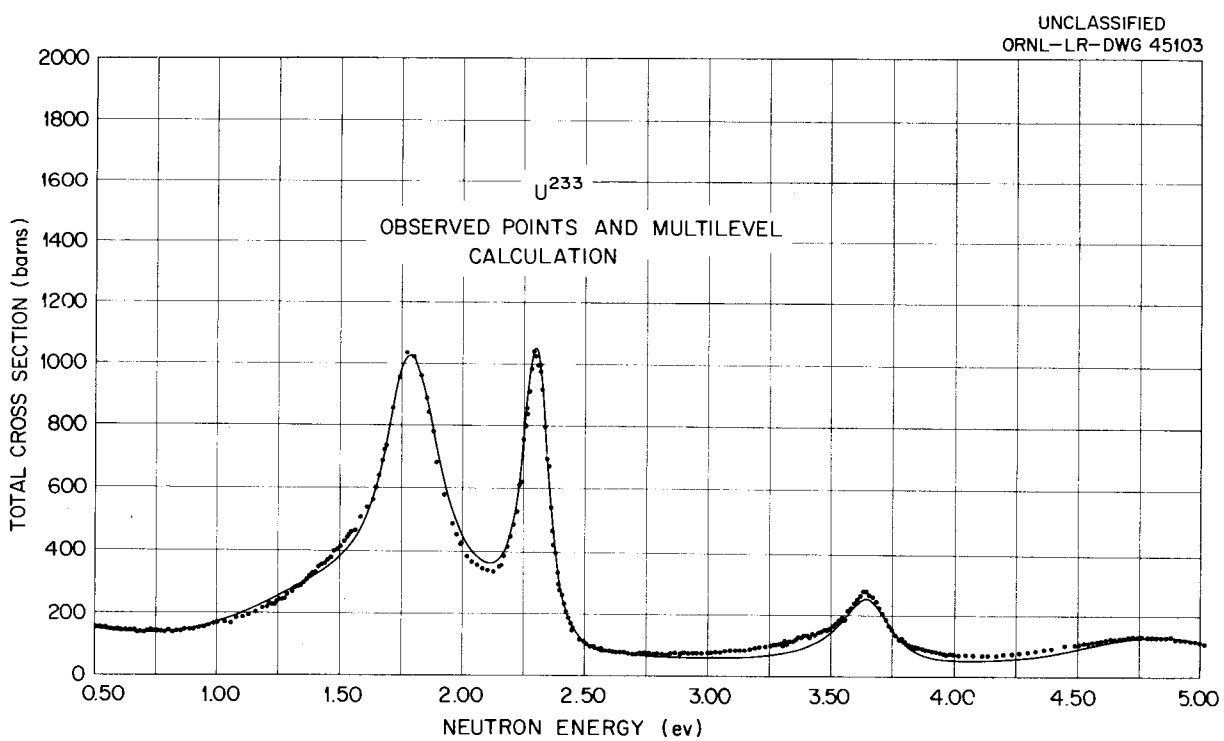

Fig. 2. Total Cross Section of U^{233} from 0.5 to 5 ev.

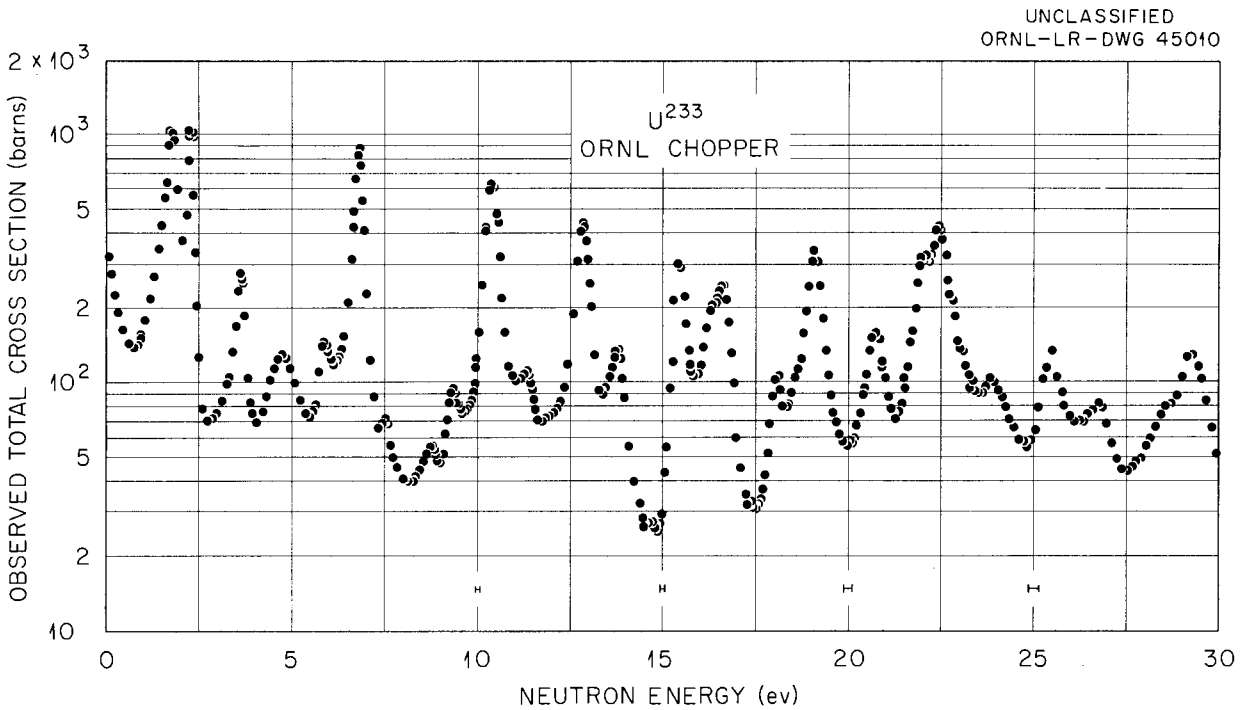

Fig. 3. Total Cross Section of U^{233} from 0 to 30 ev.

in each spin state. Table 1 shows the resonance parameters used in the analysis, including the interference parameters and the assumed grouping into spin states. Except for one level, a constant radiation width of 45 mev has been used in the analysis, since the actual radiation widths are not known but are unlikely to vary appreciably from this value. In general, the total widths are largely due to the fission component, and, hence, errors in the radiation width assumptions will cause only small errors in the derived fission widths.

The computed cross-section curve should be considered provisional, since we are currently engaged in improving the fit and extending the curve to a neutron energy of about 25 ev.

Figure 4 shows a plot of observed level spacing (irrespective of spin state) against neutron energy, which gives an indication that levels are being missed at energies above 6 ev. Since the spin of U^{233} is $5/2$, the level spacings of the two spin states are expected to be approximately equal. However, many fewer observed levels can be attributed to the broad-width group than the narrow group; this is not inconsistent since with such a small spacing levels with broad widths are more difficult to observe. Where individual resonances are not observed, the contribution of the broad group would appear as a background cross section, which on the average varies inversely as the square root of neutron energy. This might explain

Table 1. U^{233} Resonance Parameters

E_0 (ev)	Γ_γ (mev)	Γ_F (mev)	$2g\Gamma_n^0$ (mev)	θ (deg)
		Narrow-Width Levels		
−1.0	45	170	0.10	165
0.185	40	55	6.0×10^{-4}	165
1.775	45	220	0.243	0
2.310	45	50	0.116	135
3.66	45	180	0.073	210
6.82	45	160	0.203	210
		Broad-Width Levels		
−0.30	45	960	0.0465	150
1.62	45	720	0.152	0
4.82	45	750	0.152	120

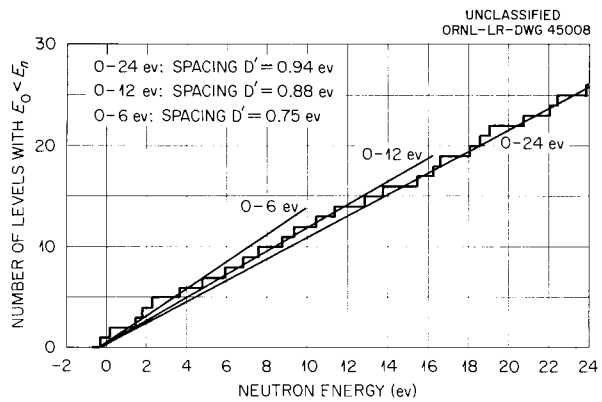

Fig. 4. U^{233} Level Spacing Below 24 ev.

the fact that between the observed resonances the computed curve in general falls lower than the observations.

CONCLUSIONS

It is possible to describe the observed low-energy neutron cross section of U^{233} in terms of a multilevel analysis based on the Wigner-Eisenbud theory of resonance reactions. A two-fission-channel analysis was used; however, this probably means that a few, but more than one, fission channels exist. The unobservable bound levels included in the analysis have parameters which are entirely reasonable when compared with those of the observed levels. Some inconclusive evidence exists that one spin state has levels characterized by large fission widths; if this is the case, it is likely that most of the observed resonances are in the other spin state.

ABSOLUTE MEASUREMENT OF ETA OF U^{233} AND U^{235}[1]

R. L. Macklin G. deSaussure J. D. Kington, Jr. W. S. Lyon

The absolute thermal value of η for U^{233} and U^{235} was measured directly by a method of total absorption which involves relative counting of manganese bath activations and some minor corrections. A thermal neutron beam (defined by cadmium difference) is introduced in the center of a 1-m-dia sphere filled with a dilute solution of manganous sulfate in water. The beam is first made to activate the bath directly, then it is totally absorbed in the fissionable sample whose fission neutrons then activate the bath. The ratio of the two activities is equal to η, except for small corrections. The results obtained for η corrected to 2200 m/sec were, for U^{233}, 2.296 ± 0.010; and for U^{235}, 2.077 ± 0.010.

[1]Abstract of paper submitted to *Nuclear Science and Engineering.*

RARE-EARTH SPECTROSCOPY

K. L. Vander Sluis

Since most of the Zeeman effect data pertaining to the Er II spectrum has been exhausted, the extension of the energy level system is now dependent upon the use of measured transition energies. To handle this problem, a program for the IBM-704 computer has been written by J. Boatman of the ORGDP computing group. This program is designed to add or subtract up to 20,000 measured transition energies from up to 100 established energy levels. The results of this operation are arranged in numerical order and scanned in the following manner. Starting with a given E_0, the number of results falling in the interval E_0 to $E_0 + \epsilon$ (where ϵ is an arbitrary, but fixed wave number interval) is counted. If this number is equal to or greater than a specified i, then the contents of this interval and the two adjacent intervals are printed out. If the number is less than the specified i, no printout occurs and the results falling in the interval $E_0 + \epsilon$ to $E_0 + 2\epsilon$ are counted. This printout cycle is continued until a specified value of $E_0 + n\epsilon = E_{max}$ is reached.

This routine has been tested in the case of Er II as a means of extending a known energy level system. It has also been used in an attempt to

break into the Er I spectrum. In the latter case, transitions which have common values of total angular momentum J, and of Landé g factor, were assumed to terminate on a common level. In this manner an assumed set of energy levels were constructed. A third application involved the setting up of a proposed set of energy levels from a set of reversed furnace lines which were suspected of having a common terminus in the ground state.

The conclusions that are reached from these tests are:

1. The generated set $E_i \pm \nu_{ij} = E_j$ behaves according to the binominal distribution as described previously,[1] except where a real regularity exists.

2. If as few as 15% of the allowed transitions from the present set of Er II upper levels to a new lower level were listed in the existing table of wavelengths, this lower level would have been detected by this method. This points out the need for a much more complete set of ν_{ij}'s than now exists. Supporting this conclusion are echelle spectrograms of 2-hr exposure which have recorded a line density about four times that of the existing table of wavelengths. These spectrograms are presently being reduced to provide the necessary data.

[1]K. L. Vander Sluis, *J. Opt. Soc. Am.* 49, 944–47 (1959).

HYPERFINE STRUCTURE AND ISOTOPE SHIFT OF Po^{209}

G. W. Charles

During the past year measurements have been carried out on interferograms of the spectrum of polonium. Preliminary results of these measurements are presented, including hyperfine structure splittings of Po^{209} and isotope shifts of Po^{209} from Po^{208}.

The interferograms were made by Vander Sluis and Griffin,[1] who reported the nuclear spin of Po^{209} to be $\frac{1}{2}$. Measurements on a Gaertner comparator have yielded the data on hyperfine structure components listed in Table 1 in order of intensity and in terms of displacements in cm^{-1} from the Po^{208} components. Table 1 also summarizes data on approximate wavelength and classification from a previous investigation.[2]

Analysis of the data of Table 1 has led to the structures and isotope shifts listed in Table 2, where, again, the intervals are referred to the Po^{208} components.

Mrozowski has given a supplementary classification of the polonium spectrum.[3] Two of his classified lines, λ5939.6 and λ4611.5, were observed in this investigation. If Mrozowski's assignments of these two lines are assumed to be correct, then the structure of $6p^4\ {}^3P_2$ shown in Table 3 is obtained. The corresponding isotope shifts are −0.02 and −0.03 cm^{-1}, respectively. These results suggest the correctness of Mrozowski's assignment of these lines.

Further evidence on this point will come through the measurement of wavelength from the interferograms, which is now in progress.

[1]K. L. Vander Sluis and P. M. Griffin, *J. Opt. Soc. Am.* 45, 1087 (1955).

[2]G. W. Charles *et al.*, *J. Opt. Soc. Am.* 45, 869 (1955).

[3]S. Mrozowski, *J. Opt. Soc. Am.* 46, 663 (1956).

Table 1. Hyperfine Structure Components of Po^{209}

Wavelength (Å)	Transition	Separation of Components from Po^{208} (cm^{-1})
8618.3	$7s\ ^5S_2 - 7p\ ^5P_1$?	−0.09, +0.09
8433.8	$7s\ ^5S_2 - 7p\ ^5P_2$?	−0.09, +0.09
7962.5	$7s\ ^5S_2 - 7p\ ^5P_3$?	−0.09, +0.02
6245.5		−0.12, −0.22, +0.35
5939.6		−0.09, +0.15
5928.3		−0.05, +0.08
5744.8	$6p\ ^1D_2 - 7s\ ^5S_2$	−0.05, +0.22, +0.40, −0.22
5227.6	$6p\ ^1D_2 - 7s\ ^3S_1$	−0.15, +0.37
4946.9		−0.08, +0.09
4867.2		−0.16, +0.31
4825.9		−0.16, +0.17
4780.5		−0.13, +0.09
4611.5		+0.15, −0.24
4550.4		+0.21, −0.28
4493.1	$6p\ ^3P_1 - 7s\ ^5S_2$	+0.18, −0.19
4490.0		+0.14
4170.5	$6p\ ^3P_1 - 7s\ ^3S_1$	+0.09
3286.4	$6p\ ^1D_2 - 2_3^0$	−0.16, +0.29
3240.2	$6p\ ^1D_2 - 3_1^0$	−0.16, +0.29
3069.3	$6p\ ^1D_2 - 5_1^0$	−0.17, +0.30
2824.1	$6p\ ^1D_2 - 9_1^0$	−0.20, +0.43

Table 2. Hyperfine Structure and Isotope Shifts of Some Levels of Po^{209}

Level	Displacements of States from Po^{208} (cm^{-1})	Isotope Shift of Level from Po^{208} (cm^{-1})
$6p^3(^4S)7s\ ^5S_2$	$\frac{5}{2}$ +0.09 $\frac{3}{2}$ −0.09	+0.02
$6p^4\ ^1D_2$	$\frac{5}{2}$ +0.14 $\frac{3}{2}$ −0.31	−0.04
$6p^4\ ^3P_1$	$\frac{1}{2}$ +0.10 $\frac{3}{2}$ −0.09	−0.03
$6p^3(^4S)7s\ ^3S_1$	$\frac{1}{2}$ +0.06 $\frac{3}{2}$ −0.01	+0.01
2_3°	$\frac{7}{2}$ −0.02 $\frac{5}{2}$ −0.02	−0.02
3_1°	$\frac{3}{2}$ −0.02 $\frac{1}{2}$ −0.02	−0.02
5_1°	$\frac{3}{2}$ −0.03 $\frac{1}{2}$ −0.01	−0.02

Table 3. Structure of $6p^4\ ^3P_2$

Wavelength (Å)	Classification According to Mrozowski	Structure	Structure of $6p^4\ ^3P_2$
5939.6	$6p^4\ ^3P_1 - 6p^4\ ^3P_2$	−0.09, +0.15	$\frac{5}{2}$ 0.00 $\frac{3}{2}$ −0.05
4611.5	$6p^4\ ^1D_2 - 6p^4\ ^3P_2$	+0.15, −0.24	$\frac{5}{2}$ −0.01 $\frac{3}{2}$ −0.07

INFRARED SPECTRA OF SOLID AMMONIA

H. W. Morgan P. A. Staats

The observation of the infrared spectra of NH_3 in a stable cubic phase and in two metastable phases of unknown structure was previously reported.[1] The different solid phases were obtained by depositing thin films of ammonia upon a cooled surface, and studies were made down to 77°K.

The isotopic species NH_3, NH_2D, NHD_2, and ND_3 have now been studied in these three phases, and the majority of the observed bands assigned to specitic vibrational motions. An infrared cell has been constructed for operation at 4°K, and some of the spectra restudied at this lower temperature in an effort to obtain better resolution of the absorption bands.

The spectra of ammonia in the two metastable phases show marked similarities to the gas-phase absorption spectra. Intermolecular bonding is weaker in metastable phase I, existing between 125 and 90°K, than in the cubic phase, and is weakest in metastable phase II, existing below 90°K. The spectrum of metastable phase II at 4°K gives clear evidence of molecular inversion, the first observed in a solid phase. The observed splitting of 22 cm^{-1} in the ν_2 vibrational mode, compared to 37 cm^{-1} in the gas spectrum, indicates a remarkably weak coupling between molecules in this phase. The observed spectra determine only that these solid crystalline phases have very low symmetry. With reasonable assumptions, the spectra could arise from any one of many different possible crystal structures.

Further studies of the infrared spectra of the stable cubic phase have shown the existence of two modifications, with a reversible transition occurring at about 170°K. The changes in the spectrum which indicate this transition appear to be primarily associated with frequencies of the molecular torsional motions in the lattice. Thus, they involve primarily the proton positions and motions, and do not affect the cubic symmetry of the nitrogen atoms. This explanation is compatible with the more detailed x-ray structure given by Olovsson.[2] The observed vibrational frequencies show appreciable anharmonicity and coupling with the torsional modes, and a part of the observed spectrum has not yet been interpreted. It is believed that studies of the cubic phase at 4°K will lead to a complete assignment of the absorption bands and to a full correlation between the spectrum and the cubic structure.

[1] P. A. Staats and H. W. Morgan, *Phys. Ann. Prog. Rep. Mar. 10, 1959*, ORNL-2718, p 34.

[2] I. Olovsson and D. H. Templeton, *X-Ray Study of Solid Ammonia*, UCRL-8700 (April 1959).

NEUTRON DIFFRACTION INVESTIGATION OF MAGNETIC ORDERING IN THE TRIFLUORIDES OF 4*d* TRANSITION ELEMENTS

M. K. Wilkinson E. O. Wollan H. R. Child J. W. Cable

INTRODUCTION

The magnetic properties of compounds containing ions of the 4*d* and 5*d* transition series are of considerable interest, because they appear to be quite different from those of similar compounds containing ions of the 3*d* series. The values of the atomic magnetic moments obtained from susceptibility measurements on 4*d* and 5*d* compounds are generally quite small, and they do not correspond to the spin-only values characteristic of the iron group. Furthermore, there has previously been no direct experimental confirmation of ordering of the atomic magnetic moments in these higher transition series.

In a recent neutron diffraction investigation of the iron-group trifluorides[1] it was shown that the magnetic structures which develop at low temperatures can be accounted for in terms of the orbitals which result from the splitting of the *d* levels by the crystal field. The crystal field splits the 3*d* levels of an iron-group ion in an octahedral site into a lower triplet (t_{2g}) and an upper doublet (e_g), the latter orbitals being of a type which point toward and overlap the *p* orbitals of the anions located between adjacent metal ions. The indirect magnetic coupling which results from this overlap depends on the electron

[1] E. O. Wollan *et al.*, *Phys. Rev.* 112, 1132 (1958).

occupation of the e_g orbitals of the particular cations involved.

Since the magnetic ordering properties of the iron-group trifluorides could be correlated with their d-electron configurations, it was felt that a study of the trifluorides of the second transition group elements might give information on the electron configuration of the $4d$ shell. This report contains the results which were obtained on PdF_3, RuF_3, and MoF_3.

CRYSTAL STRUCTURES

Both PdF_3 and RuF_3 have been reported by Hepworth *et al.*,[2] to crystallize with a bimolecular rhombohedral unit cell of space group $R\bar{3}c$ containing two metal atoms at 000 and $\frac{1}{2}\ \frac{1}{2}\ \frac{1}{2}$ and six fluorine atoms at $\pm(x,\ \frac{1}{2}-x,\ \frac{1}{4})$, $\pm(\frac{1}{2}-x,\ \frac{1}{4},\ x)$, and $\pm(\frac{1}{4},\ x,\ \frac{1}{2}-x)$, where values of x were given as -0.10 for RuF_3 and -0.083 for PdF_3. However, MoF_3 was reported by Gutman and Jack[3] to have the cubic ReO_3 structure. The samples of PdF_3 and RuF_3 used in this investigation were found to have crystal structures in agreement with those reported, but the samples of MoF_3 were also found to have the bimolecular rhombohedral unit cell of the $R\bar{3}c$ space group,[4] and the value of x was determined to be -0.12 ± 0.01.

EXPERIMENTAL RESULTS

PdF_3 and RuF_3

Neutron diffraction patterns were obtained on powdered specimens of PdF_3 and RuF_3 at sample temperatures of 298 and 4.2°K. There was no evidence of magnetic ordering in either compound. Furthermore, the diffuse scattering at room temperature showed little or no angularly dependent paramagnetic diffuse scattering. Unfortunately, the diffraction patterns for the samples which were studied showed a considerable line broadening of the nuclear reflections, so that background measurements were difficult and an accurate analysis of the angular variation of the diffuse scattering was not possible.

MoF_3

Powder diffraction patterns were obtained on MoF_3 at temperatures ranging from 425 to 4.2°K, and, as shown in Fig. 1, antiferromagnetic

[2] M. A. Hepworth *et al.*, *Acta Cryst.* 10, 63 (1957).

[3] V. Gutman and K. H. Jack, *Acta Cryst.* 4, 244 (1951).

[4] D. E. LaValle, R. M. Steele, M. K. Wilkinson, and H. L. Yakel (to be published in *J. Am. Chem. Soc.*).

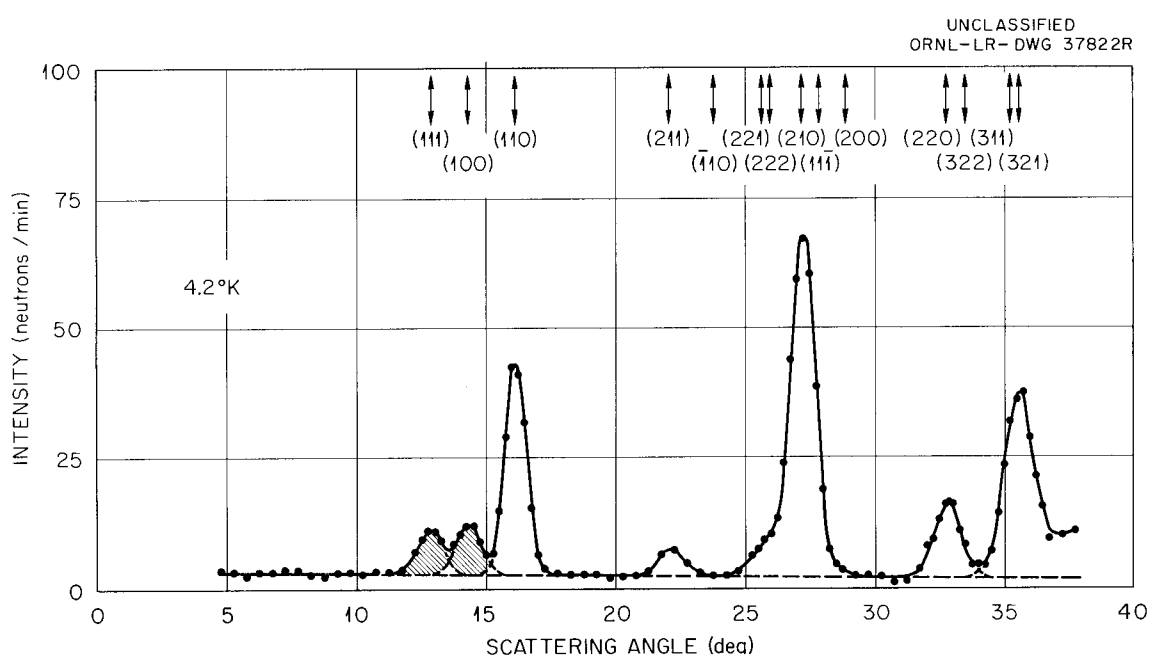

Fig. 1. Neutron Diffraction Powder Patterns for MoF_3 at 4.2°K ($\lambda = 1.08$ Å).

ordering was observed at 4.2°K. The two cross-hatched reflections represent magnetic reflections which occurred at low temperatures, and these are the only two magnetic reflections which are observable in the pattern. This pattern closely resembles that which was reported[3] for the corresponding iron-group compound, CrF_3, and the magnetic structures appear to be identical. They are *G*-type antiferromagnetic lattices[5] in which each metal atom is antiferromagnetically coupled through the intervening fluorine atoms to each of its six nearest neighbors. Furthermore, the relative intensities of the two reflections show that the magnetic moments are oriented in a direction closely perpendicular to the unique axis of the rhombohedral unit cell.

The value of the antiferromagnetic transition in MoF_3 was determined by the variation of the (111) magnetic reflection with temperature, and the intensity of this reflection has a Brillouin-type dependence with a Néel temperature near 185°K. This value is considerably higher than that of 80°K observed for antiferromagnetic ordering in CrF_3, thereby indicating that the magnetic coupling in MoF_3 is stronger than it is in the corresponding compound of the 3*d* series.

In addition to establishing the antiferromagnetic structure of MoF_3, it was of interest to determine the value of the atomic magnetic moments and the magnetic form factor associated with the scattering. The latter determination was particularly interesting since no such experimental data had previously been obtained for electrons in the 4*d* shell. Furthermore, a comparison of the experimental form factor to that obtained from theoretical calculations would indicate whether there was a contribution to the atomic moments from the orbital currents. Since there were only two magnetic reflections and these occurred at comparable scattering angles, very little form factor information could be obtained from the coherent scattering, and it was necessary to determine this form factor from the paramagnetic diffuse scattering. Two types of diffuse scattering analyses are possible, and both were performed, as shown in Fig. 2.

The points in Fig. 2*a* represent average values of many determinations of the diffuse scattering from MoF_3 at 425°K, a temperature well above the Néel transition, so that short-range-order effects should be negligible. These points have been corrected for background scattering, and corrections have also been made for the thermal motion of the atoms on the basis of the Debye theory of independent oscillators. A Debye temperature of 280°K was determined from intensity changes of the (110), (210), and (321) nuclear reflections at a series of temperatures from 425 to 4.2°K, and the estimated error of 25° in this determination is primarily responsible for the long feet on the points at large scattering angles. The angularly dependent scattering in this plot corresponds to the paramagnetic diffuse scattering, and the differential cross section of this scattering is proportional to $\mu_p^2 f^2$, where μ_p is the effective moment per atom in the paramagnetic state and f is the magnetic form factor. An extrapolation of the data to zero scattering angle gives a cross-section value which corresponds to a spin-only paramagnetic moment with $S = 1.38$. Since the relatively large errors in the points do not permit a good determination of the nuclear scattering level, this moment value is consistent with a spin-only moment for $S = 3/2$, corresponding to three unpaired electrons.

Figure 2*b* gives points which represent average values of several determinations of the difference in the diffuse scattering from MoF_3 at 425 and 4.2°K, and these points have been corrected for thermal effects by the method previously stated. Since these two temperatures are well above and well below the Néel transition, to a first approximation the difference in diffuse scattering is proportional to $\mu^2 f^2$, where μ is the average atomic magnetic moment in the ordered lattice. This difference method has the advantages of eliminating temperature-independent nuclear scattering effects and of establishing the zero position on the scale for magnetic scattering. In this analysis of the MoF_3 data, the extrapolation to zero scattering angle is in excellent agreement with the value calculated for a spin-only moment with $S = 3/2$. It is interesting to note the two points representing the (111) and (100) magnetic reflections that are plotted in Fig. 2*b*. These intensities are also proportional to $\mu^2 f^2$, and the excellent agreement with the diffuse scattering data is additional evidence that the stated antiferromagnetic structure is correct and that the moment is equal to 3 Bohr magnetons. Analysis of the coherent magnetic

[5] E. O. Wollan and W. C. Koehler, *Phys. Rev.* 100, 345 (1955).

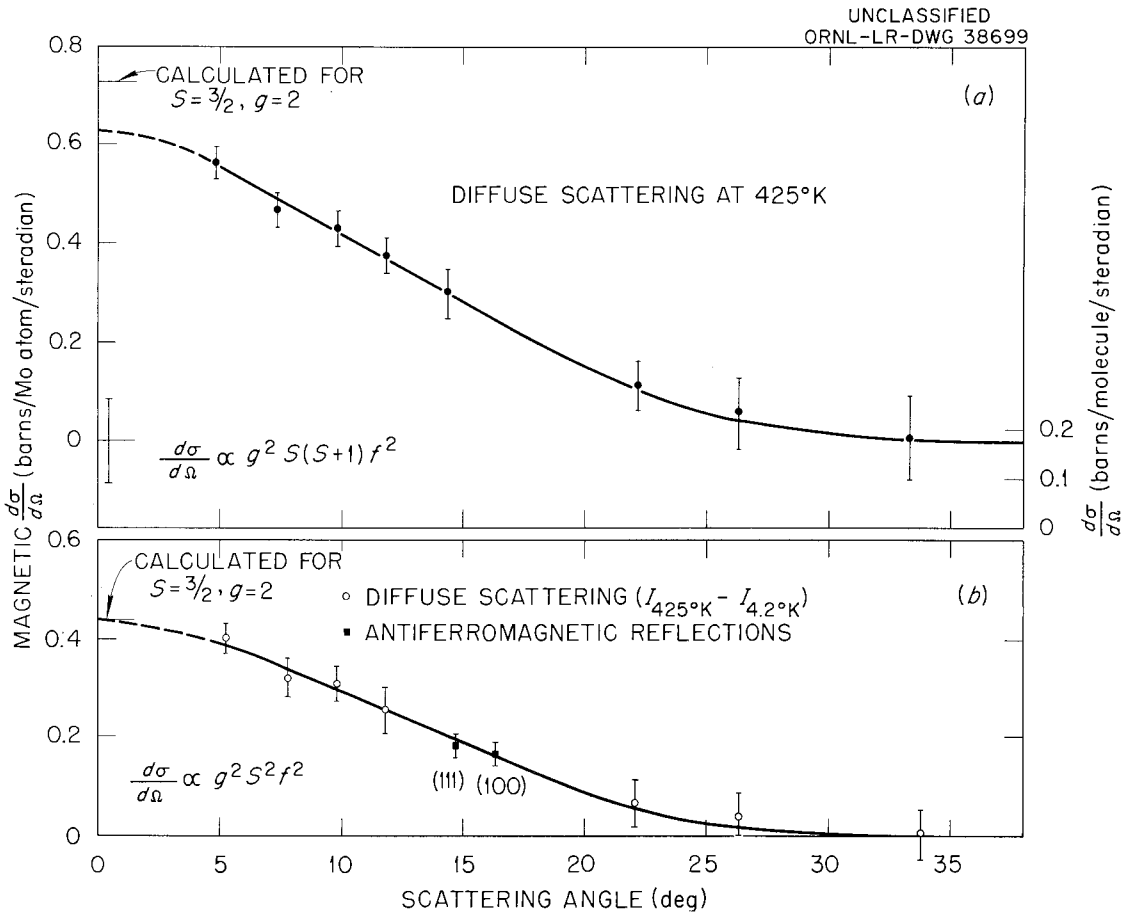

Fig. 2. Magnetic Scattering from MoF_3 Powder ($\lambda = 1.22$ Å).

scattering requires a knowledge of the ordered lattice, whereas the diffuse scattering analysis is independent of the type of magnetic ordering.

The data shown in Fig. 2 were converted to magnetic form factors by taking ratios of the plotted points to the extrapolated values in the forward direction, and the results are shown in Fig. 3. The estimated accuracy of the points is indicated for the results obtained from Fig. 2*b*, and the points obtained from the diffuse scattering at 425°K are less significant because of the uncertainty in the nuclear scattering level. The solid curve in this figure is the calculated form factor for Mo^{+++} as determined by the method of Pauling and Sherman[6] by using their recommended screening constant corresponding to $Z - S = 10$. More accurate form factor calculations are not yet

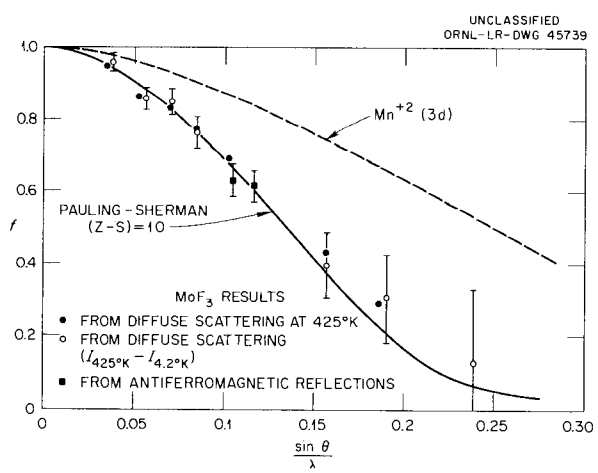

Fig. 3. Comparison of Observed and Calculated Magnetic Form Factors for MoF_3.

[6] L. Pauling and J. Sherman, *Z. Krist.* 81, 1 (1932).

available for the $4d$ series, but the very satisfactory agreement between experiment and theory shown in Fig. 3 is certainly indicative that the atomic magnetic moments in MoF_3 have little or no orbital contribution. The very rapid decrease of the Mo^{+++} form factor with scattering angle is seen from a comparison with the experimental Mn^{++} form factor, shown by the dotted curve. It is this form factor behavior which is primarily responsible for the observation of only two magnetic reflections for the ordered antiferromagnetic lattice in MoF_3.

CONCLUSIONS

The results of this investigation indicate that the magnetic properties of the $4d$ compound MoF_3 are very similar to those of the corresponding $3d$ compound, CrF_3. Molybdenum trifluoride becomes antiferromagnetic at temperatures below 185°K with a structure identical with that of CrF_3, and the atomic magnetic moment value is the expected spin-only value for a magnetic ion with three unpaired d electrons. Any theoretical considerations regarding the behavior of Cr^{+++} ions in octahedral sites might therefore be expected to apply also to Mo^{+++} ions in similar surroundings. However, neither PdF_3 nor RuF_3 showed magnetic properties similar to those of the corresponding iron-group trifluorides. No magnetic ordering was observed in these compounds at low temperatures, and any paramagnetic scattering from them was below the limit of detection.

The behavior of these three compounds can be qualitatively explained if it is assumed that Hund's rule does not apply to ions in the $4d$ transition series. The failure of this rule for ions of the higher transition series was originally suggested by Van Vleck[7] as a possible explanation for the results of the magnetic susceptibility measurements, and more recently Orgel[8] has pointed out that the splitting of the levels in $4d$ transition-metal complexes is in line with this hypothesis. In this case, the lower (t_{2g}) triplet would presumably be filled with six electrons before any electrons were placed in the e_g orbitals. Since Mo^{+++} contains only three $4d$ electrons, all would be in the t_{2g} levels with parallel spins, and there would be no difference between this ion and the corresponding ion, Cr^{+++}, of the iron-group series. However, both Pd^{+++} and Ru^{+++} would have only one unpaired electron instead of three and five, respectively, which would be expected if Hund's rule were applicable. The sensitivity of the measurements in the current investigation was not sufficient to observe either magnetic ordering or paramagnetic scattering from ions having a spin-only magnetic moment resulting from a single electron with a $4d$ magnetic form factor. It would be of considerable interest to test this hypothesis by obtaining the magnetic moment values in these two compounds from paramagnetic susceptibility measurements.

[7] J. H. Van Vleck, *Electric and Magnetic Susceptibilities*, p 311, Oxford University Press, London, 1932.

[8] L. E. Orgel, *J. Chem. Phys.* 23, 1819 (1955).

NEUTRON DIFFRACTION STUDY OF THE MAGNETIC PROPERTIES OF RARE-EARTH–IRON PEROVSKITES[1]

W. C. Koehler E. O. Wollan M. K. Wilkinson

A neutron diffraction study has been made of the magnetic properties of the rare-earth–iron perovskites $NdFeO_3$, $HoFeO_3$, and $ErFeO_3$ at temperatures ranging from 955 to 1.25°K. The iron ions in each of these compounds undergo a transition to an antiferromagnetic configuration in which each moment has six oppositely directed moments at nearest-neighbor distances. The Néel temperatures are 760, 700, and 620°K, respectively, for the compounds of Nd, Ho, and Er. The moment directions in $HoFeO_3$ and $ErFeO_3$ are parallel and antiparallel to the orthorhombic [100] direction at room temperature; at 43°K the moments are found to be in a $(1\bar{1}0)$ plane. In $HoFeO_3$ the iron ion moments at 1.25°K are parallel to [001]; in $ErFeO_3$ at the same temperature they are parallel to [110]. The magnitudes of the ordered iron moments at temperature saturation are 4.5_7, 4.6_0, and 4.6_2

[1] Abstract of paper submitted to the *Physical Review*.

Bohr magnetons in $NdFeO_3$, $HoFeO_3$, and $ErFeO_3$, respectively. In the liquid-helium temperature range magnetic ordering transitions of the rare-earth ions in $HoFeO_3$ (T_N = 6.5°K) and $ErFeO_3$ (T_N = 4.3°K) are observed. The Er^{+++} ion moments form a nearly ideal antiferromagnetic configuration in which a chain of parallel moments is surrounded by four chains of oppositely directed moments at nearest-neighbor distances. In this compound the Er^{+++} ion moments are parallel and antiparallel to [001] and at 1.25°K have a magnitude of 5.8 Bohr magnetons. In $HoFeO_3$ the ions are ordered in a distorted antiferromagnetic configuration in which, at 1.25°K, each Ho^{+++} moment, with magnitude of 7.5 Bohr magnetons, makes an angle, in the (001) plane, of about 27° with the [010] direction so as to produce a net ferromagnetic moment of 3.4 Bohr magnetons per $HoFeO_3$ molecule parallel to [100].

NEUTRON DIFFRACTION INVESTIGATIONS OF THE MAGNETIC ORDERING IN RARE-EARTH NITRIDES[1]

M. K. Wilkinson H. R. Child J. W. Cable E. O. Wollan W. C. Koehler

Neutron diffraction investigations on HoN and TbN at low temperatures show that both compounds become ferromagnetic with Curie temperatures of about 18 and 43°K, respectively. Although the paramagnetic scattering is consistent with moment values calculated for the free trivalent rare-earth ions, the observed ferromagnetic moments are lower than the calculated values and indicate the effect of crystalline field interactions. Diffraction patterns from both compounds at 1.3°K show considerable ferromagnetic short-range-order scattering with characteristics which are different from those associated with critical magnetic scattering.

[1] Abstract of paper scheduled for publication in the April 1960 issue of the *Journal of Applied Physics*.

NEUTRON DIFFRACTION STUDIES OF ANTIFERROMAGNETISM IN CrF_2 AND $CrCl_2$[1]

J. W. Cable M. K. Wilkinson E. O. Wollan

Neutron diffraction observations have been made on powder samples of CrF_2 and $CrCl_2$ from 298 to 4.2°K. These materials, which have crystal structures similar to rutile but distorted from tetragonality, become antiferromagnetic, with different magnetic structures, at low temperatures. For CrF_2 the magnetic unit cell is identical with the chemical cell and the moments at the corner sites are directed oppositely to those at the center of the cell. The magnetic unit cell of $CrCl_2$ requires doubling of the *b* and *c* axes of the orthorhombic chemical cell, and the structure consists of ferromagnetic (011) planes with adjacent planes antiparallel. In neither case were the intensities compatible with a magnetic axis directed along a simple crystallographic direction. Unique magnetic axes could not be definitely established, but the data suggest that they lie parallel to the longest Cr-F and Cr-Cl bonds. Néel temperatures of 53 and 20°K were observed for CrF_2 and $CrCl_2$, respectively.

[1] Abstract of paper submitted to the *Physical Review*.

NEUTRON DIFFRACTION INVESTIGATION OF ANTIFERROMAGNETISM IN $CrCl_3$[1]

J. W. Cable M. K. Wilkinson E. O. Wollan

Neutron diffraction observations have been nade on powder and single-crystal samples of ınhydrous $CrCl_3$ at temperatures from 298 to 1.2°K. This hexagonal layer-type crystal undergoes a transition at 16.8°K to an antiferromagnetic state in which the magnetic moments within each hexagonal layer of metal ions are aligned parallel but adjacent layers of moments are oppositely directed. The axis of spontaneous sublattice magnetization is closely perpendicular to the *c* axis.

Observations of the (003) antiferromagnetic reflection in an external magnetic field show that the antiferromagnetic lattice is completely disrupted with a relatively small magnetic field and that a net magnetization can be effected with extremely small fields.

[1]Abstract of paper to be submitted to the *Physical Review.*

MAGNETIC COUPLING IN CRYSTALLINE COMPOUNDS – A PHENOMENOLOGICAL THEORY OF MAGNETISM IN 3*d* METALS[1]

E. O. Wollan

Magnetic coupling processes are considered in terms of the orbitals which result from the splitting of the *d* levels by the crystalline field. It is shown that the antiferromagnetic and ferromagnetic structure properties of many crystalline compounds can be qualitatively accounted for on the basis of indirect coupling processes which depend on the overlap of magnetic cation *d* orbitals with *p* orbitals of intervening anions and on the electron spin occupation appropriate to the particular cations involved.

The orbital approach has also been used in considering the magnetic properties of the 3*d* metals, and a coupling mechanism has been proposed which is consistent with much of the magnetic data relating to the iron-group metals and their alloys.

[1]Abstract of paper to be published in the *Physical Review.*

ANGULAR DISTRIBUTION OF ALPHA PARTICLES EMITTED BY ORIENTED Np^{237} NUCLEI

S. H. Hanauer[1] J. W. T. Dabbs L. D. Roberts G. W. Parker[2]

In previous work,[3] the alpha particles emitted by Np^{237} nuclei oriented in monocrystalline neptunyl rubidium nitrate were found to be enhanced in the direction perpendicular to the crystalline *c* axis. This result placed current ideas about the electronic structure of the neptunyl ion in conflict with a simple barrier-penetration picture of alpha-particle emission. The present work was undertaken to clarify the matter.

The hyperfine coupling in neptunyl rubidium nitrate has been determined by Bleaney *et al.*,[4,5] who expressed their results in terms of a spin Hamiltonian

$$\mathcal{H} = AI_z S_z + B(I_x S_x + I_y S_y) + P\left[I_z^2 - \frac{1}{3} I(I+1)\right] , \quad (1)$$

[1]On loan from Instrumentation and Controls Division.

[2]Chemistry Division.

[3]J. W. T. Dabbs, L. D. Roberts, and G. W. Parker, *Physica* **24**, S59 (1958); L. D. Roberts, J. W. T. Dabbs, and G. W. Parker, *Proc. U.N. Intern. Conf. Peaceful Uses Atomic Energy, 2nd, Geneva, 1958* **15**, 322 (1958).

[4]B. Bleaney *et al.*, *Phil. Mag.* **45**, 992 (1954).

[5]P. M. Llewellyn, *Some Applications of Paramagnetic Resonance*, chap. 4, Ph.D. Thesis, St. John's College, England, 1957.

with the experimentally determined values

$$A = \pm 0.16547 \pm 0.00005 \text{ cm}^{-1} ,$$
$$|B| = 0.01782 \pm 0.00003 \text{ cm}^{-1} ,$$
$$P = \mp 0.03015 \pm 0.00005 \text{ cm}^{-1} .$$

Only the relative sign of A and P was determined experimentally. The upper signs ($A > 0$, $P < 0$) were thought more probable on the basis of a theory of the electronic structure of uranyl-like ions given by Eisenstein and Pryce.[6] In this theory, the bonding electrons of the uranyl ion are thought to form a column of charge along the O-U-O axis. The extra electron in the neptunyl ion probably lies in a $5f_{\phi}$ orbit, as far away as possible from the central charge column. The neptunium nucleus – presumably prolate in this region of N and Z – would be aligned with its symmetry axis parallel to the O-Np-O axis. Since all the neptunyl groups are parallel to the c axis in this crystal,[7] cooling a monocrystalline sample would align the nuclei parallel to the c axis.

The angular distribution of alpha particles emitted by oriented spheroidal nuclei was predicted by Hill and Wheeler.[8] They pointed out that the potential barrier was both lower and thinner at the "tips" of a prolate nucleus, and that the probability for barrier penetration is a rapidly varying function of barrier height and thickness. On this basis, the alpha particles would be expected to be emitted preferentially along the nuclear symmetry axis. This prediction, taken together with the nuclear alignment direction given by Eisenstein and Pryce's theory, led to the result that the alpha-particle emission was expected to be enhanced along the crystalline c axis when a monocrystalline sample was cooled to temperatures comparable to the hyperfine splitting of about 0.65°K. The earlier experimental results were in disagreement with this prediction, and the alpha particles were observed to be emitted preferentially perpendicular to the c axis.

The uneven spacing of the energy levels made it possible to determine unambiguously the signs of the hyperfine coupling constants A and P by studying the alpha-particle anisotropy as a function of temperature over a range extending down to at least 0.5°K. In the present experiment, this was done over the temperature range 0.2 to 4.2°K. A schematic diagram of the experimental arrangement is shown in Fig. 1. In an isothermal enclosure filled with He^3 gas for heat transfer were located a monocrystalline sample in a rotatable holder, a germanium alpha-particle counter,[9] rotation indicators, and a resistance thermometer. The sample was prepared by growing a thin layer (0.75 mg/cm^2) of neptunyl rubidium nitrate upon a single crystal of the isomorphous compound uranyl rubidium nitrate. X-ray diffraction studies[10] have confirmed that the neptunyl salt grows onto the base crystal in the same structure and orientation. The sample capsule was in thermal contact with a large (0.5 mole) volume of manganous ammonium sulphate (MAS), and the assembly was suspended on cotton threads in a vacuum enclosure so that the MAS could be cooled by adiabatic demagnetization. The vacuum chamber was mounted within Dewar vessels for liquid helium and liquid nitrogen; thermal contact was made – and broken – between the low-temperature assembly and the liquid helium bath by means of a mechanical heat switch.[11]

Counts were taken as a function of the temperature and of the angle θ between the sample crystal c axis and a line joining the counter and the sample. The results of two typical runs are shown in Fig. 2, where the observed counting rate, including a correction for sample shape, $V(\theta)$, is plotted as a function of $P_2(\cos\theta)$. A general angular-momentum-theory treatment[12] predicts that the corrected counting rate, $W(\theta)/V(\theta)$, will vary as

$$\frac{W(\theta)}{V(\theta)} = 1 + b_2 F(T) P_2(\cos\theta) . \qquad (2)$$

This neglects a term in $P_4(\cos\theta)$ which was in fact not observed. The factor b_2 corrects for the

[6] J. C. Eisenstein and M. H. L. Pryce, *Proc. Roy. Soc. (London)* **229A**, 20 (1955).

[7] J. L. Hoard and J. D. Stroupe, quoted in G. H. Dicke and A. B. F. Duncan, *Spectroscopic Properties of Uranium Compounds*, McGraw-Hill, New York, 1949.

[8] D. L. Hill and J. A. Wheeler, *Phys. Rev.* **89**, 1102 (1953).

[9] F. J. Walter, J. W. T. Dabbs, and L. D. Roberts, *Rev. Sci. Instr.* (submitted); *Large Area Germanium Surface-Barrier Counters*, ORNL-2877 (Feb. 8, 1960).

[10] R. D. Ellison, private communication.

[11] F. J. Webb and J. Wilks, *Proc. Roy. Soc. (London)* **A230**, 549 (1955).

[12] M. E. Rose, *Elementary Theory of Angular Momentum*, sec 34, Wiley, New York, 1957.

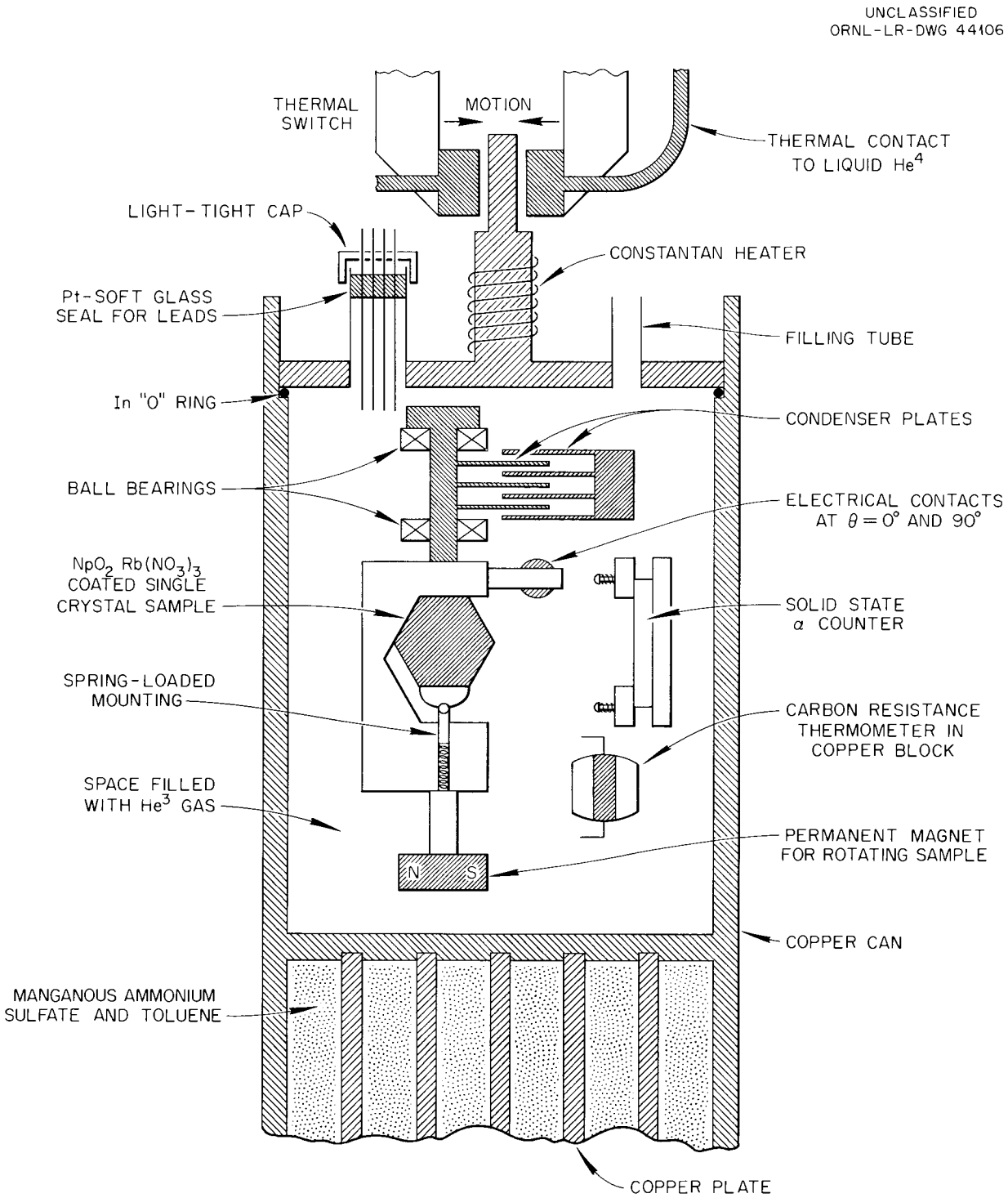

Fig. 1. Schematic Diagram of Apparatus.

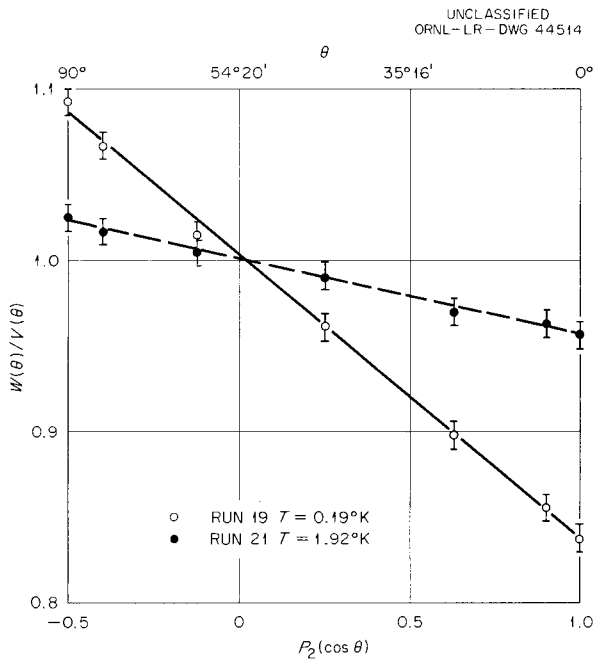

Fig. 2. Angular Distribution for Runs 19 and 21.

finite solid angle. It can be seen from Fig. 2 that the variation of corrected counting rate with the angle θ is in good agreement with the prediction. The quantity $F(T)$ is given by:

$$F(T) \propto a_2\, G_2(T) = a_2 \frac{\sum_i \langle T_{20} \rangle_i\, e^{-E_i/kT}}{\sum_i e^{-E_i/kT}}\,, \quad (3)$$

where the energies E_i are the eigenvalues of the spin Hamiltonian [Eq. (1)], and $\langle T_{20} \rangle_i$ is the expectation value of the quantity

$$T_{20} = \sqrt{\frac{180(2I-2)!}{(2I+3)!}} \left[I_z^2 - \frac{1}{3} I(I+1) \right]\,, \quad (4)$$

using the eigenfunction appropriate to the ith level. The number a_2 is a proportionality constant which was determined, for this experiment, from the earlier measurements. In Fig. 3 are plotted as a function of temperature the experimentally determined values of $b_2\, F(T)$, obtained for each of the 21 runs, by a least-squares fit of the data to Eq. (2). Also plotted in Fig. 3 are the two theoretical curves of $a_2\, G_2(T)$, calculated according to Eqs. (3) and (4) from the experimentally determined hyperfine coupling constants, with the two possible sign choices. It is evident

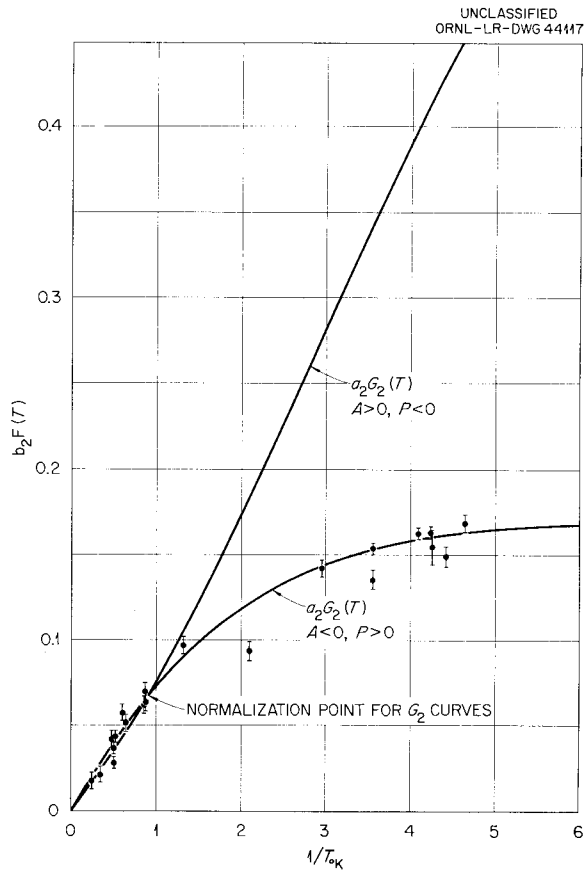

Fig. 3. Size of Anisotropy Compared with Normalized G_2 Functions for the Two Possible Nuclear Alignments.

that the data are in good agreement with the curve for the choice $A < 0$, $P > 0$, and that the choice $A > 0$, $P < 0$ is excluded. The original prediction of Eisenstein and Pryce is therefore incorrect.

Since at 0.2°K the states with the greatest populations are those for which $m_I = \pm \frac{1}{2}$, the observed enhancement of alpha-particle emission perpendicular to the c axis gives the result that the alpha particles are emitted preferentially along the nuclear angular momentum vector. If one makes the usual assumption that $K = I$, then the experiment has shown that the alpha particles are emitted preferentially along the nuclear symmetry axis, in accordance with the prediction of Hill and Wheeler.

Since the above result was obtained, Pryce[13] has pointed out an error in the theoretical calculation of A, which leads to the new theoretical

[13] M. H. L. Pryce, *Phys. Rev. Letters* 3, 375 (1959).

result $A < 0$, in agreement with experiment. The theory still requires P and the nuclear quadrupole moment Q to be of opposite sign; so Pryce has suggested that Np^{237} may have a negative quadrupole moment. This would resolve the disagreement between the experiment and the "column-of-charge" picture of the electronic structure of the neptunyl ion. On the other hand, nuclear systematics[14] predict a positive quadrupole moment in this region, and we point out that optical hyperfine spectra for the neighboring nuclides U^{233} and U^{235} have been interpreted[15] as giving evidence for $Q > 0$ in both cases. Also, if $Q < 0$, the experimental result would mean that the alpha particles were emitted preferentially from the "flat" sides of the oblate nucleus, contrary to the prediction of barrier penetrability. Resolution of this matter awaits further experiment.

[14]D. L. Hill, "Matter and Charge Distributions within Atomic Nuclei," p 221 in *Encyclopedia of Physics*, Vol 39, ed. by S. Flugge, Springer, Berlin, 1957.

[15]K. L. Vander Sluis and J. R. McNally, Jr., *J. Opt. Soc. Am.* 44, 87 (1954), also private communication; N. I. Kaliteevskii and M. P. Chaika, *Optika i Spektroskopiya* 1, 809 (1956), A.E.C. Translation 2890; A. G. Zimin and N. M. Iashin, *Soviet Phys. "Doklady"* 1, 419 (1956).

FISSION FRAGMENTS FROM ALIGNED U^{233} AND U^{235} NUCLEI

J. W. T. Dabbs F. J. Walter L. D. Roberts
G. W. Parker[1] J. O. Thomson[2]

A new apparatus has been used to restudy the angular distribution of fission fragments produced by thermal neutron bombardment of aligned U^{233} in monocrystalline $UO_2Rb(NO_3)_3$ in the temperature range 77 to 1.3°K. In this new apparatus (Fig. 1) a germanium surface-barrier counter 1 in. in diameter was held at 77°K while the temperature of the sample crystal was varied. A thin (0.25 mg/cm^2) nickel window separated the sample space (containing He^4 heat-exchange gas) from the counter space (*in vacuo*). The window had pinholes of about 1 μ diameter, but these were plugged to give a gas-tight window by evaporating a 1% solution of VYNS in cyclohexanone on the surface of the nickel foil. Another feature of the apparatus was a design utilizing the typical variation of expansion coefficient for metals with temperature. At 77°K and below, only small amounts of expansion and contraction take place. Thus by isolating the length-determining wall of the cryostat from gas flows in the region between 77°K and room temperatures, and placing bellows in other walls and tubes, an essentially constant length is secured for the distance of the sample from the room-temperature end of the cryostat, while the sample temperature is varied between 77°K and the low temperatures. This gives a very small vertical motion of the sample in the

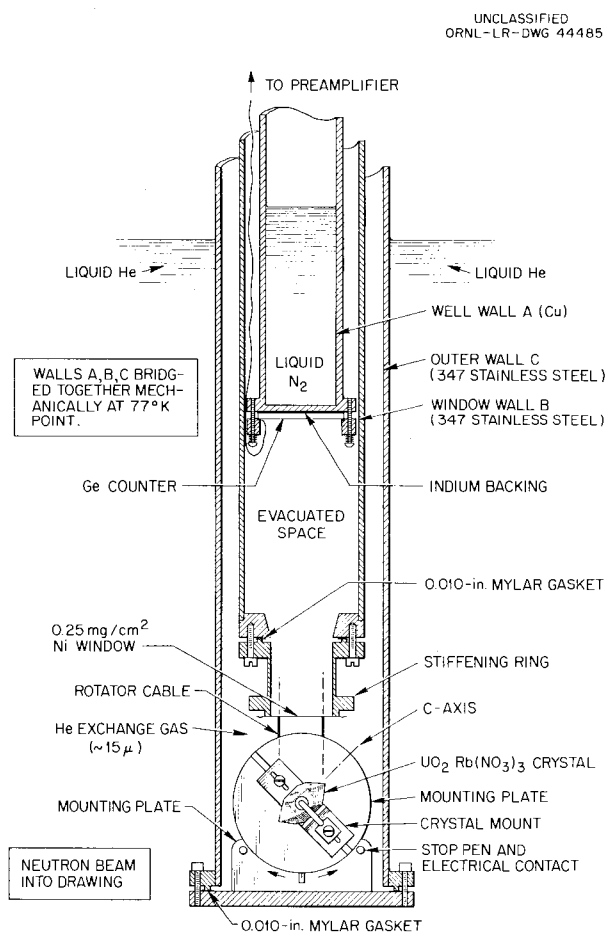

Fig. 1. Apparatus for Study of Angular Distribution of Fission Fragments from Oriented Nuclei.

[1]Chemistry Division.

[2]Consultant and summer research participant, University of Tennessee.

neutron beam with temperature changes in this range. Thus two important sources of possible systematic error have been removed.

In an earlier report,[3] a description of the Bohr[4] picture of fission anisotropies in a quantitative formulation for oriented nuclei was given. There, an expression for the angular distribution $W(\theta)$ was obtained as follows:

$$W(\theta) \propto \sum_{\nu} (-)^{j-(1/2)-K-\nu} C(I,I,\nu;K,-K) \times \times W(j,I,j,I;\tfrac{1}{2},\nu) G_{\nu} P_{\nu} \ . \quad (1)$$

In this expression, j is the spin of the target nucleus, I the total angular momentum of the compound state after capture of an s-wave neutron, and K its projection on the nuclear symmetry axis; G_{ν} is the alignment parameter associated with the target nucleus, C is a Clebsch-Gordan coefficient, W is a Racah coefficient, and the $P_{\nu}(\cos\ \theta)$ are Legendre polynomials. In this picture, each channel for fission is characterized by I and K. If the alignment is brought about through a spin Hamiltonian associated with pure quadrupole coupling (as is thought to be the case in UO_2^{++}),

$$\mathcal{H} = P\left[I_z^2 - \frac{1}{3} I(I+1)\right] \ , \quad (2)$$

one obtains expressions for $G_2/G_0 = -\tfrac{2}{3}\sqrt{14}\ P/kT$ for $j = \tfrac{5}{2}$, and $G_2/G_0 = -\sqrt{21}\ P/kT$ for $j = \tfrac{7}{2}$. Thus to terms in $P_2(\cos\ \theta)$, the angular distribution (1) would be for U^{233} ($j = \tfrac{5}{2}^+$):

$$W(\theta) = 1 - \frac{4}{9}(3K^2 - 6)\frac{P}{kT} P_2(\cos\ \theta) \ , \quad I = 2^+ \ ; \quad (3a)$$

$$W(\theta) = 1 - \frac{1}{3}(3K^2 - 12)\frac{P}{kT} P_2(\cos\ \theta) \ , \quad I = 3^+ \ . \quad (3b)$$

For U^{235} ($j = \tfrac{7}{2}^-$):

$$W(\theta) = 1 - \frac{5}{12}(3K^2 - 12)\frac{P}{kT} P_2(\cos\ \theta) \ , \quad I = 3^- \ ; \quad (4a)$$

$$W(\theta) = 1 - \frac{1}{4}(3K^2 - 20)\frac{P}{kT} P_2(\cos\ \theta) \ , \quad I = 4^- \ . \quad (4b)$$

Bohr[4] suggests that the lower values of K should predominate. If one assumes that $P = +0.04°K$ in U^{233} and $P = +0.02°K$ in U^{235} (corresponding to equal over-all quadrupole splittings in the two cases),[5] the predictions of Eq. (1) are as given in Table 1.

[3] L. D. Roberts, J. W. T. Dabbs, and G. W. Parker, *Phys. Semiann. Prog. Rep. Sept. 10, 1957*, ORNL-2430, p 51.

[4] A. Bohr, *Proc. Intern. Conf. Peaceful Uses Atomic Energy, Geneva, 1955* **2**, 151 (1956).

[5] This sign choice is that which has been found to be correct in NpO_2^{++}; see preceding paper of this report.

Table 1. Coefficients of $P_2(\cos\ \theta)$ for Fission of U^{233} and U^{235}

U^{233}		U^{235}	
Channel (I, K)	Coeff. of P_2 $P = 0.04°K$	Channel (I, K)	Coeff. of P_2 $P = 0.02°K$
2^+, 0	$+0.106/T$	3^-, 0	$+0.100/T$
2^+, 1	$+0.053/T$	3^-, 1	$+0.075/T$
2^+, 2	$-0.106/T$	3^-, 2	0
		3^-, 3	$-0.125/T$
3^+, 0	(parity-forbidden)	4^-, 0	(parity-forbidden)
3^+, 1	$+0.120/T$	4^-, 1	$+0.085/T$
3^+, 2	0	4^-, 2	$+0.04/T$
3^+, 3	$-0.20/T$	4^-, 3	$-0.035/T$
		4^-, 4	$-0.140/T$

The experimental results obtained for U^{233} are shown in Fig. 2. It is seen that the fission fragments are emitted essentially isotropically from the oriented nuclei, as previously reported.[6] It is not known at present which I value is involved at thermal energies. Excluding the 3^+, 2 channel, it seems clear that more than one channel is involved and that the channels of smallest possible K do not strongly predominate.

[6] L. D. Roberts, J. W. T. Dabbs, and G. W. Parker, *Phys. Semiann. Prog. Rep. Mar. 10, 1957*, ORNL-2302, p 31; *Bull. Am. Phys. Soc.* 3, 6 (1958).

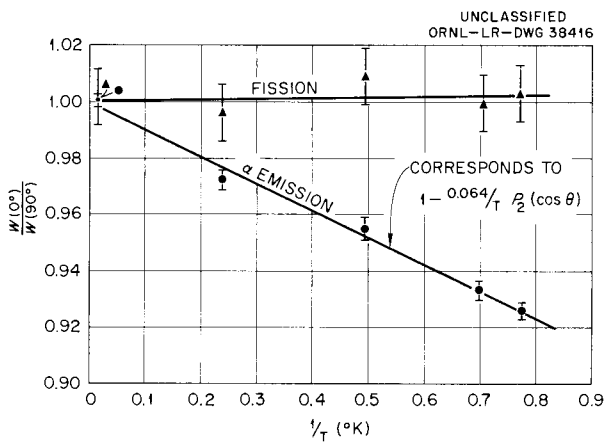

Fig. 2. Anisotropies of Thermal Fission Fragments and of Alpha Particles Emitted from Same Sample of Oriented $U^{233}O_2Rb(NO_3)_3$. Lines are fitted by least squares.

We have also studied the thermal fission of U^{235} in the apparatus shown in Fig. 1, and these results are shown in Fig. 3. Here, a positive anisotropy is observed. This result seems to correspond to the lower K channels under the assumption that P is positive, but again it seems clear from the magnitude of the observed anisotropy that the lowest K value is not the only K value involved. It should be pointed out that the assumption $P < 0$ would lead to a predominance of the $K = I$ channels, which seems unlikely on the basis of the Bohr idea that the lowest K values lie lowest in energy, and hence tend to be more probable in the fission process.

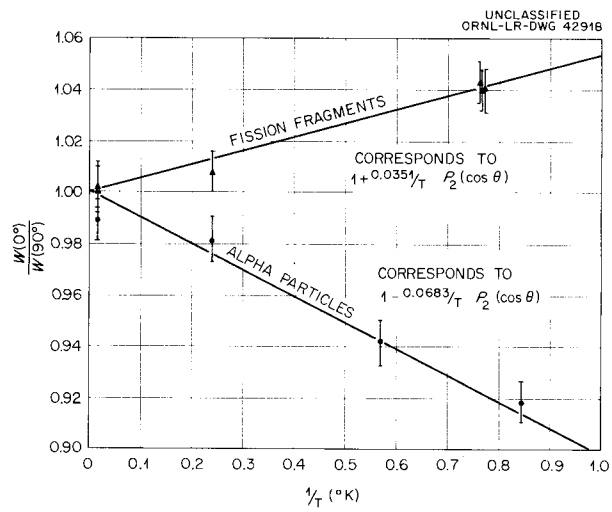

Fig. 3. Anisotropy of Thermal Fission and Alpha-Particle Emission from Aligned U^{235} Nuclei.

SIGN OF THE NUCLEAR QUADRUPOLE COUPLING IN UO_2^{++} AND NpO_2^{++} IONS

L. D. Roberts J. W. T. Dabbs

As has been pointed out earlier (see "Angular Distribution of Alpha Particles Emitted by Oriented Np^{237} Nuclei," this report), our experimental results on the anisotropy of alpha emission from Np^{237} nuclei oriented in the group NpO_2^{++} demonstrate that the sign of the nuclear electric quadrupole coupling constant P [see Eq. (1) of above-named paper] in this group is positive. In that

$$P = -\frac{3e^2 Q}{2I(2I-1)} \sum_i \left\langle i \left| \frac{P_2(\cos\theta)}{r^3} \right| i \right\rangle ,$$

we find that the nuclear quadrupole moment Q and

$$\zeta = \sum_i \left\langle i \left| \frac{P_2(\cos\theta)}{r^3} \right| i \right\rangle$$

must be of opposite sign. The index i represents the wave functions for the electrons contributing to ζ. As will be discussed below, however, nuclear evidence would suggest that Q should be positive. Chemical and microwave evidence as discussed by Eisenstein and Pryce[1] would indicate that ζ should also be positive. To help resolve this conflict we have undertaken to extend the calculation of ζ given by Eisenstein and Pryce. This work is only partially completed, but some definite conclusions are given.

COVALENT CHARACTER OF THE BOND

The UO_2^{++}, NpO_2^{++}, PuO_2^{++}, and AmO_2^{++} linkages are chemically novel structures. Until the discovery of the transuranic elements the UO_2^{++} group was a unique chemical form, and it has been the object of extensive chemical investigation.

The fact that the UO_2^{++} group behaves as a tightly bonded ionic chemical entity in many solutions and crystalline solids is demonstrated amply by the following facts. Freezing point studies[2] of uranyl chloride and uranyl nitrate solutions have shown that they behave as completely dissociated ternary electrolytes. Later studies by Crandall[3] have shown that two uranyl oxygens exchange only very slowly with solvent water in a uranyl chloride solution and are thus tightly bonded to the uranium, compared with the Cl^- ions or the water of solvation. Zachariasen[4] has shown that in uranyl compounds and in numerous uranates, the bond length to two of the oxygens is substantially shorter than to the other oxygens or associated groups. Studies[5] of the fluorescence and infrared spectra of uranyl salts and of the Raman spectra of aqueous uranyl solutions show that the three vibrational frequencies of the linkage are to a high degree independent of environment. This includes a symmetric stretching frequency at 860 to 880 cm^{-1}, an asymmetric stretching frequency at 930 to 960 cm^{-1}, and a bending frequency at 199 to 210 cm^{-1}.

All the above facts strongly support the picture that UO_2^{++} is highly covalently bonded. Additional direct evidence for this covalent bonding comes from our nuclear alignment studies. From the magnitude of the anisotropy of alpha emission as a function of temperature[6] we find that $|P| \sim 0.02$ cm^{-1}. If we should take $|Q| \sim 10$ barns, a U-O bond length of 1.63 Å, and should assume that the UO_2^{++} linkage is not covalent but entirely ionic, the calculated coupling is found to be too small by more than an order

[1] J. C. Eisenstein and M. H. L. Pryce, *Proc. Roy. Soc.* (*London*) **A229**, 20 (1955).

[2] C. Dittrich, *Z. physik. Chem.* **29**, 449 (1899).

[3] H. W. Crandall, *J. Chem. Phys.* **17**, 602 (1949).

[4] W. H. Zachariasen, *Acta Cryst.* **1**, 281 (1948).

[5] L. H. Jones and R. A. Penneman, *J. Chem. Phys.* **21**, 542 (1953) and associated references.

[6] J. W. T. Dabbs, L. D. Roberts, and G. W. Parker, *Physica* **24**, 456 (1958); L. D. Roberts, J. W. T. Dabbs, and G. W. Parker, *Proc. U.N. Intern. Conf. Peaceful Uses Atomic Energy, 2nd, Geneva, 1958* **15**, 322 (1958).

of magnitude. The observed magnitude of $|P|$ can be understood only in terms of a high degree of covalent bonding.

Extensive chemical and x-ray crystal structure studies of NpO_2^{++} show that it is physically very similar to the UO_2^{++} group. Of particular interest is the work by Jones and Penneman[5] on the infrared spectra of aqueous solutions of UO_2^{++}, NpO_2^{++}, PuO_2^{++}, and AmO_2^{++} as the perchlorates. They find that the asymmetric stretching frequency for XO_2^{++} corresponds to 965, 969, 962, and 939 cm^{-1} for U, Np, Pu, and Am. The remarkable constancy of these frequencies and thus of the corresponding force constants suggests that the detailed nature of the covalent bond is very similar throughout the sequence. This would similarly suggest that the contribution of this covalent bond to ζ should be very similar in magnitude and detailed character for each of these XO_2^{++} groups.

We note that there is ample crystallographic and microwave evidence that these XO_2^{++} groups are linear.

SIGN OF NUCLEAR QUADRUPOLE MOMENT

We are here interested only in UO_2^{++} and NpO_2^{++} groups. With Elliott,[7] Eisenstein and Pryce,[1] and Bleaney *et al.*,[8] we would suggest that the hyperfine structure coupling in NpO_2^{++} has a magnetic term very probably due predominantly to a $5f$ state, and an electric quadrupole coupling coming in part from this $5f$ charge distribution and in part from the covalent bonding charge. Eisenstein and Pryce consider the bonding charge to make the predominant contribution to ζ and suggest that ζ should be positive. On this basis, and from the fact that Q and ζ must have opposite signs, Pryce suggests $Q < 0$.

Other fairly direct experimental information on the sign of Q is meager in this region of Z. With increasing Z, the nuclear quadrupole moment Q (ref 9) falls from positive values to near zero at Bi, goes to a negative value at Ac^{227} ($Q = -1.7$ barns).[10] It then rises to $\sim +10$ barns for U^{233} and U^{235} and $\sim +5$ barns for Am^{241} and Am^{243} (ref 11). But these values for Ac, U, and Am are the only measured ones beyond Bi. These values do, however, accord with predictions of the nuclear shell model[12] which would also predict a positive Q for Np^{237}. Further, our results on the fission of an alpha emission from oriented U^{233} and U^{235} (ref 6; see "Fission Fragments from Aligned U^{233} and U^{235} Nuclei," immediately preceding this paper) would fit more easily in current barrier concepts if one assumed $Q > 0$ and $\zeta < 0$. One is therefore led to inquire whether there is a reasonable model for the XO_2^{++} covalent bond for which ζ would be negative.

---

[7] R. J. Elliott, *Phys. Rev.* **89**, 659 (1953).

[8] B. Bleaney *et al.*, *Phil. Mag.* **45**, 992 (1954).

[9] D. L. Hill, *Handbuch der Physik*, vol 39, 1957.

[10] F. S. Tomkins, M. Fred, and W. F. Meggers, *Phys. Rev.* **98**, 1514 (1955).

[11] T. E. Manning, M. Fred, and F. S. Tomkins, *Phys. Rev.* **102**, 1108 (1956).

[12] B. R. Mottelson and S. G. Nilsson, *Mat. Fys. Skr. Vid. Selsk.* 1(8) (1959) and associated references.

CALCULATION OF ζ

Cohen[13] has calculated the relativistic Hartree wave functions for atomic uranium, and using his code we have further calculated those for U^{5+}. It is these functions which we have used for both Np and U in our calculations. The states we have considered are the single-electron $5f^{5/2}$, $5f^{7/2}$, $6d^{3/2}$, $6d^{5/2}$, $7s^{1/2}$, $7p^{1/2}$, and $7p^{3/2}$ around a radon core. We note that in the inner region of the atom, which contributes predominantly to ζ, the change of charge from atomic uranium to U^{5+} only modifies the amplitude of the wave functions, that is to say, only changes them in the sense of a normalization but does not alter the "shape." These wave functions will almost certainly be substantially modified in the overlap region of the bond. Again, however, in the inner region of the atom important to ζ, the potential due to the nucleus vastly predominates over effects due to the bond. Thus modification of the wave function due to bond formation will again only affect the wave function in the important region for quadrupole coupling in the sense of a normalization. This should also be true of exchange effects. The above s, d, f, and p functions should also be the only ones which contribute importantly to ζ, since states of higher angular momentum or principal quantum number have a much smaller amplitude near the nucleus. Thus we propose that these states are the predominant ones in the description of the nuclear quadrupole coupling, that is, in the value of ζ.

We now wish to calculate ζ for all possible hybrids of these functions. The relativistic wave functions which we have are states of good total angular momentum j and j_z, whereas chemical bonds, at least for the lighter elements, generally are thought to correspond more to states of good orbital angular momentum l and m_l. That is, formation of the chemical bond tends to maximize the charge density along the bond axis at the expense of the "double lobe" associated with spin-orbit coupling. Thus one will certainly have hybrid states, for example, of the form $(\cos\alpha\, 6d^{3/2} + \sin\alpha\, 6d^{5/2})$. In general, in taking the expectation value $\langle i|P_2(\cos\theta)|i\rangle$, only states of a given j_z mix. States of different j_z simply add in their contribution to ζ. Then for the calculated uranium wave functions, the following equations summarize the possible values of ζ for a single electron in atomic units.

SUMMARY OF BONDING CALCULATION FOR s-d HYBRIDIZATION

$j_z = 1/2$:

$$\zeta_{1/2}^{sd} = 3.83386N_{2,3/2}^2 + 3.27655N_{2,5/2}^2 - 2.08800N_{2,3/2}N_{2,5/2} - 5.77476N_{0,1/2}N_{2,3/2} - 0.20881N_{0,1/2}N_{2,5/2} \; .$$

$j_z = 3/2$:

$$\zeta_{3/2}^{sd} = -3.83387N_{2,3/2}^2 - 0.81914N_{2,5/2}^2 - 5.14068N_{2,3/2}N_{2,5/2} \; .$$

$j_z = 5/2$:

$$\zeta_{5/2}^{sd} = -4.09569N_{2,5/2}^2$$

[13] S. Cohen, private communication.

SUMMARY OF BONDING CALCULATION FOR *f*-*p* HYBRIDIZATION

$j_z = \frac{1}{2}$:

$$\zeta^{fp}_{1/2} = 11.29398N^2_{1,3/2} - 45.90766N_{1,1/2}N_{1,3/2} + 2.59459N^2_{3,5/2} - 0.70641N_{3,5/2}N_{3,7/2} + $$
$$+ 2.49243N^2_{3,7/2} + 0.11456N_{1,1/2}N_{3,5/2} + 0.02259N_{1,3/2}N_{3,5/2} + 0.01133N_{1,3/2}N_{3,7/2} \ .$$

$j_z = \frac{3}{2}$:

$$\zeta^{fp}_{3/2} = -11.29398N^2_{1,3/2} + 0.64865N^2_{3,5/2} + 5.0402N_{3,5/2}N_{3,7/2} + $$
$$+ 1.49538N^2_{3,7/2} + 0.05532N_{1,3/2}N_{3,5/2} + 0.00844N_{1,3/2}N_{3,7/2} \ .$$

$j_z = \frac{5}{2}$:

$$\zeta^{fp}_{5/2} = -3.24323N^2_{3,5/2} - 5.60478N_{3,5/2}N_{3,7/2} - 2.48543N^2_{3,7/2} \ .$$

$j_z = \frac{7}{2}$:

$$\zeta^{fp}_{7/2} = -3.48940N^2_{3,7/2} \ .$$

In the above, the N are the coefficients of admixture of the state described by the subscript. The first number in the subscript is the orbital angular momentum and the second the total angular momentum. For example, $N_{2,5/2}$ corresponds to the coefficient of the $d_{5/2}$ state admixed into the hybrid bond. Figures 1, 2, and 3 give the corresponding values of P in cm^{-1} calculated from the above equations for a nucleus of spin $\frac{5}{2}$ and $Q = +10$ barns for various degrees of hybridization expressed in degrees (α).

The small component of these relativistic wave functions is found to play an important role particularly for the *s*-*d* hybrids.

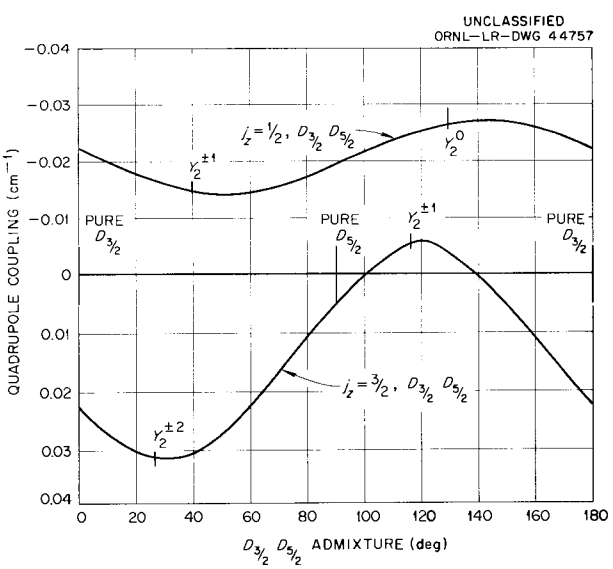

Fig. 1. Nuclear Quadrupole Coupling $Q = +10$ Barns, $I = \frac{5}{2}$. U^{5+} wave functions.

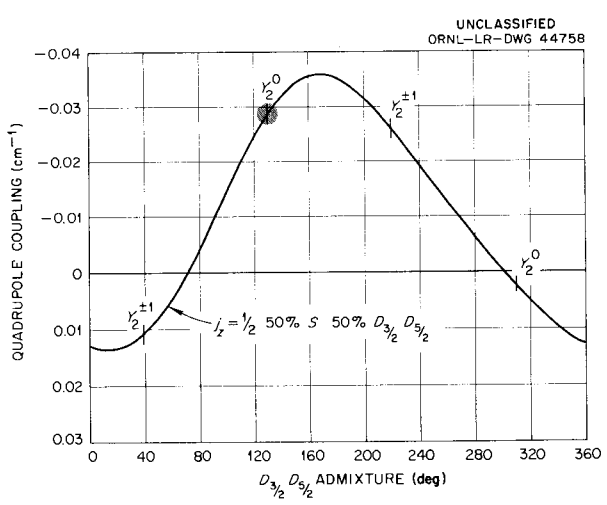

Fig. 2. Nuclear Quadrupole Coupling $Q = +10$ Barns, $I = \frac{5}{2}$. U^{5+} wave functions.

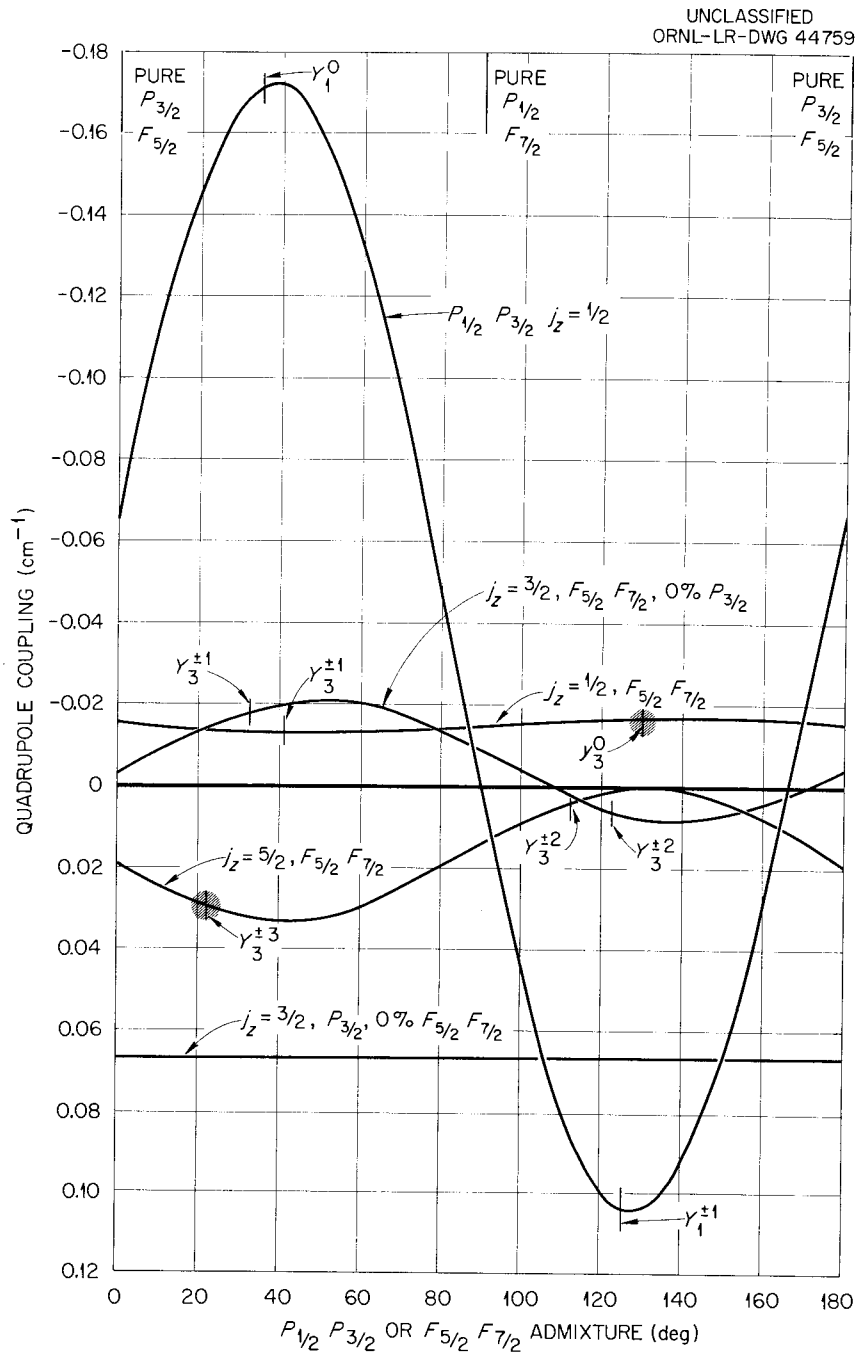

Fig. 3. Nuclear Quadrupole Coupling $Q = +10$ Barns, $I = 5/2$. U^{5+} wave functions.

INTERFERENCE EFFECTS

The principal point demonstrated by these graphs is that there are no important interference effects arising from the radial properties of the wave functions such that the sign of $\langle i|P_2(\cos\theta)/r^3|i\rangle$ is different from $\langle i|P_2(\cos\theta)|i\rangle$. In more pictorial terms, it is not possible to construct a hybrid single-electron state which would appear as a "column" of charge at large distances from the uranium nucleus but nevertheless as a "ring" of charge at small radius.

π BONDING

The above equations and graphs correspond to eigenvectors for which j_z is a good quantum number, and for $j_z \neq 0$ they describe a paramagnetic state.

Our earlier discussion of the near equality of the infrared absorption frequencies of UO_2^{++} and NpO_2^{++} suggested the great similarity of the covalent bonding in these ions. The UO_2^{++} is only very weakly magnetic and this magnetism is temperature independent. It certainly does not arise from the orientation of free electron spins. Thus if states with $j_z \neq 0$ are involved in the bond, the magnetism must be quenched by combining in equal amounts states with $j_z = +|j_z|$ and $j_z = -|j_z|$. This presents no problem for hybrids involving $m_l = 2$, 3, or greater. Here the coupling is independent of the sign of j_z and is given by the above equations and graphs. For hybrid bonds involving $m_l = \pm 1$, that is, π bonding, quenching the orbital moment leads to an electric field axis (and thus to a symmetry axis for quadrupole coupling) perpendicular to the O-X-O direction. The Hamiltonian for the hyperfine structure coupling in NpO_2^{++} as given by Bleaney *et al.* [Eq. (1) of "Angular Distribution of Alpha Particles Emitted by Oriented Np^{237} Nuclei," this report] corresponds to a higher degree of symmetry around the O-X-O axis than this, and thus quenched π bonding is excluded to a high degree in NpO_2^{++}. Because UO_2^{++} is not paramagnetic and because of its structural similarity to NpO_2^{++}, a large percentage of π bonding would seem to be unlikely here. Figure 3 shows that the coupling from the P state is large and could make a large contribution to ζ with only a small percentage admixture. However, on the basis of the above, this could only appear as a quenched π bond, and thus this state probably does not make an important contribution to the bond.

The above argument may be presented more formally as follows: The operator corresponding to quadrupole coupling is given by

$$\mathcal{H} = K\left[(I\cdot J)^2 + \frac{1}{2}(I\cdot J) - \frac{1}{3}I^2J^2\right] ,$$

where I and J are the nuclear and electronic angular momentum operators. This may be rewritten in a form with terms diagonal in the j, m representation plus other terms involving the operators L_+^2 and L_-^2. For a quenched π bond the wave function will be of the form

$$\psi_\pi = \frac{1}{\sqrt{2}}\,(Y_l^1 + Y_l^{-1}) ,$$

where the $Y_l^{\pm 1}$ are spherical harmonics. With ψ_π, the operators L_+^2 and L_-^2 lead to off-diagonal terms in the energy matrix. Comparison of a detailed calculation of this type with experimentally observed energy levels of Bleaney *et al.*[8] rejects any appreciable amount of π bonding in NpO_2^{++}.

δ BONDING

We note from the graph, Fig. 3, that delta bonding, that is, a wave function involving predominantly $Y_l^{\pm 2}$, gives only a very small value of P for $l = 3$. For a pure $Y_3^{\pm 2}$ state, $P = 0$, and the small value calculated above arises from the fact that relativistic $f_{5/2}$ and $f_{7/2}$ states have somewhat different radial wave functions and thus a pure l value at all radii cannot be separated. The points marked Y_l^m on the graphs correspond to "pure" functions at large radius, that is, in the bonding region.

SUMMARY

In the above discussion we have made the points that (1) the bond is clearly covalent, (2) no important interference effects occur, (3) π bonding is excluded, and (4) that f_δ bonding will not contribute to P in any case. Thus P must arise either from σ bonding or from bonding states dominated by $Y_3^{\pm 3}$ or $Y_2^{\pm 2}$. The conclusion of Eisenstein and Pryce that Np^{237} has a negative quadrupole moment rests on the assumption that σ bonding dominates. We make the point that one can only reverse their conclusion by assuming the bond to have roughly half its charge (two electrons) involved in the covalent aspect of the bond and the other two electrons in a nonbonding configuration constructed from $Y_2^{\pm 2}$ or $Y_3^{\pm 3}$. The $Y_3^{\pm 3}$ appears to be improbable in NpO_2^{++} because of the Pauli principle, since g-factor measurements strongly indicate that the magnetic electron is in this state. This leaves only $Y_2^{\pm 2}$. However, this has problems also. It is unusual in the chemistry of bonding to find such a strong covalent bond with the oxygens effectively monovalent and with two seemingly available electrons on an adjacent atom in a nonbonding configuration. Here one is forced to consider this strange suggestion because the chemically much more reasonable configuration proposed by Eisenstein and Pryce leads to rather unexpected nuclear results. The XO_2^{++} bond is unique in many ways, however, so a further theoretical study of the Slater integrals involved in the actinide bonding configuration may be worthwhile.

SAMPLE SCATTERING CORRECTIONS IN NEUTRON BEAM EXPERIMENTS[1]

H. W. Schmitt

Calculations have been made of the effect of single and multiple neutron scattering in a disk of sample material. This effect (frequently referred to as average path length effect or correction), which increases the effective thickness of the sample relative to the geometric thickness in the direction of the incident neutrons, must be considered in a large class of neutron measurements, cross-section measurements in which the total number of reactions in a sample is measured, for example. The integrals, taking account of exponential attenuation, have been evaluated for the case of a beam of neutrons incident along the axis of the disk. Results are given analytically and graphically in the report[1] abstracted.

[1]Abstract of ORNL-2883.

MILLIMICROSECOND TIME-OF-FLIGHT: INSTRUMENTATION

J. H. Gibbons W. M. Good R. F. King[1] J. Judish[1]

The measurement of neutron total and capture cross sections has been routine during the last year; the results are described under these headings in this report. The future work with the millimicrosecond-pulsed beam and time spectrometer depends upon the success of some developments under way but not entirely completed. Among these developments is a better understanding of the circumstances surrounding the production of ion bursts of a specified burst duration. Following is the abstract of a paper on this subject by T. K. Fowler[2] and W. M. Good that has been submitted for publication:[3]

Many modern-day experiments in nuclear physics, particularly neutron physics, require short-duration bursts of ions whose definition in energy and angle corresponds to an ion beam of rather high quality. This paper treats the problem of producing bursts of ions by sweeping a beam across an operture. By considering several examples of electric-field-sweeping, it is shown that (1) an essential equivalence exists between different time-varying wave forms that may be employed, and that (2) the beom quality, as measured by energy and/or angular spread, is necessarily diminished in the process of burst production. In a general way it is shown that if a steady "monoenergetic" beam, characterized by y component of momentum spread Δp_y and object size Δy, is chopped by beam sweeping, then there is a relation which in its simplest form is given by $\Delta E \Delta t = \Delta p_y \Delta y$. In this relation ΔE is the energy that must be introduced into a monoenergetic beam in order to produce bursts as short as Δt. Finally, it is shown that beam bunching results in diminished beam quality. An example is klystron bunching of a nearly parallel pulsed beam. In this case there is a relation, the simplest form of which is

$$\Delta E_a \Delta t_a = \Delta E_b \Delta t_b \ ,$$

relating the product $\Delta E \Delta t$ before bunching to that which exists after bunching.

From a better understanding of the conditions that limit the shortness of burst achievable with a given ion beam, a deliberate step has been taken to produce ion bursts of 0.5 to 1 mμsec duration for 1 ma peak current of protons. The scheme is to preacceleration-chop a beam to a duration of 10 mμsec or less and by synchronized postacceleration chopping to further clip the 10-mμsec bursts to 1 mμsec or less. The post-acceleration chopping is to be achieved by means of approximately ½-m-long deflector plates to which is applied a 12-Mc/sec sweep voltage synchronized with the 10-mμsec ion bursts.

Terminal modifications have been completed in preparation for installing the Duo-Plasmatron ion source. Principally, these modifications include a new 400-cps 3-kw alternator, an enlarged spinning for greater volume for components, and a circulating Freon cooling system to permit cooling of components in the high-voltage terminal.

[1] Instrumentation and Controls Division.

[2] Neutron Physics Division.

[3] "A Theory on Obtaining Short Bursts of Ions from a Beam of Ions," submitted to *Nuclear Instruments*.

SEMICONDUCTOR SURFACE BARRIER COUNTERS

F. J. Walter J. W. T. Dabbs L. D. Roberts S. H. Hanauer[1]

In a previous semiannual report[2] a theoretical model was presented to describe the behavior of semiconductor surface barrier counters. Experimental evidence was presented which demonstrated that this model described the observed characteristics of germanium counters quite adequately provided that the counter was operated at a temperature where the bulk resistivity of the semiconductor was relatively small.

At very low temperatures, where the resistivity of the bulk material is very large, the equations[2] for pulse height and rise time based on the Schottky

[1] Instrumentation and Controls Division.

[2] F. J. Walter *et al.*, *Phys. Ann. Prog. Rep. Mar. 10, 1959*, ORNL-2718, p 53.

barrier remain good approximations in the absence of applied potential bias. However, when a bias is applied, the assumption that significant electric fields do not exist outside the barrier region is no longer valid. Thus as the temperature is lowered the total applied potential difference may be shared in some manner between the barrier region and the remainder of the crystal. An upper limit on the potential gradient in the bulk material is assumed to be set by the breakdown field, which is about 10 v/cm in rather pure n-type germanium at very low temperatures. When significant fields exist in the bulk material, the counter behavior may approach that of a conduction counter; that is, the counter becomes sensitive to radiation throughout its volume, and its effective capacitance approaches that determined by its over-all dimensions and dielectric constant. If C in the equation for pulse height is replaced by this new capacitance, then the approximate pulse height can be calculated.

It is difficult to make an estimate of the pulse rise times for this case, since the sharing of the potential distribution between the barrier region and the bulk region is unknown. However, for counters many times thicker than the barrier region, the rise time at liquid-helium temperatures may in general be expected to be significantly longer than at 77°K. In the limit of an approximately uniform field throughout the bulk region, the minimum traversal time for the electrons may be estimated from

$$t \cong \frac{d}{\mu_e E_c}, \qquad (1)$$

where d is the crystal thickness and E_c is the breakdown field. Assuming[3] that $\mu_e E_c = 1.3 \times 10^6$ cm/sec for rather pure germanium at helium temperatures, we obtain $t \cong 7 \times 10^{-7}$ sec/cm.

The behavior of the counter in both temperature regions can be discussed in terms of a simplified equivalent circuit. In Fig. 1, all external circuits, including means for applying the potential bias, are to be considered as connected to points 1 and 2. The effective resistance and capacitance associated with the barrier region are represented by R_1 and C_1. Similarly, R_2 and C_2 represent these quantities for the remainder of the crystal;

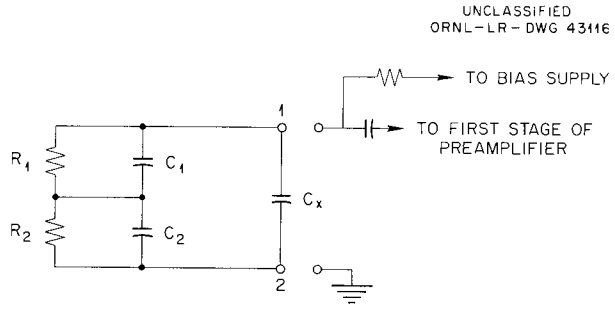

Fig. 1. Equivalent Circuit for Surface Barrier Counter.

C_x represents the total stray capacitance in external circuits.

When an ionizing event produces free charge carriers in the crystal, the drift of the carriers in the electric field induces charges at the terminals 1 and 2.

At higher temperatures, R_1 is very large, R_2 is essentially zero, and C_1 is just the Schottky capacitance of the barrier region times the area (A) of the counter.

When the resistivity of germanium is very large, there can be a significant potential gradient throughout the crystal associated with an applied bias and the steady-state current flow. In this case the charge carriers may be separated across the total thickness of the crystal and the correct capacitance (CA) approaches $CA = C_1C_2/(C_1+C_2)$.

In the absence of applied bias, the Schottky barrier equations predict that at any temperature a significant surface barrier should exist provided that $-q\psi_0 > kT$. Consequently, it would be expected that the counters would detect ionizing events even under this circumstance. However, it should be pointed out that when no external bias is applied the charge carriers will traverse only the barrier region during the time intervals of interest, regardless of the resistivity of the bulk material. At very low temperatures, where the resistivity of the germanium[3] is very large, the absence of significant potential gradients in the bulk material may be represented by a large value for R_2. If it is assumed that this R_2 is essentially infinite compared with the impedance of C_2, the pulse height at zero external bias at very low temperatures is given by

$$V = \frac{qWC_2}{C_1C_x + C_1C_2 + C_2C_x}\,\frac{\eta}{\epsilon}. \qquad (2)$$

[3] S. H. Koenig and G. R. Gunther-Mohr, *Phys. and Chem. Solids* 2, 268 (1957).

One counter has been operated successfully at temperatures as low as 0.2°K. Figure 2 shows the pulse height resulting from bombardment of this counter with alpha particles from a relatively thick Np^{237} source, as a function of applied bias at 77 and 0.2°K. In this case, both pulse-height curves correspond to the largest pulses observed from the thick source. The value of ϵ/η corresponding to the plateau region of the 0.2°K curve is 2.8 ev/pair and the values ϵ/η for the 77°K curve are 2.9, 2.8, and 2.8 ev/pair for the 1-, 2-, and 3-v points respectively. These values of ϵ/η are based on the measured effective capacitances obtained by injecting a known amount of charge into the counter circuit with a precision pulser. The rather striking difference between the two curves of Fig. 2 illustrates the difference between the behavior of these counters in the high and low temperature regions.

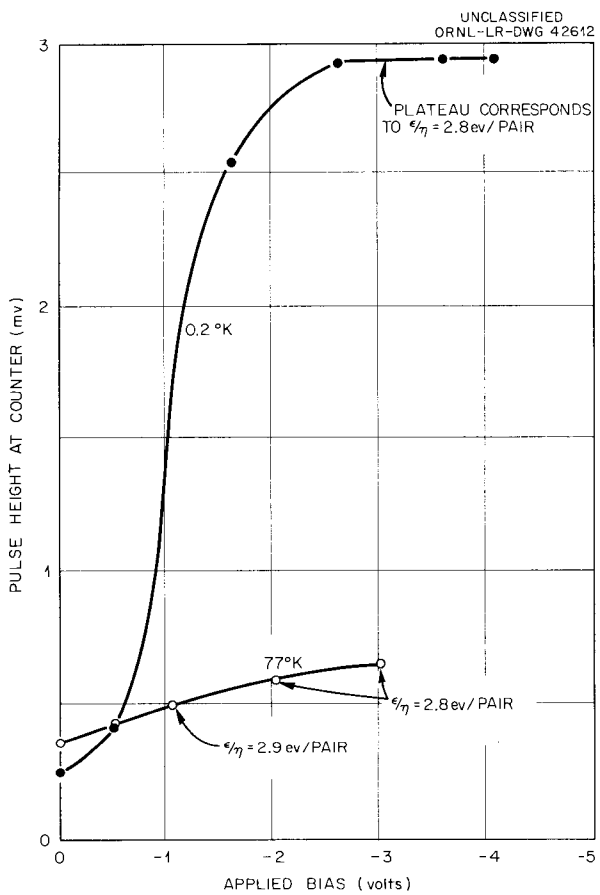

Fig. 2. Comparison of Behavior of Germanium Surface Barrier Counter at "High" and Low Temperatures.

The rise times of pulses resulting from bombardment with monoenergetic alpha particles at 77°K were measured for a 0.7-cm-thick counter and for a 0.1-cm-thick counter. In both cases, the experimentally determined rise time was $\leq 2 \times 10^{-8}$ sec, which is in reasonable agreement with the predictions of simple surface barrier theory. At 4.2°K, the pulse rise time for the 0.7-cm-thick counter was 2×10^{-7} sec. Since the carrier mobilities would be expected to be larger at 4.2°K than at 77°K, this relatively long pulse rise time, as well as the results shown in Fig. 2, indicates that at very low temperatures (where the resistivity of germanium approaches that of a good insulator) there were significant electric fields extending through a substantial portion of the crystal when external bias was applied.

It was noted that these counters are sensitive to the presence of magnetic fields, particularly when they were operated in the liquid-helium temperature range. At these temperatures, application of magnetic fields of a few hundred gauss appeared to have a slight effect on the pulse height at a given bias voltage. Fields of a few kilogauss parallel to the counting surface completely suppressed the pulses resulting from alpha-particle bombardment.

POLARIZED ION SOURCE

J. E. Sherwood S. J. Ovenshine R. F. King[1]

There is considerable interest at this time in medium-energy nuclear reactions in which one of the reactants is polarized. Such conditions may be obtained by ionizing a beam of neutral atoms having nuclear polarization, and then accelerating these ions to the desired energy. Efforts of this type are under way at the University of Minnesota and Yale University in this country and at several European universities.

It was decided to build a test model of such an ion source independent of the accelerator. The

[1] Instrumentation and Controls Division.

machine would employ deuterium gas since the resultant deuterons can conveniently be tested for polarization by the $T(d,n)He^4$ reaction at 100 kv, as pointed out by Galonsky, Willard, and Welton.[2]

The present status of the apparatus, which consists of the following units, can conveniently be described in terms of the block diagram (Fig. 1):

Atomizer. – The gas (hydrogen at present) is fed into a Woods-type discharge tube which operates at 15 kv. This tube is mounted in a vacuum chamber and contains a slit, ¾ in. high by 0.030 in. wide, which serves as a molecular beam source. The optimum gas pressure for beam generation, some tenths of a millimeter of mercury, supports the discharge very nicely. Examination of the discharge by means of a hand spectroscope reveals that it is rich in Balmer radiation, which is characteristic of atomic hydrogen. However, quantitative determination of the extent of dissociation has not yet been made.

The atomizer chamber is pumped by means of a 10-in. oil diffusion pump and Freon-cooled baffle. A separation chamber equipped with a 6-in. oil diffusion pump and baffle is provided to isolate the source chamber from the polarizer chamber.

Polarizer. – Polarization is achieved by selection of appropriate atomic hyperfine states by means of the "flop-in" technique. Inasmuch as a premium is placed on intensity, the beam must be as short as possible. Thus the stray fields of the A and B magnets constitute a strong field in the C or transition region. In the present machine, this field is about 1630 gauss, which corresponds to a flop frequency of about 4300 Mc/sec. Since the line width cannot reasonably be much greater than ½ Mc/sec, the magnetic field must be stable to 1 part in 10^4. The r-f exciter (under construction) consists of a high-Q resonant hairpin fed by the fifth harmonic of an 800-Mc/sec oscillator. The polarizer chamber is evacuated by a 4-in. mercury diffusion pump and liquid-nitrogen-cooled baffle.

Detector and Ionizer. – The neutral beam intensity is measured by means of a modified Pirani gage which is so mounted as to permit traversal across the beam or removal from the beam.

The ionizer is shown schematically in Fig. 2. The beam is seen to pass between two parallel cathodes from which electrons are accelerated to about 100 ev energy. The grid structure is arranged in 12 segments along the beam in such a way that small potentials can be applied between adjacent segments in order to facilitate collection of the ions. The ionizer is undergoing tests to determine optimum operating conditions. The detector and ionizer are mounted in a chamber which is evacuated by means of a 6-in. mercury diffusion pump equipped with a liquid-nitrogen-cooled baffle.

Results to Date

The neutral beam detector has been calibrated for hydrogen by exposing it to known pressure changes. Measurements were then made of the direct beam intensity. The result, 3×10^{14} $cm^{-2} \cdot sec^{-1}$, agrees with the gas-kinetic estimate.

UNCLASSIFIED
ORNL-LR-DWG 45571

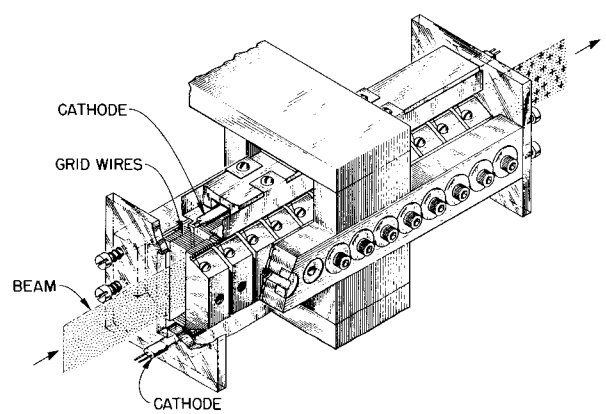

Fig. 2. Schematic Sketch of Atomic Beam Ionizer.

UNCLASSIFIED
ORNL-LR-DWG 45570

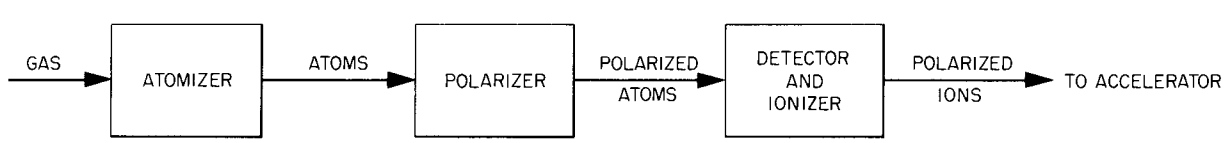

Fig. 1. Block Diagram of Polarized Ion Source.

[2] A. Galonsky, H. B. Willard, and T. A. Welton, *Phys. Rev. Letters* **2**, 349 (1959).

One can distinguish between atoms and molecules by turning on the deflecting magnet. A drop in detector output indicates the presence of atoms. Such a drop was indeed observed, but the detector circuit was sufficiently unstable as to make a quantitative determination of dissociation unfeasible.

SPHERICAL ABERRATION OF GRID-TYPE ELECTROSTATIC LENSES

N. B. Alexander[1] R. M. Chester[2] D. G. Maeder[3]

INTRODUCTION

In contrast to the situation in light optics, efforts to produce low-aberration electron (or ion) optical systems have so far met with limited success only. In particular, the aperture defect, which constitutes the essential limitation in the performance of most electron optical devices, can be shown to be incurable[4] as long as one requires the electromagnetic fields to be produced by charges (or currents) located entirely outside the beam region. This is certainly the case for designs of all electrostatic lenses that are easy to construct (Fig. 1), namely, those consisting of two cylinders, two parallel plates with apertures, or cylinder–aperture-plate combinations. The general field pattern produced by the basic two-element lens cannot be changed very much by combining cylinders and/or apertures of different diameters. Three-element combinations allow a greater variety, leading to various lens designs with reduced spherical aberration.[5] In spite of several efforts aimed at optimizing the unipotential three-element lens configuration (*Einzel-Linse*), its residual spherical aberration calls for further developments. A generalization of the unipotential lens concept[6] would approach the ideal field pattern with increasing number of elements, but its practical application is made difficult by the requirement of having large voltages across many small gaps between adjacent elements.

Drastic variations of the field pattern can, however, be produced when one accepts the presence of conducting obstructions in the cross section of the beam, such as a wire grid. The loss of beam current caused by this technique is more than compensated by a newly gained versatility in fighting the aberrations. Grid-type lenses have in fact been constructed, and some performance data experimentally determined, by Liebmann. The object of our paper is to present (1) systematic calculations of the focusing properties of the basic (plane grid + cylinder) element, which is easy to construct, (2) a search for a zero-spherical-aberration arrangement, (3) additional numerical data that show the dependence of focusing and spherical aberration on geometrical parameters such as gap orientation, gap width, and curvature of gap corners. Finally, a few calculations on two-dimensional fields were done.

We shall not be concerned with space-charge effects, except for quoting estimates of the corrections they will introduce under conditions where such corrections are known to be small.

[1]Mathematics Panel.

[2]Instrumentation and Controls Division.

[3]Now at CERN, Geneva, Switzerland.

[4]O. Scherzer, *Z. Physik* 101, 593 (1936).

UNCLASSIFIED
ORNL-LR-DWG 45564

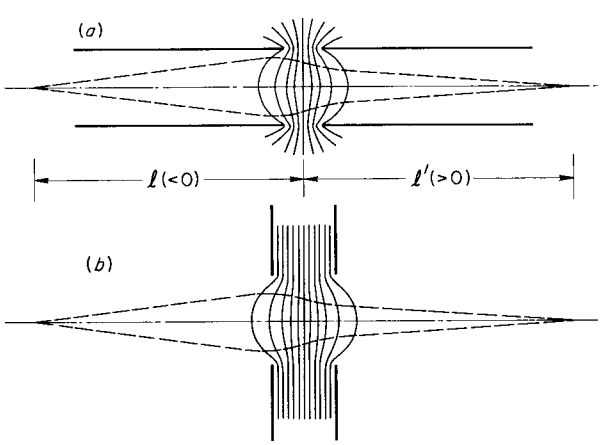

Fig. 1. Electrostatic Lens Designs: (*a*) Two Cylinders; (*b*) Parallel Plates with Apertures.

[5]V. K. Zworykin *et al.*, *Electron Optics and the Electron Microscope*, chap. 17, Wiley, New York, 1945.

[6]A. Recknagel, *Z. Physik* 117, 63 (1940); O. Scherzer, *Z. Physik* 101, 593 (1936).

ABERRATION-FREE LENSES

In describing the characteristics of a lens system, we shall use the notations shown in Fig. 2, with the understanding that f, f', p, and p' are no longer constants, but are functions of r: $f(r)$, $f'(r)$, $p(r)$, and $p'(r)$, when aberrations are taken into account. Thus, the principal planes are bent into "principal surfaces" $P(r)$ and $P'(r)$, and the focal points are replaced by "focus-position curves" $F(r)$ and $F'(r)$, where r is the intersection of the ray with $z = 0$. These modifications are illustrated in Fig. 3 for those rays which enter the system parallel to the z axis from the left; the symbols are distinguished by a prime from the corresponding symbols applying to rays emerging parallel to the z axis to the right. In considering configurations containing electrodes that reach into the particle beam, the double wire grid (Fig. 4*a*) presents a direct analog to a refracting lens in light optics,[7] and should therefore allow exact annulation of spherical aberration by properly shaping the grids. However, the difficulty of shaping two highly transparent grids into complicated surfaces within narrow tolerances – and of maintaining their shapes and relationship – seems to preclude practical use of this scheme.

The unipotential-type design proposed in Fig. 4*b* is the analog of the Fresnel lens in light optics. As the electric field between the concentric cylinders is most effective for deflecting the particles (rather than changing their energy), such a system should be capable of extremely large aperture-to-focal-length ratios. The distortion caused by the necessarily finite number of cylinders (or toroids) and the difficulty that all the leads must be shielded appear to have prevented any practical applications so far.

[7] M. Knoll and E. Ruska, *Ann. Physik* [5]12, 607 (1932).

UNCLASSIFIED
ORNL-LR-DWG 45974

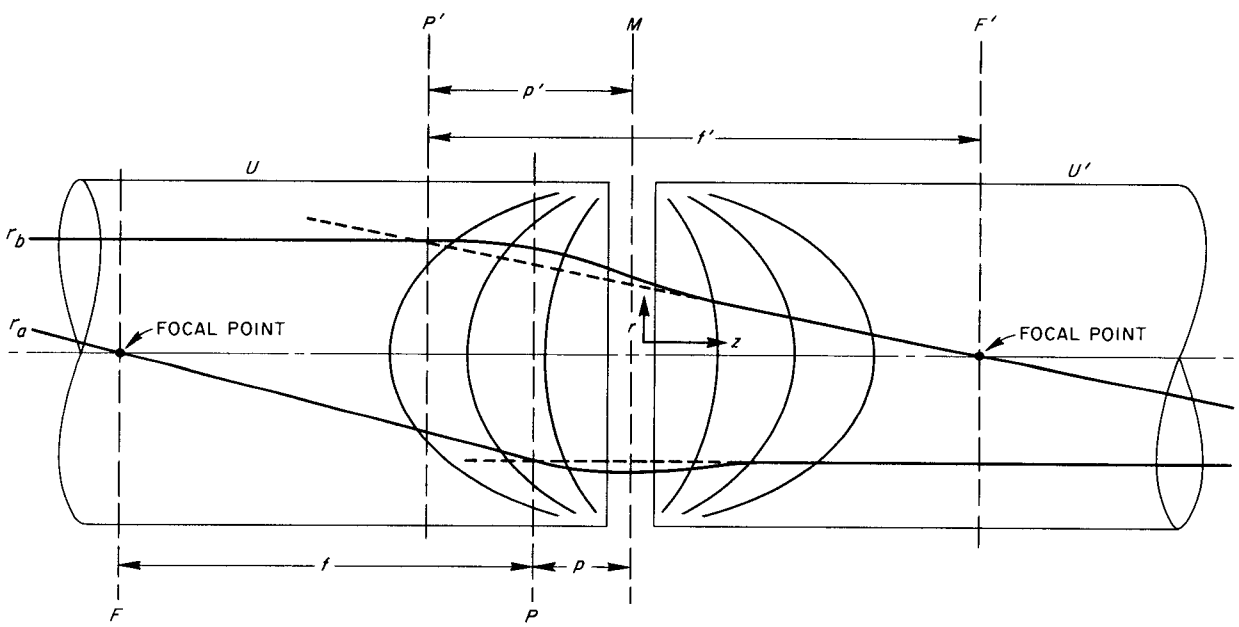

M = REFERENCE PLANE OF LENS
r_a = FIRST PRINCIPAL RAY
r_b = SECOND PRINCIPAL RAY
$U'/U > 1$

P = FIRST PRINCIPAL PLANE
P' = SECOND PRINCIPAL PLANE
f = FIRST FOCAL LENGTH
f' = SECOND FOCAL LENGTH

Fig. 2. Thick-Lens Terminology.

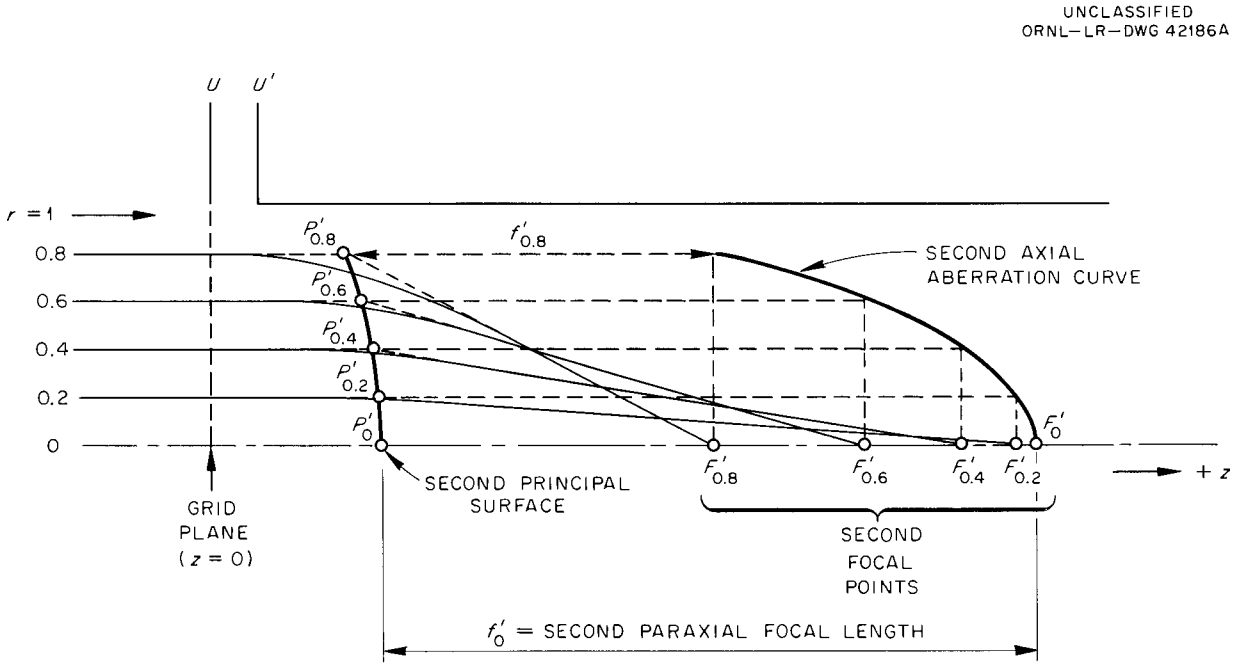

Fig. 3. Terminology as Applied to Grid-Type Lenses.

Figure 4*c* shows the design principle which we shall follow in this paper. While it may still be considered difficult to accurately maintain *one* grid in a prescribed shape, this problem should be less critical than for the configurations 4*a* and 4*b*. The special case of a plane grid was studied in some detail, in order to show the influence of gap width and gap shape on the characteristics of a lens system that is easy to construct, and on which some experimental data are already available from Liebmann. Various grid shapes were then assumed in a trial-and-error search for a low-aberration system. The most favorable grid shape was then tried with different gap widths for a final adjustment. In addition, two cases of two-dimensional lenses were investigated.

The trial-and-error procedure was based mainly on the calculation of "second" parameters p' and f' (at a fixed U/U' ratio), which were considered more descriptive of typical applications than p and f.

ELEMENTARY THEORY OF BASIC (PLANE GRID + CYLINDER) LENSES

Dependence of Paraxial Focal Lengths on Voltage Ratio

In order to abbreviate our notation, all lengths [in particular, r, z, $p(r)$, $f(r)$] are expressed in units of the inner cylinder radius ($r = R = 1$).

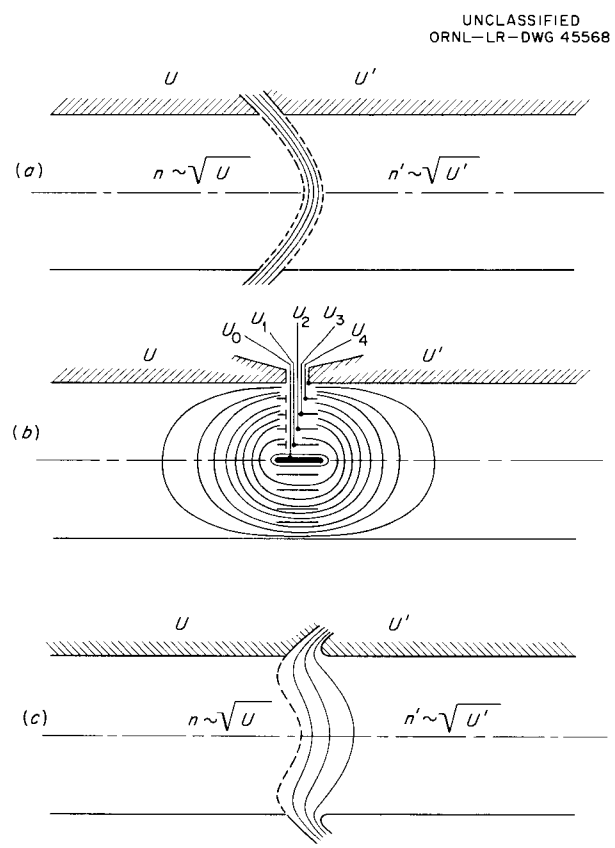

Fig. 4. Electrostatic Lens Configurations: (*a*) Double Wire Grid; (*b*) Concentric Cylinders; (*c*) Single, Shaped Wire Grid.

Furthermore, we set $2e/m = +1$ and assume the particle to have zero velocity at ground potential, so that its velocity at a potential $U < 0$ can be written

$$v = \sqrt{-U} \ . \tag{1}$$

The grid coincides with $z = 0$, reference plane, and p_0' and f_0' are the limiting values of $p'(r)$ and $f'(r)$ for $r \to 0$, as indicated in Fig. 5. Unprimed symbols will be reserved for describing the backward (or "first") focus, F, which is located in the region of potential U (i.e., to the left of the grid). Correspondingly, the potential of the cylinder (which encloses the forward focus, F') is called U'.

To calculate f', we note that practically all the radial acceleration takes place within the region $z = 0 \ldots 2p$, or during a transit time

$$\tau \cong \frac{2p}{\sqrt{1/2\,(-U - U')}} \ , \tag{2}$$

assuming an average potential $1/2\,(U + U')$. The average radial potential gradient in this region is related to the axial gradient by a geometry-dependent function which is roughly proportional to r, so that we may write

$$\left\langle \frac{\partial U}{\partial r} \right\rangle_{0\ldots 2p} = \frac{r}{g(r)} \cdot \frac{U' - U}{2p} \ , \tag{3}$$

where $g(r)$ is approximately constant for a given gap configuration. Particles entering parallel to the axis will therefore acquire a radial velocity component

$$-v_r' = \tau \frac{e}{m} \left\langle \frac{\partial U}{\partial r} \right\rangle = \tau \cdot \frac{1}{2} \cdot \frac{r}{g(r)} \cdot \frac{U' - U}{2p}$$

$$= \frac{r}{g(r)} \cdot \frac{U' - U}{\sqrt{2(-U' - U)}} \tag{4}$$

during the period τ, while their total velocity changes from $v = \sqrt{-U}$ to $v' \cong \sqrt{-U'}$. For $z > 2p$, the particle trajectory approximates a straight line whose angle against the z axis is given by

$$\sin \alpha' = \frac{v_r'}{v'} = \frac{-r}{g(r)} \frac{U' - U}{\sqrt{2U'(U' + U)}} = \frac{-r}{g(r)\,\Phi'} \ , \tag{5'}$$

where

$$\Phi' \equiv \frac{\sqrt{2U'(U' + U)}}{(U' - U)} \ . \tag{6'}$$

UNCLASSIFIED
ORNL-LR-DWG 45565

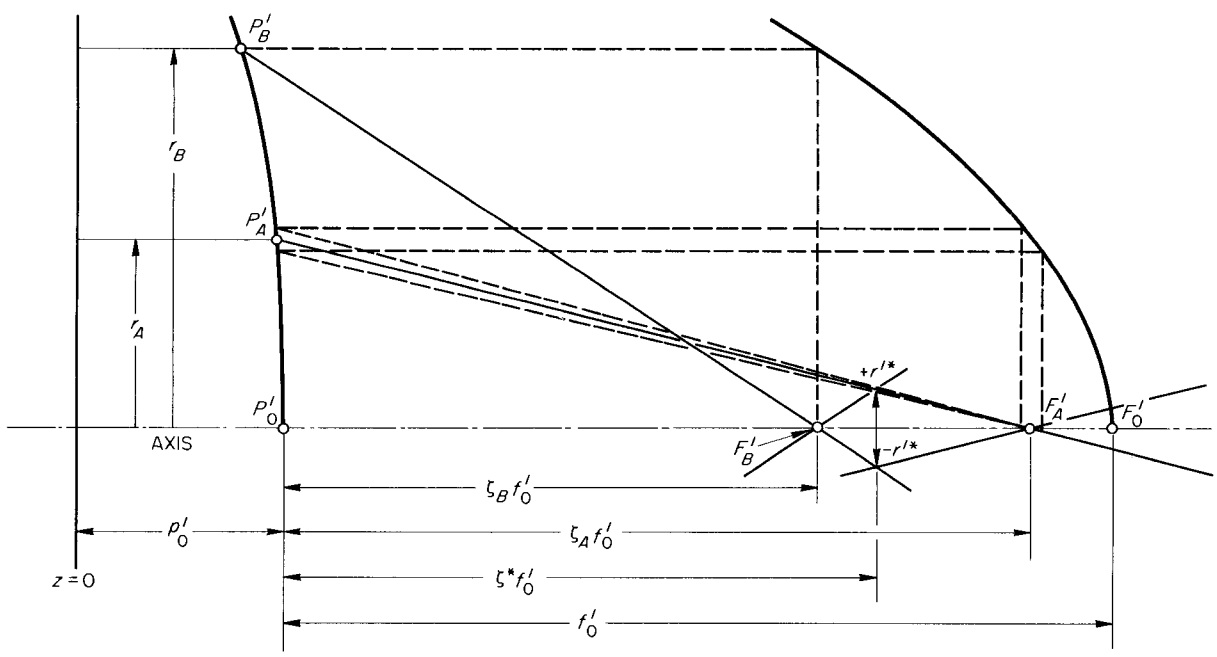

Fig. 5. Terminology Used in Approximate Calculations.

This straight line, originating at point $P = \left(p(r), r\right)$, intersects the axis at

$$z_F' = p'(r) - r \cot \alpha' ,$$

so that the focal length as a function of the radius of incidence becomes

$$f'(r) = z_F' - p'(r) = -r \cot \alpha' . \qquad (7')$$

First-order approximation now gives the paraxial focal length

$$f_0' = \lim_{\alpha' \to 0} \frac{r}{\sin \alpha'} = g_0 \cdot \Phi' , \qquad (8')$$

where g_0 stands for $\lim_{r \to 0} g(r)$.

Similar arguments, applied to the trajectories of particles coming from the backward focus, F, suggest that the radial velocity $+v_r$ should initially be equal to expression (4) in order to approach zero for $z > 2p$ if the radius r' in that region is to approach the r value inserted in (4). The angle of the incident ray against the axis (at $z = 0$) is therefore given by

$$\sin \alpha = \frac{v_r}{v} = \frac{+r}{g(r)\,\Phi} , \qquad (5)$$

where

$$\Phi \equiv \frac{\sqrt{2U\,(U' + U)}}{U' - U} = \sqrt{\frac{U}{U'}} \cdot \Phi' , \qquad (6)$$

and the focal length becomes

$$f(r) = -r \cot \alpha , \qquad (7)$$

or in the limit $r \to 0$

$$f_0 = -g_0 \Phi = -\sqrt{\frac{U}{U'}}\, f_0' . \qquad (8)$$

The voltage dependences of the two focal lengths, as given by (8), are shown in Fig. 6 as functions of the ratio U/U'. These relations, together with the assumption $p_0 \cong p_0' \cong$ const, determine the approximate position of the focal points once the geometrical constant g_0 is known. For several of the lens arrangements discussed later in this article, the validity of this formula has been

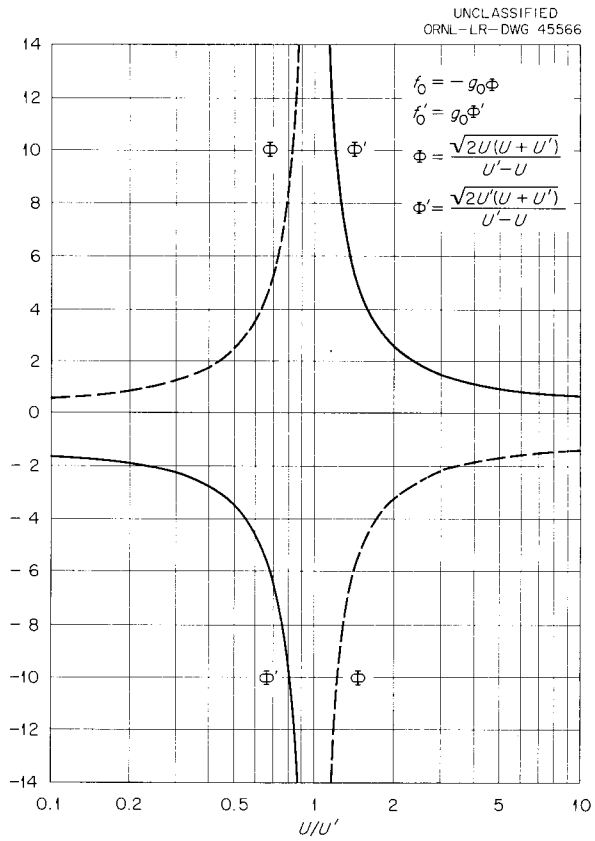

Fig. 6. Voltage Dependences of Focal-Length Parameters as Functions of the Ratio U/U'.

verified by ray-tracing calculations and agreement within 1% was found over a wide range of potential ratios. For the three geometries pictured in Fig. 7, g_0 lies between 1.92 and 1.80, while p_0 = 0.89 ... 0.84 and p_0' = 0.71 ... 0.68, and these parameters are practically independent of voltages over the range U'/U = 1.25 ... 5 (convergent lenses). The same formulas, (5) and (8), hold whether the potential ratio is $U/U' > 1$ (convergent lens, particles are decelerated in traveling from the grid towards the cylinder, $\Phi > 0, \Phi' > 0$) or $U'/U < 1$ (divergent lens, particles accelerated, $\Phi < 0$, $\Phi' < 0$), except that g_0 assumes a slightly different value. A rough estimate is

$$g_0^{\text{div}} \cong g_0^{\text{conv}} - \frac{p_0}{2\Phi} .$$

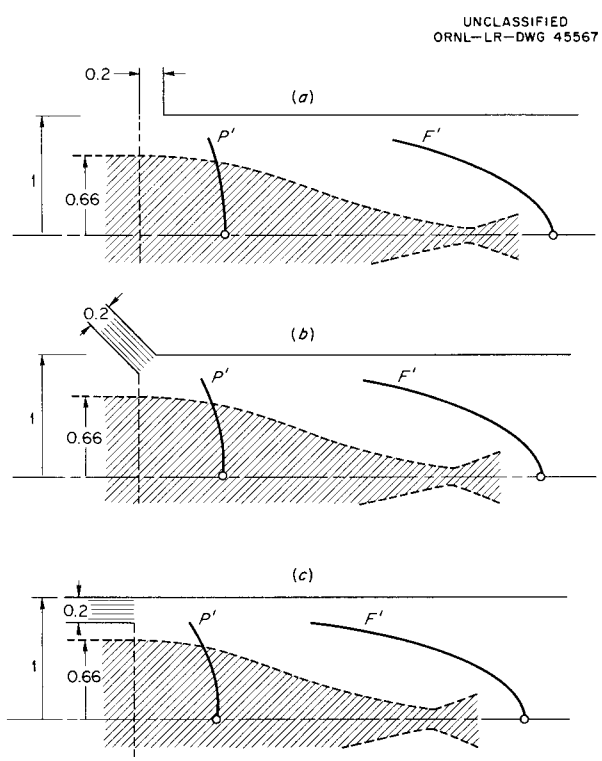

Fig. 7. Plane-Grid Configurations.

Axial Aberration

Third-order approximation in expanding Eq. (7′) yields

$$f'(r) \cong -r\left(\frac{1}{\sin\alpha'} - \frac{\sin\alpha'}{2}\right)$$

$$= g(r)\,\Phi' - \frac{r^2}{2g(r)\,\Phi'} \,. \qquad (9)$$

In order to write this in the form

$$f'(r) = \xi'(r)\cdot f_0' \cong f_0'\,(1 - a'r^2) \,, \qquad (10)$$

we put $g(r) = g_0$ in the second term of (9), and thus obtain

$$f'(r) \cong f_0'\left[\frac{g(r)}{g_0} - \frac{1}{2}\left(\frac{r}{f_0'}\right)^2\right] \,. \qquad (11)$$

For this to be identical with (10), we must have

$$g(r) = g_0\left[1 - a'r^2 + \frac{1}{2}\left(\frac{r}{f_0'}\right)^2\right]$$

$$= g_0\,(1 - br^2) \,. \qquad (12)$$

Since g has been introduced as a purely geometrical factor, the coefficient b cannot depend on the voltage ratio. Therefore,

$$a' = \frac{1}{2g_0^2\,\Phi'^2} + b \qquad (13)$$

gives the dependence of the spherical-aberration coefficient a' on the voltage ratio, through the auxiliary function Φ' as given by (6′) or the graph reproduced in Fig. 6. For example, ray-tracing for the lens shown in Fig. 7*a* gave $a' = 0.64$ at $\Phi' = \sqrt{2}$ (corresponding to $U/U' = 3$). Using $g_0 = 1.92$, we find the voltage-dependent term in (13) to be $1/(2\,g_0^2\Phi'^2) = 0.068$ at $\Phi' = \sqrt{2}$ so that $b = 0.57$. It is evident that b predominates unless we go to extreme values of the voltage ratio. In other words, the *coefficient of third-order axial spherical aberration does not change appreciably upon variation of paraxial focal length.*

Radial Aberration

Since in all practical cases the variance of $p'(r)$ is much smaller than that of $f'(r)$, let us assume $p'(r) = p_0' =$ const. A plane screen, perpendicular to the z axis, shall be specified by a certain ζ'^* value, according to

$$z = z'^* = p_0' + \zeta'^*\,f_0'$$

(see Fig. 5). A particle pointed from P' toward F' then hits that screen at a radius

$$r'^* = r\frac{\zeta'(r) - \zeta'^*}{\zeta'(r)} \qquad (14)$$

or, taking ζ' from (10),

$$r'^* = r\,\frac{1 - \zeta'^* - a'r^2}{1 - a'r^2} \,. \qquad (15)$$

In the special case $\zeta'^* = 1$, we obtain

$$r_0'^* = \frac{-a'r^3}{1 - a'r^2} \cong -a'r^3 \,,$$

which is the radial aberration in the paraxial focal plane.

Caustic

For any given $\Delta \equiv 1 - \zeta'^*$ in the region of interest, where $0 < \Delta \lesssim 1/4$, there exists a radius of

incidence r_A such that r'^* becomes stationary (see Fig. 5). Setting the derivative of (15) equal to zero gives

$$\Delta - a'r^2(3 - \Delta) + a'^2r^4 = 0 \ ,$$

whose useful solution satisfies $a'r_A^2 \ll 1$ and therefore can be written as

$$a'r_A^2 \cong \frac{\Delta}{3 - \frac{4}{3}\Delta} \ ; \qquad (16)$$

then

$$r_A \cong \sqrt{\frac{\Delta}{3a'}}\left(1 + \frac{2}{9}\Delta\right) \ . \qquad (17)$$

The corresponding r'^* value from (15) is

$$r_A'^* \cong \frac{2}{3}\sqrt{\frac{\Delta^3}{3a'}}\left(1 + \frac{1}{3}\Delta\right) \qquad (18)$$

or, expressed as a function of radius of incidence,

$$r_A'^* \cong 2a'r_A^3\,(1 - a'r_A^2) \ . \qquad (19)$$

Circle of Least Confusion

For the same Δ as considered above, there exists another radius of incidence r_B such that $r_B'^* = -r_A'^*$ (see Fig. 5). Putting (15) equal to the negative of (19) and eliminating Δ by use of (16) yields

$$r_B(3r_A^2 - r_B^2 - 4a'r_A^4) \cong -2r_A^3(1 - a'r_A^2)\,(1 - a'r_B^2) \ . \qquad (20)$$

As Fig. 5 shows r_B to be approximately twice r_A, we may replace r_B^2 in the higher-order terms by $r_B^2 \cong 4(1 + 2\epsilon)\,r_A^2$, so that (20) is simplified to

$$r_B \cong \frac{+2r_A(1 - 5a'r_A^2)}{1 + 8\epsilon + 4a'r_A^2} \ .$$

Comparing this with the assertion

$$r_B = 2\,r_A(1 + \epsilon) \ ,$$

ϵ is found to be $\epsilon = -a'r_A^2$, which is $\ll 1$ indeed. We can now express r_A in terms of r_B, namely,

$$r_A \cong \frac{1}{2}\,r_B(1 - \epsilon) \cong \frac{1}{2}\,r_B\left(1 + \frac{1}{4}a'r_B^2\right) \ ,$$

and eliminate r_A from (19), to obtain

$$r'^* \cong \frac{a'}{4}r_B^3\left(1 + \frac{a'}{2}r_B^2\right) \ . \qquad (21)$$

The length r_B may be considered as the radius of a parallel beam of particles passing through the grid plane, which is related, by (21), to the radius of its narrowest constriction, situated at

$$Z'^* \cong p_0' + (1 - \Delta)\,f_0' \cong p_0' + f_0'\left(1 - \frac{3}{4}a'r_B^2\right) \ . \qquad (22)$$

These formulas are useful for wide-aperture beams in the plane-grid arrangements such as shown in Fig. 7. For example, with $a' = 0.64$ and $r_B = 0.66$ as in Fig. 7*a*, (21) and (22) yield $r'^* = 0.056$ and $\Delta \cdot f_0' = 0.60$, while the ray-tracing results are 0.061 and 0.65 respectively.

The fact that the voltage ratio enters (21) only through the rather small influence on a' given by (13) implies that a given lens arrangement always produces approximately the same spot size when operated at different focal lengths. On the other hand, if all lengths in a given lens arrangement are scaled up, by a factor of 2, for example, except for keeping the beam diameter constant, $a'r_B^3$ drops by a factor of 8 since the unit for expressing r_B is doubled. The absolute spot size thus drops by a factor of ~ 4 as lens size and focal length are doubled. But the focal length may then even be reduced to its original value by increasing the voltage ratio, without much further effect on focus quality, due to the slow variation of a' predicted by (13) as long as the new focal length continues to satisfy

$$f_{0\,\mathrm{new}}' \gg \frac{r_{\mathrm{cylinder}}}{\sqrt{2b}} \ ,$$

where b is the aberration coefficient of the geometrical factor $(r/r_{\mathrm{cylinder}})$, and the cylinder radius (now $\neq 1$) characterizes the scaling factor.

COMPUTER CALCULATIONS

Potential Distributions

The general procedure used is the relaxation method of solution to Laplace's equation.[8] An

[8] F. B. Hildebrand, *Methods of Applied Mathematics*, p 295 ff., Prentice-Hall, New York, 1952.

Oracle program (problem No. 631) was written for cylindrical and also two-dimensional rectangular Cartesian coordinates. The computer program is of a general type allowing variation in the total dimensions of the net as well as in boundary shapes and values.

Geometries Studied. – The lens is approximated with a finite cylinder and modified by a gap configuration. The equipotentials in Figs. 8, 9, and 10 were traced at $U(r,z)$ = 49, 40, 30, 20, 10, 0, −10, −20, −30, and −40. Here $U = 50$; $U' = -50$. The r coordinate is r in the text × 35 ($r_{max} = 50$); the z coordinate is z in the text × 35 ($z_{max} = 125$). As shown by these maps, replacing the complicated gap structure by a linear interpolation between U and U' has little effect on the total potential distribution throughout the lens. Linear interpolation has the effect of producing a sharp-cornered gap. Replacing the complicated gap structure also shortens necessary computer time by approximately 30% and is used whenever possible.

The shaped grid (equipotential) is produced by assuming

$$U(r,0) = \begin{cases} U\ , & R \geqq r \geqq r_0\ , \\ U + [U(0,0) - U]\left(\dfrac{r}{r_0}\right)\left[\left(\dfrac{r}{r_0}\right) - 2\right]\ , & r_0 \geqq r \geqq 0\ , \end{cases}$$

where r_0 and $U(0,0)$ are arbitrary parameters. The quadratic potential variation along $z = 0$ was selected by trial and error, since the trajectories produced by this shape seemed to yield a marked improvement over those obtained from $U(r,0)$ = const $\cdot R \geqq r \geqq 0$. The resultant equipotential, $U(r,z)$ = const, from the quadratic approximation along $U(r,0)$ produces $z(r)$ that is roughly sinusoidal, Figs. 8, 9, and 10. Also, a quadratic potential variation along $z = 0$ produces a smoother equipotential than assignment of boundary values to net points nearest the space position of the curve.

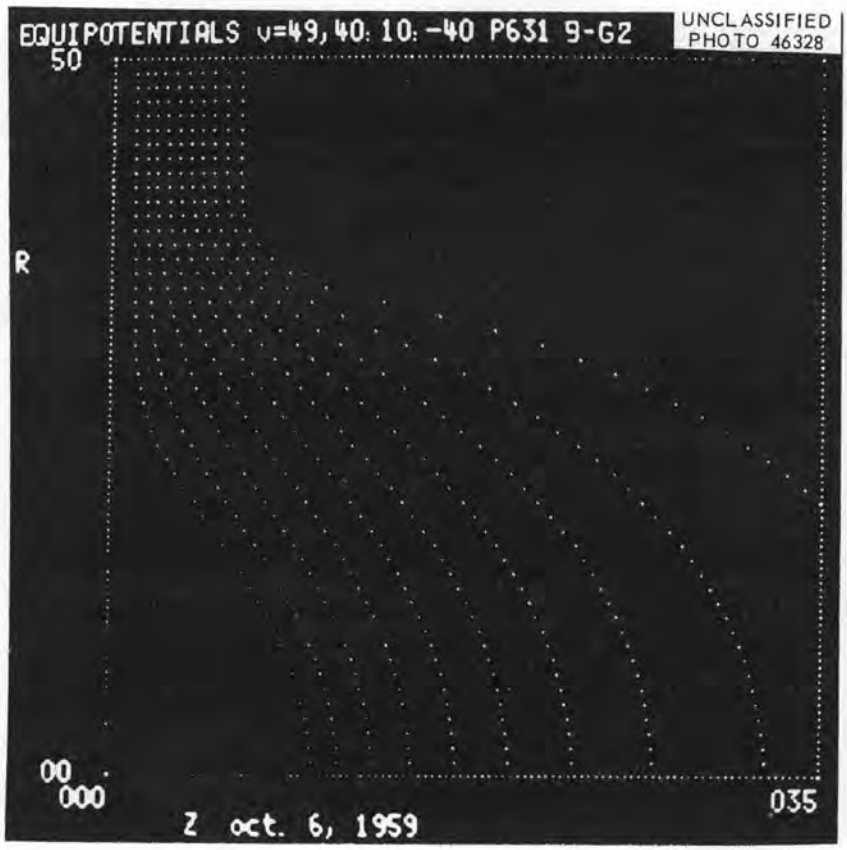

Fig. 8. Equipotential Map.

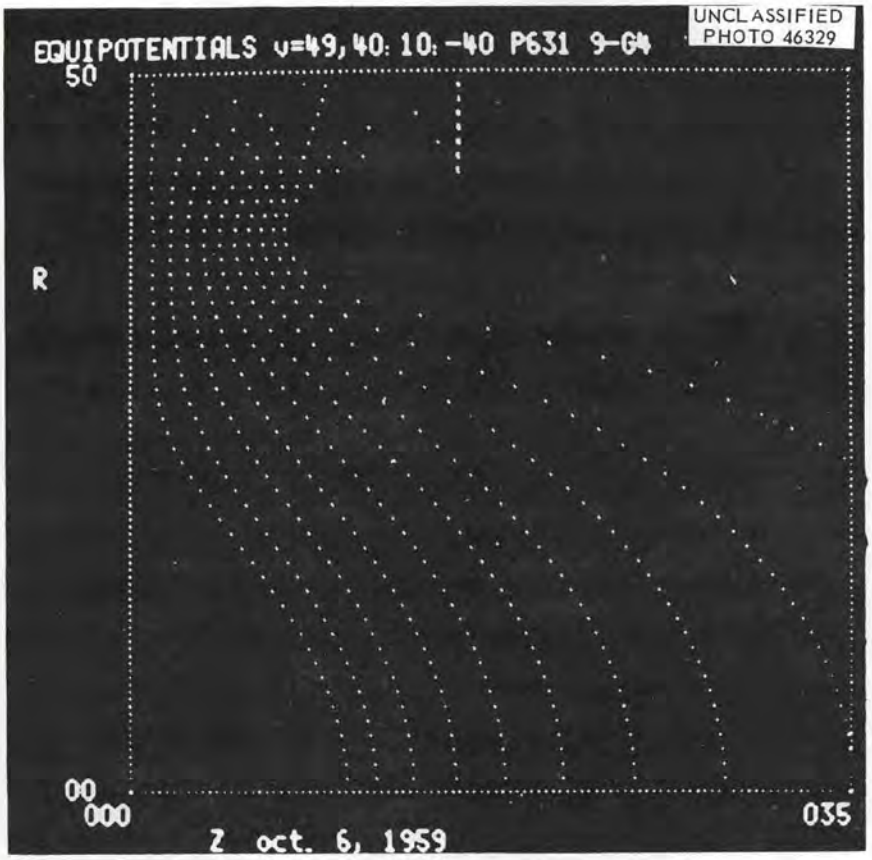

Fig. 9. Equipotential Map.

Details of the Calculation. – For convenience the following parameter values were used:

$$U' = 50 \ , \qquad U = -50 \ ,$$

$$\Delta r = \Delta z = \frac{1}{35} \ , \qquad R = 1 \ , \qquad z_{max} = \frac{125}{35} \ .$$

An over-relaxation factor ω was introduced to speed convergence:

$$U(r,z) = \frac{\omega}{4} \times \text{residual} + U(r,z) \ , \qquad 1 \leqq \omega \leqq 2 \ ,$$

where

$$\begin{aligned} \text{residual} = {} & U(r+\Delta r,z) + U(r-\Delta r,z) + \\ & + U(r,z+\Delta z) + U(r,z-\Delta z) + \\ & + \frac{U(r+\Delta r,z) - U(r-\Delta r,z)}{2r} - 4U(r,z) \ . \end{aligned}$$

For $r > \frac{1}{7}$, ω was set equal to the Cartesian coordinate value,

$$\omega = 1 + \left(\frac{\mu}{1 + \sqrt{1-\mu^2}} \right)^2 \ ,$$

$$\mu = \frac{1}{2} \left(\cos \frac{\pi \Delta r}{R} + \cos \frac{\pi \Delta z}{z_{max}} \right) \ .$$

For $0 < r \leqq \frac{1}{7}$, ω was decreased approximately 5% and, along the axis, the following modification was used:[9]

$$U(0,z) = \frac{1}{6} \left[U(0,z+\Delta z) + U(0,z-\Delta z) + \right.$$
$$\left. + 4U(\Delta r,z) \right] \ .$$

[9] K. R. Spangenberg, *Vacuum Tubes*, p 74, McGraw-Hill, New York, 1948.

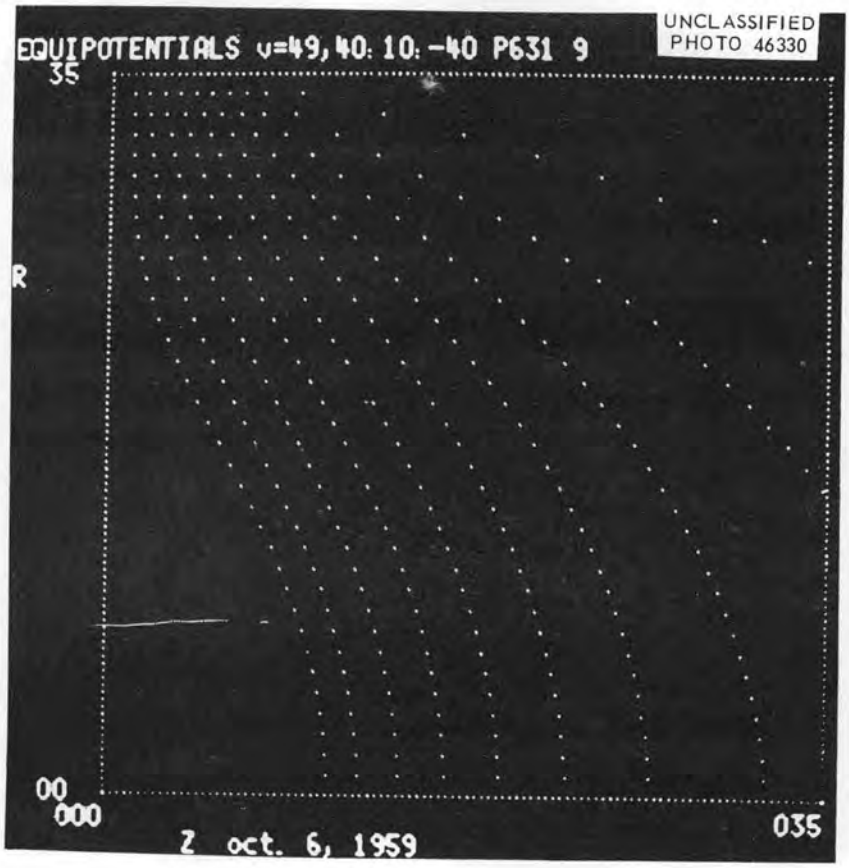

Fig. 10. Equipotential Map.

The initial total residual was reduced by linear interpolation of the boundary values at $z = 0$ and $z = 125/35$.

Convergence Criterion. – Over the entire map,

$$\frac{\frac{1}{4}\text{ residual}}{U(r,z)} \leq 10^{-8} .$$

Particle Trajectories

The calculated paths of a particle with a given velocity vector, starting at a particular point on the grid, in a specified potential distribution were traced on the Oracle by using the following formulas:

$$v_{r_0} = 0 ,$$

$$v_{z_0} = \sqrt{4U} , \quad U = 150, 200, 300, 500 ,$$

$$z_{n+1} = z_n + 1 ,$$

$$r_{n+1} = r_n + \frac{v_{r_n} \cdot \Delta z}{W} + \frac{F + F^*}{2W^2} \cdot \Delta z^2 ,$$

$$v_{r_{n+1}} = v_{r_n} + \frac{F + F^*}{W} ,$$

$$v_{z_{n+1}} = v_{z_n} + \frac{G + G^*}{W} , \tag{23}$$

where

$$W = v_{z_n} + \frac{v_{z_n}(G + G^*)}{2v_{z_n}^2 + (G + G^*)} ,$$

$$F \equiv -\frac{\partial U(r,z)}{\partial r} , \quad F^* \equiv -\frac{\partial U[r + (v_r/v_z), z + 1]}{\partial[r + (v_r/v_z)]} ,$$

$$G = -\frac{\partial U(r,z)}{\partial z} , \quad G^* \equiv -\frac{\partial U[r + (v_r/v_z), z + 1]}{\partial[r + (v_r/v_z)]} ,$$

$$r = \frac{5}{35}, \frac{7}{35}, \frac{10}{35}, \frac{12}{35}, \frac{15}{35}, \frac{20}{35}, \frac{25}{35}, \frac{28}{35}, \frac{30}{35} .$$

Each complete path was computed and results recorded on paper tape in 1.5 min for 125 positions within the potential distribution. The focal point was calculated by a linear extrapolation from the last position of the particle and its velocity components before the particle crossed the center ($r = 0$). The principal surface was likewise calculated by determining the intersection of the above straight line with the r_0 line.

RESULTS ON PLANE GRID CONFIGURATIONS

Influence of Gap Orientation

Without regard to the occurrence of sharp corners, the plane parallel gap of the configuration shown in Fig. 7*a* was tilted by 45° to give 7*b*, or by 90° to give 7*c*. It is somewhat surprising that these rather drastic changes did not increase the spherical aberration by more than 20% and 40% respectively. For purposes of illustration, the envelope of a beam which fills the grid plane to $(0.66)^2 = 43\%$ of the cylinder cross section has been indicated in Fig. 7. Thus, the changes in r'^* and z'^* for a constant $r_B = 0.66$ are seen to be fairly small.

The lens 7*a* has a special interest in that it constitutes exactly one half of the conventional two-cylinder configuration, Fig. 1*a*. From sufficiently detailed data on 7*a* (including the case $U'/U < 1$ which makes a divergent lens) one can therefore construct the detailed behavior of lens 1*a*.

In addition, case 7*a* offers an analytical solution which we found valuable as a check on the accuracy of our potential distributions found by the relaxation method. Formula (11.85) in Zworykin *et al.*[10] reads, with V_0, V_1, V_2, a, R replaced by our notations $V_0 \to U$, $V_1 = V_2 \to U'$, $a \to w$ = gap width, R = cylinder radius $\to 1$, as follows:

$$U(z,r) = U' + (U - U')\frac{z}{z_{max}} + 2(U - U')\sum_{n=1}^{\infty}\left(1 + \frac{z_{max}}{w}\cos n\pi\right)\frac{\sin(n\pi z/z_{max})\, I_0(n\pi r/z_{max})}{n\pi\, I_0(n\pi/z_{max})} , \tag{24}$$

where

w = gap width (a in previous notation),
$r = 1$ = cylinder radius,
z_{max} = "cylinder" height,
$U = V_0$,
$U' = V_1 = V_2$,
z is measured from the grid.

The $U(z,r)$ values obtained by the relaxation method were found to coincide with those calculated from (24) within $10^{-6}\ U$ when the iterations had become stationary within $10^{-8}\ U$. Such checks were made along the axis at $z = 0.2$, 0.4, 0.6, 0.8, 1.0, 1.4 and along $r = 0.8$ at $z = 0.0857$, 0.2, 0.4.

Influence of Gap Width and Corners

A common feature of all results presented in Fig. 11 is that third-order theory is adequate up to $r = 0.8$. This is evident from the smallness of a_4' when the formula

$$f'(r) = f_0'(1 - a_2' r^2 - a_4' r^4) , \qquad 0 \leq r \leq 1 , \tag{25}$$

is fitted to the ray-tracing results. For example, the sharp-corner geometry, Fig. 11*a*, gives

$$a_2' = 0.486 , \qquad a_4' = 0.119 .$$

The well-known fact that wider gaps tend to improve focusing is confirmed by a comparison of 11*b*, *c*, and *e*, but it is also evident that the improvement is of no practical importance.

Finally, the influence of corners at $r > 1 + w$ (i.e., outside the cylinder by more than one gap width) is seen to be negligible when comparing 11*c* and 11*d*.

PRACTICAL LIMITATIONS

Requirements on Grid Mesh Size

Assuming a square wire grid net with a uniform spacing δ, the number of meshes per unit grid area is δ^{-2} and we can apply a formula quoted in Von Ardenne's reference book[11] to estimate the

[10] V. K. Zworykin *et al.*, *Electron Optics and the Electron Microscope*, sec 11.7, p 382, Wiley, New York, 1945.

[11] M. von Ardenne, *Tabellen der Elektronenphysik, Ionenphysik und Übermikroskopie*, vol 1, p 50, VEB Deutscher Verlag der Wissenschaften, Berlin, 1956.

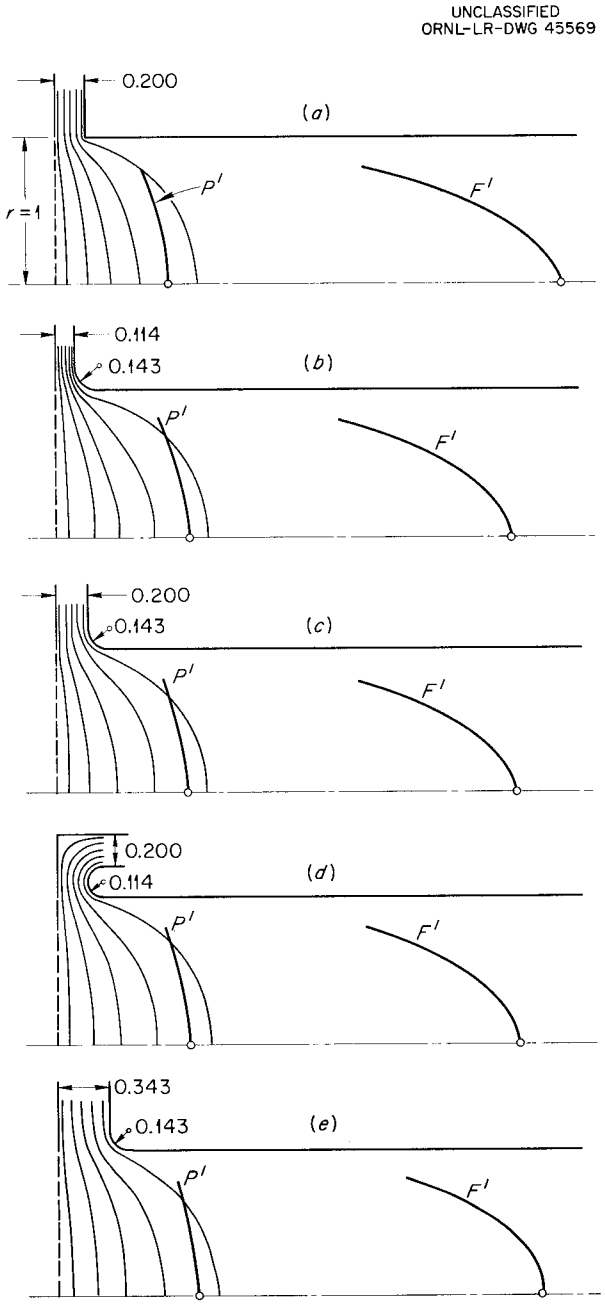

Fig. 11. Influence of Gap Width and Corners.

median scattering angle:

$$\alpha'_{Sc} \cong 0.2\delta \frac{U - U'}{p'} \cdot \frac{1}{U} . \qquad (26)$$

Here the average field strength near the grid is replaced by the approximation $(U - U')/p'$ which is suggested by the arguments used in "Elementary Theory of Basic (Plane Grid + Cylinder) Lenses," in this paper. The additional factor $\sqrt{U/U'}$ was inserted to take the change $\alpha \to \alpha'$ into account. When this expression, multiplied by the focal length f', exceeds the radius of least confusion for a given incident-beam radius r_B, then grid scattering becomes the predominant lens defect. Given r_B and the axial aberration coefficient a'_2, we therefore can define a critical mesh size by putting $\alpha'_{Sc} f' = r'^*$, or, using (3), (6′), (8′), (21), in first-order approximation:

$$0.2 \frac{\delta}{p'} \cdot \frac{U - U'}{\sqrt{UU'}} g_0 \phi' \cong 0.2\delta \frac{g_0}{p'_0} \sqrt{2\left(1 + \frac{U'}{U}\right)}$$

$$= r'^* \cong \frac{a'}{4} r_B^3 .$$

Most of the lens configurations considered here have $g_0/p'_0 \cong 2.7$, so that

$$\delta_{crit} \cong \frac{a'}{3} r_B^3 \sqrt{\frac{U}{U + U'}} . \qquad (27)$$

For the beam pictured in Fig. 4*a*, $\delta_{crit} \cong 0.05$ from (27); $\delta = 0.025$ might be considered satisfactory for a practical application.

Space-Charge Effect on a "Point" Focus

We shall from now on use the actual e/m values characterizing the particles in our beam. Consider a homocentric beam (i.e., a bundle of rays free from spherical aberration) of uniform density over the cross section πr_B^2, carrying a current

$$I = \pi r_B^2 \rho v_Z \cong \pi r_B^2 \rho \sqrt{-2 \frac{e}{m} U}$$

along the z axis, assuming that $|v_r/v_Z| \ll 1$. The electric field E produced by the uniform charge density ρ in the region $0 \leq r \leq r_B$ is then governed by the Poisson equation, in which we may neglect the z component:

$$\frac{1}{r} \frac{d}{dr} (rE_r) = \frac{\rho}{\epsilon_0} .$$

Its solution,

$$E_r = \frac{r\rho}{2\epsilon_0} = \frac{r}{r_B} \cdot \frac{I\sqrt{m}}{2\pi r_B \epsilon_0 \sqrt{-2eU}} ,$$

shows that radial accelerations produced by space-charge repulsion are proportional to the momentary radial distances of individual particles. Thus, the space-charge effect *does not introduce spherical aberration into a homocentric beam, nor does it tend to destroy a uniform density distribution.* It does, however, *shift the focus of a homocentric beam toward infinity* as the trajectories approach the axis.

The paraxial solution for an initially convergent beam, as discussed by Pierce,[12] predicts a finite constriction radius

$$r_{min} = r_B e^{-(S/f')^2} \tag{28}$$

if the beam, on crossing some $z = z_0$ plane, where its radius is r_B, is pointing toward a focus at $z_F = z_0 + f'$.[13] The space-charge parameter S is defined:

$$S = \sqrt{2 \cdot 2\pi\epsilon_0 \left(\frac{kl}{m}\right)^{1/2} |U'|^{3/2} I^{-1}}$$

$$= \left\{\begin{matrix} 1.01 \\ \text{or} \\ 0.15 \end{matrix}\right\} \cdot |U'|^{3/4} \cdot \left(\frac{1}{I}\right)^{1/2} , \tag{29}$$

with numerical factors calculated for electrons (1.01) and protons (0.15); U' is in kilovolts, I is in amperes, and l is length of line focus. The beam constriction is located at

$$z_{r_{min}} - z_0 = 2Se^{-(S/f')^2} \int_{y=0}^{S/f'} e^{y^2} dy . \tag{30}$$

In the case of a weak space charge, this is slightly larger than f'.

We can now compare (28) with (21) in order to define a critical beam current above which space-charge spreading spoils the focusing quality of a given lens system. Equality requires

$$S^2_{crit} = f'^2 \ln \frac{r_B}{r'^*} = f'^2 \ln \frac{4}{a' r_B^2} ; \tag{31}$$

or, making use of (6′), (8′), and (29):

$$I_{crit} = \frac{\sqrt{2}\,\pi\epsilon_0 \sqrt{|e|/M}}{g_0^2 \ln (4/a' r_B^2)} \cdot \frac{(U - U')^2 \sqrt{|U'|}}{U + U'} . \tag{32}$$

For most of the lenses considered here, $g_0 \cong 1.85$, so that the formula may be rewritten with approximate numerical factors for electrons (150) and protons (3.2):

$$I_{crit} \cong \left\{\begin{matrix} 150 \\ \text{or} \\ 3.2 \end{matrix}\right\} \frac{1}{\ln (4/a' r_B^2)} \cdot \frac{(U - U')^2 \cdot \sqrt{|U'|}}{|U + U'|} , \tag{33}$$

where U is in kilovolts, I_{crit} is in milliamperes. If the beam pictured in Fig. 7*A* is run at $|U| = 15$ kv, $|U'| = U/3 = 5$ kv, the voltage-dependent factor becomes 11.2, and at $r_B = 0.66$ the formula gives

$$I_{crit} \cong \begin{cases} 630 \text{ ma} , & \text{for electrons} , \\ 13.5 \text{ ma} , & \text{for protons} . \end{cases} \tag{34}$$

Space-Charge Effect on a Line Focus

Analogous treatment of the two-dimensional case,[12] where the variable r is replaced by a Cartesian ordinate y, yields

$$y_{min} = \begin{cases} 0 , & \sigma > \dfrac{2f'}{\sqrt{y_B}} , \\ y_B - \left(\dfrac{\sigma y_B}{2f'}\right)^2 , & \sigma < \dfrac{2f'}{\sqrt{y_B}} , \end{cases} \tag{35}$$

where

$$\sigma = \sqrt{8\sqrt{2}\,\epsilon_0 \left(\frac{|e|}{M}\right)^{1/2} |U'|^{3/2} (iy_B)^{-1}}$$

$$= \left\{\begin{matrix} 1.16 \\ \text{or} \\ 0.177 \end{matrix}\right\} \cdot (|U'|)^{3/4} \cdot \left(\frac{1}{iy_B}\right)^{1/2} , \tag{36}$$

i = current per unit depth of beam = I,

I = total beam current,

l = length of line focus.

---

[12] J. R. Pierce, *Theory and Design of Electron Beams*, Von Nostrand, New York, 1949.

[13] In Pierce's notation, the initial condition is specified in terms of a parameter $R_0' = S(r'/r)_{z=z_0}$ rather than by the focal length $f' = -(r/r')_{z=z_0}$.

Since y_{min} according to (35) increases rapidly when σ falls below $2f'/\sqrt{y_B}$, we may define this as the critical σ value (without taking actual lens aberrations into account) and introduce it into (36) to obtain the critical total beam current

$$I_{crit} = \frac{l}{g_0^2}\sqrt{2}\,\epsilon_0\sqrt{|e|/M}\cdot\frac{(U-U')^2\sqrt{|U'|^2}}{|U+U'|} \quad . \tag{37}$$

Assuming $g_0 \cong 2$ for the lenses of interest, the explicit numerical formulas for electrons and protons become

$$I_{crit} \cong \left\{\begin{matrix}42\\ \text{or}\\ 1\end{matrix}\right\} l\cdot\frac{(U-U')^2\cdot\sqrt{|U'|}}{|U+U'|} \quad , \tag{38}$$

where I_{crit} is in milliamperes. In contrast to the case of cylindrical symmetry, the sheet-beam geometry permits ideally sharp focusing even with a finite beam current, as long as $I < I_{crit}$. Within this range, space charge merely shifts the focal length from f_0' to

$$f'(\sigma) = \sigma^2\frac{y_B}{2f_0'}\left[1-\sqrt{1-\left(\frac{\sigma_{crit}}{\sigma}\right)^2}\right] . \tag{39}$$

In the limiting cases, this expression yields:

$$f'(I) \cong f_0'\left[1+\left(\frac{I}{4I_{crit}}\right)^2 + 2\left(\frac{I}{4I_{crit}}\right)^4\right] , \quad \text{(low current)} , \tag{40}$$

$$f'_{max} = 2f_0' , \quad \text{(critical current)} . \tag{41}$$

For a two-dimensional lens operated at the same potentials as assumed in our previous example, Eq. (34), space-charge spreading allows a maximum electron current of 470 ma, or proton current of 11 ma, through each centimeter of an ideal line focus, which then appears at twice the zero-current focal length. It is of interest to note here that the focal-length shift becomes quite small (1.6%) if one reduces the currents to one-half of their critical values.

PUBLICATIONS

Alburger, D. E., "7.656-Mev $E0$ Transition in C^{12}," *Phys. Rev. Letters* **3**, 280 (1959).

Becker, R. L., and M. E. Rose, "Polarization of Conversion Electrons Following Beta Decay," *Nuovo cimento* **13**, 1182 (1959).

Block, M. M., E. B. Brucker, I. S. Hughes, T. Kikuchi, C. Meltzer, F. Anderson, A. Pevsner, E. M. Harth, J. Leitner, and H. O. Cohn, "Observation of He^4 Hyperfragments from K^--He Interactions: The K^--Λ Relative Parity," *Phys. Rev. Letters* **3**, 291 (1959).

Brolley, J. E., Jr., and J. L. Fowler, "Monoenergetic Neutron Sources: Reactions with Light Nuclei," p 73–111 in *Fast Neutron Physics. Part I: Techniques* (ed. by J. B. Marion and J. L. Fowler), Interscience, New York, 1960.

Campbell, E. C., and P. F. Fettweis, "Mise en evidence de quelques nouveaux etats isomeriques," *Nuclear Phys.* **13**, 92 (1959).

Cohn, H. O., and J. L. Fowler, "Differential Elastic Scattering of Neutrons from Neon," *Phys. Rev.* **114**, 194 (1959).

Galonsky, A., H. B. Willard, and T. A. Welton, "S-Wave Detector of Deuteron Polarization and 14-Mev Polarized-Neutron Sources," *Phys. Rev. Letters* **2**, 349 (1959).

Gardner, C. G., and T. A. Welton, "On the Possibility of Studying the Λ-Hyperon-Nucleon Force by Low Energy Scattering," *Phys. Rev. Letters* **3**, 281 (1959).

Gibbons, J. H., and R. L. Macklin, "Total Neutron Yields from Light Elements Under Proton and Alpha Bombardment," *Phys. Rev.* **114**, 571–80 (1959).

Gibbons, J. H., R. L. Macklin, J. B. Marion, and H. W. Schmitt, "Precision Measurement of the $Be^9(\gamma,n)$ Cross Section," *Phys. Rev.* **114**, 1319 (1959).

Gibbons, J. H., and H. W. Newson, "The $Li^7(p,n)Be^7$ Reaction," p 133–76 in *Fast Neutron Physics. Part I: Techniques* (ed. by J. B. Marion and J. L. Fowler), Interscience, New York, 1960.

Good, R. H., and M. E. Rose, "Transverse Polarization in Allowed Beta Transitions," *Nuovo cimento* **14**, 872 (1959).

Johnson, C. H., "Recoil Telescope Detectors," p 247–95 in *Fast Neutron Physics. Part I: Techniques* (ed. by J. B. Marion and J. L. Fowler), Interscience, New York, 1960.

Kisslinger, L. S., "Nuclear Structure Effects in Internal Conversion Coefficients by Configuration Mixing," *Phys. Rev.* **114**, 292 (1959).

Lamphere, R. W., "Fission Detectors," p 449–506 in *Fast Neutron Physics. Part I: Techniques* (ed. by J. B. Marion and J. L. Fowler), Interscience, New York, 1960.

Lyon, W. S., and R. L. Macklin, "Neutron Activation at 195 kev," *Phys. Rev.* **114**, 1619 (1959).

McGowan, F. K., "Excitation Coulombienne," p 225–39 in *Comptes Rendus du Congrès International de Physique Nucléaire*, Dunod, Paris, 1959.

McGowan, F. K., and P. H. Stelson, "Coulomb Excitation of the Second 2+ State in Even-Even Nuclei," p 765-71 in *Comptes Rendus du Congrès International de Physique Nucléaire*, Dunod, Paris, 1959.

McGowan, F. K., and P. H. Stelson, "Coulomb Excitation of States in Pt^{195}," *Phys. Rev.* **116**, 154 (1959).

McNally, J. R., Jr., and K. G. Kessler, "Supplementary Zeeman Data for the First Spectrum of Ruthenium (RuI)," *J. Research Natl. Bur. Standards* **63A**, 253 (1959).

Macklin, R. L., "Neutron Absorption at Intermediate Energies," 2nd UN Geneva Conference of 1958, P671, USA, Pergamon Press, p 68–71.

Moak, C. D., H. E. Banta, J. W. Johnson, and R. F. King, "A New Ion Source for Propulsion of Space Vehicles," *Am. Rocket Soc. J.* **29**, 868 (1959).

Moak, C. D., H. E. Banta, J. N. Thurston, J. W. Johnson, and R. F. King, "A Duo Plasmatron Ion Source for Use in Accelerators," *Rev. Sci. Instr.* **30**, 694 (1959).

Morgan, H. W., "A Leveling Device for Alkali Halide Pressed Disk Preparation," *Appl. Spectroscopy* **13**, 48 (1959).

Morgan, H. W., and J. H. Goldstein, "The Microwave Spectrum and Molecular Structure of Vinyl Fluoride," *J. Chem. Phys.* **30**, 1025 (1959).

Murray, R. B., and H. W. Schmitt, "Cross Section for the $Li^6(n,\alpha)H^3$ Reaction for $1.2 \leq E_n \leq 8.0$ Mev," *Phys. Rev.* **115**, 1707 (1959).

Neiler, J. H., "Time to Pulse Height Conversion," *Proceedings of Second Symposium on Advances in Fast Pulse Techniques for Nuclear Counting*, UCRL-8706, p 59 (1959).

Neiler, J. H., and W. M. Good, "Time-of-Flight Techniques," p 509–621 in *Fast Neutron Physics. Part I: Techniques* (ed. by J. B. Marion and J. L. Fowler), Interscience, New York, 1960.

Newson, H. W., R. C. Block, P. F. Nichols, A. Taylor, A. K. Furr, and E. Merzbacher, "*S*- and *P*-Wave Neutron Spectroscopy, II. Even-Even Nuclei," *Ann. Physics* **8**, 211 (1959).

Rose, M. E., "Beta Radioactivity," p 90 in *Handbook of Physics* (ed. by E. U. Condon and H. Odishaw), McGraw-Hill, New York, 1958.

Rose, M. E., "A Method for Producing Aligned Deuterons," *Phys. Rev. Letters* **3**, 387 (1959).

Sherwood, J. E., and S. J. Ovenshine, "The Nuclear Spins of I^{128} and I^{130}," *Phys. Rev.* **114**, 858–61 (1959).

Smith, E. C., G. S. Pawlicki, P. E. F. Thurlow, G. W. Parker, W. J. Martin, G. E. Creek, P. M. Lantz, and S. Bernstein, "The Total Neutron Cross Section of Xe^{135} as a Function of Energy," *Phys. Rev.* **115**, 1693 (1959).

Smith, W. G., P. H. Stelson, and F. K. McGowan, "Decay of $I^{130} \rightarrow Xe^{130}$," *Phys. Rev.* **114**, 1345 (1959).

Staats, P. A., and H. W. Morgan, "Infrared Spectrum of Phosphorous (III) Cyanide," *Appl. Spectroscopy* **13**, 79 (1959).

Staats, P. A., and H. W. Morgan, "Infrared Spectra of Solid Ammonia," *J. Chem. Phys.* **31**, 553 (1959).

Stelson, P. H., W. G. Smith, and F. K. McGowan, "Polarization of γ-Rays in Pb^{207}," *Phys. Rev.* **116**, 167 (1959).

Vander Sluis, K. L., "An Application of a Digital Computer to the Zeeman Method in Atomic Spectroscopy," *J. Opt. Soc. Am.* **49**, 944 (1959).

Wilkinson, M. K., "Neutron Diffraction Investigations of Magnetic Phenomena in Crystalline Compounds," *J. Appl. Phys.* **30**, 278S (1959).

Wilkinson, M. K., J. W. Cable, E. O. Wollan, and W. C. Koehler, "Neutron Diffraction Investigation of the Magnetic Ordering in $FeBr_2$, $CoBr_2$, $FeCl_2$, and $CoCl_2$," *Phys. Rev.* **113**, 497 (1959).

PAPERS PRESENTED AT SCIENTIFIC AND TECHNICAL MEETINGS

American Physical Society Meeting, Cambridge, Massachusetts, March 30–April 1, 1959

J. W. Cable, M. K. Wilkinson, and E. O. Wollan, "Neutron Diffraction Studies of the Magnetic Ordering in $CrCl_3$."

M. K. Wilkinson, H. R. Child, W. C. Koehler, and E. O. Wollan, "Neutron Diffraction Investigations of Metallic Cerium at Low Temperatures."

Spring Meeting – Optical Society of America, New York City, April 2–4, 1959

J. R. McNally, M. R. Skidmore, and G. K. Werner, "The Spectroscopy of a Thermonuclear System – The Magnetically Confined, High Current, Vacuum Carbon Arc."

American Chemical Society Meeting (Division of Physical Chemistry), Boston, Massachusetts, April 5–10, 1959

T. A. Carlson, F. Pleasonton, and A. H. Snell, "Dissociation of C_6H_5T Following Beta Decay."

Southeastern Section Meeting of the American Physical Society, New Orleans, Louisiana, April 9–11, 1959

H. O. Cohn (invited paper), "High Energy Experiment with the Duke Liquid Helium Bubble Chamber."

C. H. Johnson (invited paper), "The Study of the β-Decay Interaction by Recoil Experiments."

T. A. Welton (invited paper), "Progress Report on the Southern Regional Accelerator."

M. K. Wilkinson (invited paper), "The Unique Role of Neutron Diffraction in Solid State Physics."

C. P. Bhalla and M. E. Rose, "Pseudoscalar Interaction in Nuclear β Decay."

H. R. Child, M. K. Wilkinson, E. O. Wollan, and J. W. Cable, "Neutron Diffraction Investigations of the Ferromagnetic Ordering in HoN."

J. L. Fowler and H. O. Cohn, "Scattering of Neutrons from Beryllium."

J. A. Harvey, R. C. Block, and G. G. Slaughter, "Low Energy Neutron Resonance in Lanthanum."

J. R. Lawson and H. W. Morgan, "Infrared Absorption Intensities of Ions in Solid Solutions."

D. G. Maeder, "High Output Level Time-to-Voltage Converter."

H. W. Schmitt and J. Halperin, "Cross Section for the $Al^{27}(n,\alpha)Na^{24}$ Reaction as a Function of Neutron Energy."

J. E. Sherwood, S. J. Ovenshine, and G. W. Parker, "Nuclear Spin of I^{132}."

M. R. Skidmore, J. R. McNally, Jr., and G. K. Werner, "The Spectroscopy of a Thermonuclear System Component – The Magnetically Confined, High Current, Vacuum Carbon Arc."

H. B. Willard and J. K. Bair, "60° Deflection, Uniform Field, Double-Focusing Reaction Product Magnet."

Sixth Tripartite Instrumentation Conference, Chalk River, Ontario, Canada, April 20–24, 1959

D. G. Maeder, "High Output Level Time-to-Voltage Converter."

D. G. Maeder, "Circuits Recently Added to Delay-Line Memory Pulse Spectrometer."

Symposium on the Mathematical Aspects of Reactor Theory (American Mathematical Society), New York City, April 23–24, 1959

T. A. Welton (invited paper), "System Kinetics."

American Physical Society Meeting, Washington, D.C., April 30–May 2, 1959

R. L. Macklin (invited paper), "Neutron Radiative Capture Cross Sections from 10 to 150 kev."

R. C. Block, J. A. Harvey, and G. G. Slaughter, "The ORNL Neutron Fast Chopper Time-of-Flight Spectrometer."

J. W. Cable, M. K. Wilkinson, and E. O. Wollan, "Neutron Diffraction Investigations of the Magnetic Ordering in CrF_2 and $CrCl_2$."

J. H. Gibbons, R. L. Macklin, and J. H. Neiler, "Neutron Radiative Capture Cross Sections from 10 to 150 kev."

F. K. McGowan and P. H. Stelson, "Coulomb Excitation of the Second 2+ State in Even-Even Medium Weight Nuclei."

R. L. Robinson and W. G. Smith, "Decay of Rh^{106} and Ag^{106}."

P. A. Staats and H. W. Morgan, "The Infrared Spectra of Solid Ammonia."

P. H. Stelson and F. K. McGowan, "Coulomb Excitation of the First 2+ State in Some Medium-Weight Even-Even Nuclei."

M. K. Wilkinson, E. O. Wollan, and H. R. Child, "Antiferromagnetism in MoF_3."

J. H. Wise, "Classification of the Pu II Spectrum."

Annual Meeting of the French Society of Crystallography and Mineralogy, Grenoble, France, June 3–8, 1959

W. C. Koehler, E. O. Wollan, and M. K. Wilkinson, "Neutron Study of Rare Earth Perovskites."

American Nuclear Society Meeting, Gatlinburg, Tennessee, June 15–17, 1959

E. C. Campbell, "Fundamental Mode Neutron Distribution in Pulsed Composite Systems."

Symposium on Molecular Structure and Spectroscopy, Ohio State University, June 15–19, 1959

P. A. Staats, H. W. Morgan, and J. H. Goldstein, "The Infrared Spectra of Solid Ammonia."

American Physical Society Meeting, Milwaukee, Wisconsin, June 18–20, 1959

H. W. Schmitt and R. B. Murray, "Neutron-Induced Fission Cross Section of Neptunium-237 as a Function of Energy."

Summer and Pacific General Meeting and Air Transportation Conference (American Institute of Electrical Engineers), Seattle, Washington, June 21–26, 1959

D. G. Maeder, "The Nature of Radiation."

Gordon Conference on Nuclear Chemistry, Meriden, New Hampshire, June 29–July 3, 1959

G. R. Satchler (invited paper), "Theoretical Discussion of Initial Interaction."

Conference on Nuclear Forces and the Few-Nucleon Problem, University College, London, England, July 8–11, 1959

H. B. Willard, A. Galonsky, and T. A. Welton, "The $T(d,n)He^3$ Reaction as an *S*-Wave Detector of Deuteron Polarization and 14 Mev Polarized Neutron Source."

Gordon Research Conference on Inorganic Chemistry, New Hampton, New Hampshire, August 10–14, 1959

M. K. Wilkinson (invited paper), "Investigations of Magnetic Phenomena by Neutron Diffraction."

Infrared Spectroscopy Institute, Fisk University, Nashville, Tennessee, August 24–29, 1959

H. W. Morgan, "Basic Techniques in Infrared Spectroscopy."

P. A. Staats, "Qualitative and Quantitative Analyses by Infrared Spectroscopy."

American Physical Society, Honolulu, Hawaii, August 27–29, 1959

C. W. Cook and H. W. Schmitt, "Neutron Absorption Cross Sections with Sb-Be Neutrons."

International Conference on High Energy Accelerators and Instrumentation, CERN, Geneva, Switzerland, September 14–19, 1959

T. A. Welton, "A High Intensity Alternating Gradient Proton Synchrotron with Relativistic Cyclotron Injection."

International Discussion on Magnetism, Clarendon Laboratory, Oxford, England, September 15–16, 1959

E. O. Wollan, "Magnetic Coupling in Crystalline Compounds and a Phenomenological Theory of Magnetism in 3d Metals."

Conference on Magnetism, Sheffield, England, September 22–24, 1959

M. K. Wilkinson, W. C. Koehler, and E. O. Wollan, "Recent Neutron Diffraction Investigations of Rare-Earth Substances."

Conference on Neutron Capture Reactions (Topical Meeting of APS), Los Alamos Scientific Laboratory, Los Alamos, New Mexico, October 1–3, 1959

J. H. Gibbons (invited paper), "Radiative Capture Cross Sections."

R. C. Block, "A Liquid Scintillator Tank for Neutron Capture Gamma Measurements with the ORNL Fast Chopper."

J. A. Harvey, "Spin States for Low Energy Neutron Resonances in Pt^{195}."

R. L. Macklin, P. D. Miller, J. H. Neiler, and J. H. Gibbons, "Radiative Capture Measurements for kev neutrons – III. Cross Section Results."

P. D. Miller, J. H. Neiler, J. H. Gibbons, and R. L. Macklin, "Radiative Capture Measurements for kev neutrons – II. Neutron Flux Measurements and the Cross Section of Indium."

J. H. Neiler, J. H. Gibbons, R. L. Macklin, and P. D. Miller, "Radiative Capture Measurements for kev Neutrons – I. Experimental Techniques and Gamma Spectrum Measurements."

H. W. Schmitt, C. W. Cook, and J. H. Gibbons, "Absolute Neutron Absorption Cross Sections at 24 kev."

American Society for Testing Materials Spectroscopy Symposium, San Francisco, California, October 12–16, 1959

J. R. McNally, Jr. (invited paper) "Challenges in Atomic Spectroscopy."

Physics of Thermal Breeders Conference, Argonne National Laboratory, Lemont, Illinois, October 19–21, 1959

N. J. Pattenden, "Fission Product Poisoning Data."

American Institute of Electrical Engineers Conference on Magnetism and Magnetic Materials, Detroit, Michigan, November 16–19, 1959

M. K. Wilkinson, H. R. Child, J. W. Cable, E. O. Wollan, and W. C. Koehler, "Neutron Diffraction Investigations of the Magnetic Ordering in Rare-Earth Nitrides."

G. T. Trammell, "Theory of Low-Lying States of Some Rare Earth Compounds."

Subcommittee on Neutron Standards and Measurements of the National Research Council, Gatlinburg, Tennessee, November 18, 1959

R. L. Macklin, "Graphite Sphere Neutron Detector."

P. D. Miller and J. H. Neiler, "Absolute Neutron Flux Measurement in the Kilovolt Region."

H. W. Schmitt, "Cross Section Measurements with Sb-Be Sources. Cross Section of $B^{10}(n,\alpha)$ Reaction."

American Physical Society Meeting, Cleveland, Ohio, November 27–28, 1959

J. H. Gibbons, P. D. Miller, R. L. Macklin, and J. H. Neiler, "The Absorption Cross Section of U^{235} from 10 to 175 kev."

R. L. Macklin, G. DeSaussure, J. D. Kington, and W. S. Lyon, "Measurement of η for U^{233}, U^{235}, and Pu^{239} by the Manganese Bath Technique."

H. W. Schmitt, R. C. Block, and R. L. Bailey, "Total Neutron Cross Section of B^{10} in the Range $0.018 \leq E \leq 0.4$ ev."

Tennessee Academy of Science Meeting, Vanderbilt University, Nashville, Tennessee, December 11–12, 1959

A. Nickle and P. D. Miller, "DIZY, a Neutron Capture Data Processing Program for the Oracle."

D. O. Patterson, C. E. Hughey, and H. O. Cohn, "Analysis of Bubble Chamber Photographs."

H. W. Schmitt and W. F. Mruk, "An Advanced Fission Experiment."

American Physical Society Meeting, Pasadena, California, December 28–30, 1959

J. L. Fowler (invited paper), "Differential Elastic Scattering of Neutrons and Resonance Structure of Nuclei."

American Physical Society Meeting, New York City, January 27–30, 1960

C. P. Bhalla and M. E. Rose, "The Pseudoscalar Interaction in β-Decay."

R. C. Block and G. G. Slaughter, "Neutron Radiative Capture Measurements with the ORNL Fast Chopper."

E. G. Corman and J. L. Fowler, "Phenomenological Nuclear Potentials from Neutron Scattering from O^{16}."

J. W. T. Dabbs, F. J. Walter, L. D. Roberts, and G. W. Parker, "Fission Fragment Emission from Aligned U^{233} and U^{235} Nuclei."

S. H. Hanauer, J. W. T. Dabbs, L. D. Roberts, and G. W. Parker, "Direction of Alpha Emission from Oriented Np^{237} and the Quadrupole Coupling in $NpO_2Rb(NO_3)_3$."

E. M. Harth, J. Leitner, R. Gessaroli, A. Minguzzi-Ranzi, G. Puppi, M. M. Block, E. B. Brucker, C. C. Chang, T. Kikuchi, C. Meltzer, A. Pevsner, P. Schlein, and H. O. Cohn, "Hyperfragment Production in the Helium Bubble Chamber."

P. D. Miller, J. H. Gibbons, and R. L. Macklin, "Effect of p-Wave Neutrons on Total Cross Sections in the kev Region."

N. J. Pattenden, J. A. Harvey, A. Culkowski, and N. Dismuke, "The Resonance Energy Neutron Cross Section of U^{233}."

L. D. Roberts and J. W. T. Dabbs, "Emission of Alpha Particles from Oriented Np^{237} Nuclei and the Structure of the NpO_2^{++} Bond."

G. R. Satchler, "Spin-Orbit Coupling for Spin-One Particles."

G. G. Slaughter and J. A. Harvey, "The Variation of η of U^{233} with Energy."

P. H. Stelson and F. K. McGowan, "Coulomb Excitation of Li^7, F^{19}, and Na^{23} by Ne^{20} Ions."

F. J. Walter, J. W. T. Dabbs, and L. D. Roberts, "Behavior of Semiconductor Counters."

ANNOUNCEMENTS

Additions and temporary assignments to the Physics Division staff during the past year were as follows: G. R. Satchler (Theoretical Physics Group); T. Dazai[1] of the Tokyo Institute of Technology, Tokyo, Japan (High Voltage Group); G. Felsner[1] of the University of Erlangen, Erlangen, Germany (Theoretical Physics Group); R. L. Gamble[1] of the Georgia Institute of Technology (Neutron Diffraction Group); N. J. Pattenden[1] of the Atomic Energy Research Establishment, Harwell, England (Fast Chopper Time-of-Flight Spectrometer Group); and H. H. F. Wegener[1] of the University of Erlangen, Erlangen, Germany (High Voltage Group).

J. L. Duggan of Louisiana State University, A. K. Furr of Duke University, and R. C. Ritter of the University of Tennessee have been granted Oak Ridge Institute of Nuclear Studies Graduate Fellowships to complete work toward the Ph.D. degree in the Physics Division – Duggan and Ritter with the High Voltage Group, and Furr with the Fast Chopper Time-of-Flight Spectrometer Group.

Co-op students assigned to the High Voltage and High Energy Physics Groups during this period included W. A. Hartman from the University of Tennessee, J. E. Thomas from Virginia Polytechnic Institute (Norfolk), and J. H. Williams from Virginia Polytechnic Institute (Blacksburg).

W. F. Mruk of the Instrumentation and Controls Division is on loan to the Nuclear Measurements for Reactor Design Group.

H. C. Owens (High Energy Accelerator Studies Group) transferred to the Solid State Division.

The following members of the Spectroscopy Group transferred to the Thermonuclear Experimental Division: P. M. Griffin, J. R. McNally, Jr., W. F. Peed, M. R. Skidmore, and G. K. Werner.

Terminations during the past year included A. Galonsky and C. N. Inskeep (High Voltage Group); T. I. Arnette and C. G. Gardner (High Energy Accelerator Studies Group); and D. G. Maeder (Scintillation Spectrometry and Instrument Development Group).

Summer personnel during 1959 included the following:

Research Participants – R. D. Edge (Assistant Professor, University of South Carolina), High Voltage Group; R. H. Good, Jr. (Associate Professor, Iowa State University) and E. Greuling (Associate Professor, Duke University), Theoretical Physics Group; J. Kronsbein (Professor, University of Florida), High Energy Accelerator Studies Group; M. T. Rodine (Professor, Gustavus Adolphus College), Scintillation Spectrometry and Instrument Development Group; and J. O. Thomson (Assistant Professor, University of Tennessee), Low Temperature Physics Group.

Summer Visitors – E. G. Corman (University of Kansas), High Voltage Group; N. H. Fuchs (Carnegie Institute of Technology), Nuclear Measurements for Reactor Design Group; and W. G. Smith (Purdue University), High Voltage Group.

ORINS Summer Student Trainees – G. Acton (Centenary College), Theoretical Physics Group; W. L. Hedger (Carson-Newman College), High Voltage Group; and D. M. Robinson (University of Chattanooga), Spectroscopy Group.

R. L. Becker (Theoretical Physics Group) has been on a nine-month assignment at Princeton University pursuing research in the field of nuclear theory; C. D. Moak (High Voltage Group) has been on a year's assignment at the Atomic Energy Research Establishment in Harwell, England, engaged in the field of Van de Graaff techniques; and T. A. Welton (High Energy Accelerator Studies Group) has been on a nine-month assignment as a visiting investigator at the Lawrence Radiation Laboratory in Berkeley, California.

[1] Temporary assignments.

L. D. Roberts (Low Temperature Physics Group) and W. C. Koehler (Neutron Diffraction Group) have returned to the Oak Ridge National Laboratory following a year's leave of absence – Roberts at the Clarendon Laboratory in Oxford, England, and Koehler at the University of Grenoble in Grenoble, France. Both were pursuing research in their respective fields under Guggenheim Foundation Fellowships and Fulbright Scholarships.

INTERNAL DISTRIBUTION

1. C. E. Center
2. Biology Library
3. Health Physics Library
4–6. Central Research Library
7. Reactor Experimental Engineering Library
8–19. Laboratory Records Department
20. Laboratory Records, ORNL R.C.
21. A. M. Weinberg
22. L. B. Emlet (K-25)
23. J. P. Murray (Y-12)
24. J. A. Swartout
25. E. H. Taylor
26. E. D. Shipley
27–37. J. L. Fowler
38. M. L. Nelson
39. A. H. Snell
40. A. Hollaender
41. K. Z. Morgan
42. F. L. Culler
43. M. T. Kelley
44. D. Phillips
45. E. O. Wollan
46. H. E. Seagren
47. A. S. Householder
48. L. D. Roberts
49. R. B. Briggs
50. R. N. Lyon
51. W. C. Koehler
52. E. P. Blizard
53. M. E. Rose
54. G. E. Boyd
55. W. H Sullivan
56. R. W. Stoughton
57. C. E. Winters
58. W. H. Jordan
59. E. C. Campbell
60. D. S. Billington
61. M. A. Bredig
62. R. S. Livingston
63. C. P. Keim
64. F. C. Maienschein
65. F. E. Obenshain, Jr.
66. R. C. Block
67. C. D. Susano
68. C. J. Borkowski
69. M. J. Skinner
70. M. K. Wilkinson
71. J. W. Cable
72. P. M. Reyling
73. G. deSaussure
74. W. M. Good
75. G. C. Williams
76. F. K. McGowan
77. R. W. Johnson
78. J. R. McNally, Jr.
79. J. L. Gabbard
80. R. A. Charpie
81. G. G. Slaughter
82. Eugene Guth
83. R. W. Peelle
84. P. R. Bell
85. G. G. Kelley
86. C. C. Harris
87. H. G. MacPherson
88. P. H. Stelson
89. J. E. Sherwood
90. W. Zobel
91. R. B. Murray
92. H. B. Willard
93. J. Schenck
94. J. H. Neiler
95. J. A. Harvey
96. C. F. Barnett
97. N. H. Lazar
98. J. W. T. Dabbs
99. A. Simon
100. J. H. Gibbons
101. J. J. Pinajian
102. S. Bernstein
103. F. Pleasonton
104. C. A. Preskitt
105. H. R. Child
106. C. G. Gardner
107. C. J. McHargue
108. J. A. Lane
109. C. S. Harrill
110. A. J. Miller
111. S. C. Lind
112. K. L. Vander Sluis
113. R. L. Robinson
114. G. R. Satchler
115. H. W. Morgan
116. H. W. Schmitt
117. P. M. Griffin
118. A. Zucker

119. C. D. Goodman
120. E. P. Wigner (consultant)
121. J. H. Van Vleck (consultant)
122. M. S. Livingston (consultant)
123. J. R. Richardson (consultant)
124. R. F. Christy (consultant)
125. M. Goldhaber (consultant)
126. W. A. Fowler (consultant)
127. J. A. Wheeler (consultant)
128. N. F. Ramsey (consultant)
129. H. Feshbach (consultant)
130. ORNL – Y-12 Technical Library, Document Reference Section

EXTERNAL DISTRIBUTION

131–230. Given external distribution
231–840. Given distribution as shown in TID-4500 (15th ed.) under Physics and Mathematics category (75 copies – OTS)